

**Civilian Radioactive Waste Management System  
Management & Operating Contractor**

**Chapter 8  
Total System Performance Assessment-Viability Assessment (TSPA-VA)  
Analyses Technical Basis Document**

**Saturated Zone Flow and Transport**

**B00000000-01717-4301-00008 REV 00**

**August 14, 1998**

Prepared for:

U.S. Department of Energy  
Yucca Mountain Site Characterization Office  
P.O. Box 30307  
North Las Vegas, Nevada 89036-0307

Prepared by:

TRW Environmental Safety Systems Inc.  
1261 Town Center Drive  
Las Vegas, Nevada 89134

**INFORMATION COPY**

9809180073 980911  
PDR WASTE  
WM-11 PDR

10/2/8

Under Contract Number  
DE-AC08-91RW00134

*Part 2*

**Civilian Radioactive Waste Management System  
Management & Operating Contractor**

**Chapter 8  
Total System Performance Assessment-Viability Assessment (TSPA-VA)  
Analyses Technical Basis Document**

**Saturated Zone Flow and Transport**

**B00000000-01717-4301-00008 REV 00**

**August 14, 1998**

Prepared for:

U.S. Department of Energy  
Yucca Mountain Site Characterization Office  
P.O. Box 30307  
North Las Vegas, Nevada 89036-0307

Prepared by:

TRW Environmental Safety Systems Inc.  
1261 Town Center Drive  
Las Vegas, Nevada 89134

**INFORMATION COPY**

Under Contract Number  
DE-AC08-91RW00134

#### **DISCLAIMER**

This report was prepared as an account of work sponsored by an agency of the United States Government. Neither the United States nor any agency thereof, nor any of their employees, makes any warranty, expressed or implied, or assumes any legal liability or responsibility for the accuracy, completeness, or usefulness of any information, apparatus, product, or process disclosed, or represents that its use would not infringe privately owned rights. Reference herein to any specific commercial product, process, or service by trade name, trademark, manufacturer, or otherwise, does not necessarily constitute or imply its endorsement, recommendation, or favoring by the United States Government or any agency thereof. The views and opinions of authors expressed herein do not necessarily state or reflect those of the United States Government or any agency thereof.

## **DRAFT DISCLAIMER**

This contractor document was prepared for the U.S. Department of Energy (DOE), but has not undergone programmatic, policy, or publication review, and is provided for information only. The document provides preliminary information that may change based on new information or analysis, and is not intended for publication or wide distribution; it is a lower level contractor document that may or may not directly contribute to a published DOE report. Although this document has undergone technical reviews at the contractor organization, it has not undergone a DOE policy review. Therefore, the views and opinions of authors expressed do not necessarily state or reflect those of the DOE. However, in the interest of the rapid transfer of information, we are providing this document for your information.



**Civilian Radioactive Waste Management System  
Management & Operating Contractor**

**Chapter 8  
Total System Performance Assessment-Viability Assessment (TSPA-VA)  
Analyses Technical Basis Document**

**Saturated Zone Flow and Transport**

**B000000000-01717-4301-00008 REV 00**

**August 14, 1998**

Prepared by:

*Stephanie King*  
*for Bill Arnold*  
\_\_\_\_\_  
Bill W. Arnold  
Performance Assessment Operations

8-14-98  
Date

Checked by:

*Mont Howard*  
*for*  
\_\_\_\_\_  
Toya Jones  
Performance Assessment Operations

8-14-98  
Date

Approved by:

*Robert W. Andrews*  
*for*  
\_\_\_\_\_  
Robert W. Andrews  
Performance Assessment Operations

14 Aug 98  
Date

B000000000-01717-4301-00008 REV00

August 1998

INTENTIONALLY LEFT BLANK

## **ACKNOWLEDGMENT**

### **Saturated Zone Flow and Transport**

The development of the Total-System Performance Assessment-Viability Analyses Technical Basis Document has benefited from the support of people from many different organizations and disciplines from across the Yucca Mountain Project.

The following persons provided support in developing the technical basis of various components of the TBD:

In alphabetical order:

G.E. Barr (M&O/SNL) assisted in the development of the three-dimensional site-scale model, contributed guidance in the sensitivity study to evaluate dilution and vertical transverse dispersivity, and provided overall technical guidance.

K.H. Birdsell (M&O/LANL) developed the convolution-integral computer program and assisted in much of the computer modeling.

J.B. Czarnecki (USGS) developed the original three-dimensional, site-scale, saturated-zone model.

F.A. D'Agnese (USGS) and C.C. Faunt (USGS) developed the three-dimensional, regional-scale, saturated-zone model, and provided groundwater-flux estimates for the different climates.

S.A. McKenna (M&O/SNL) performed the sensitivity study to evaluate heterogeneity and flow channelization.

D. Petersen (M&O/DES) provided the model used in the sensitivity study to evaluate dilution and vertical transverse dispersivity.

B.A. Robinson (M&O/LANL) provided guidance and assistance in much of the modeling, and performed the three-dimensional particle tracking to determine the flow paths.

P. Tucci (USGS) performed an interim review and provided overall technical guidance.

A.V. Wolfsberg (M&O/LANL) and M. McGraw (M&O/LANL) performed the sensitivity study that investigated reactive colloid transport.

H. Zhang (M&O/DES) performed the sensitivity study to evaluate dual-porosity transport.

G.A. Zyvoloski (M&O/LANL) provided the FEHMN computer program.

The clarity and technical completeness of the work in this document has been greatly improved by the careful and thoughtful technical reviews and subsequent discussions provided by:

T. Jones (DES) and M. Gross (Beckman & Associates, Inc.), S.R. Alcorn (Management Solutions, LLC), H. Lent (M&O/SAIC), D. Hoxie (M&O/USGS), DOE and MTS reviewers. The transparency and traceability of the data and supporting references were ensured by the support of the following individuals:

C. Crawford (TRI), O. Pratt (SAIC), and W. Stensrud (DES) aided greatly in reference and literature review. Q/A and Records staff members.

The ability to convey the specific conceptualizations and the results of this very complex set of analyses and documentation has been enhanced due the contributions of :

K. Gaither, BDM, and RED, Inc.

## CONTENTS

8. SATURATED ZONE FLOW AND TRANSPORT .....	8-1
8.1 INTRODUCTION .....	8-1
8.1.1 Overview .....	8-1
8.1.2 Previous TSPA Modeling .....	8-2
8.1.3 Synopsis of Current Approach .....	8-4
8.1.4 Chapter Organization .....	8-5
8.1.5 Data Quality and Traceability .....	8-6
8.2 SZ FLOW AND TRANSPORT CHARACTERIZATION .....	8-7
8.2.1 Description of the SZ System .....	8-7
8.2.1.1 Regional Flow System .....	8-8
8.2.1.2 Site Flow System .....	8-11
8.2.2 Site Characterization Models .....	8-17
8.2.2.1 USGS Regional-Scale Flow Model .....	8-17
8.2.2.2 USGS Site-Scale Flow Model .....	8-20
8.2.3 Conceptual Models .....	8-23
8.2.3.1 Issues From the SZ Abstraction/Testing Workshop .....	8-23
8.2.3.2 SZ Expert Elicitation .....	8-25
8.2.3.3 Base-Case Conceptual Model .....	8-26
8.2.3.4 Alternative Conceptual Models .....	8-29
8.3 ANALYSIS APPROACH TO SZ FLOW AND TRANSPORT FOR TSPA ANALYSES .....	8-32
8.3.1 General Approach .....	8-32
8.3.2 TSPA 3-D SZ Flow Model .....	8-33
8.3.3 TSPA 1-D SZ Transport Model .....	8-37
8.3.4 Convolution Integral Method .....	8-38
8.3.5 Alternative Climate States .....	8-40
8.3.6 Assumptions .....	8-41
8.3.7 Implementation With the RIP Computer Code .....	8-44
8.4 SZ FLOW AND TRANSPORT BASE CASE .....	8-45
8.4.1 Description of the Base Case .....	8-45
8.4.1.1 Scenarios .....	8-46
8.4.1.2 Uncertainty .....	8-47
8.4.1.3 UZ Source Subregions .....	8-47
8.4.1.4 Transport Modeling .....	8-48
8.4.2 Development of Parameter Distributions and Uncertainty .....	8-49

8.4.3	Analyses .....	8-58
8.4.4	Results .....	8-58
8.4.5	Interpretation .....	8-59
8.4.6	Guidance for Sensitivity Studies .....	8-60
8.5	SENSITIVITY STUDIES.....	8-61
8.5.1	Key Issues.....	8-61
8.5.2	Analyses .....	8-62
8.5.2.1	Dilution and Vertical Transverse Dispersivity .....	8-62
8.5.2.2	Heterogeneity and Flow Channelization.....	8-65
8.5.2.3	Dual-Porosity Transport .....	8-77
8.5.2.4	Alternative Dilution Assumptions .....	8-88
8.5.2.5	Reactive Colloid Transport.....	8-90
8.5.3	Interpretation .....	8-102
8.6	SUMMARY AND RECOMMENDATIONS .....	8-105
8.6.1	Summary of Methods and Results.....	8-105
8.6.2	Implications for Repository Performance .....	8-108
8.6.3	Guidance for License Application.....	8-109
8.7	REFERENCES .....	8-112

## FIGURES

Figure 8 - 1.	Conceptual model of the saturated zone groundwater-flow system from the potential repository at Yucca Mountain. Processes that affect radionuclide travel times in the saturated zone from beneath Yucca Mountain to potential pumping wells include advection, matrix diffusion and sorption. Processes that affect the concentration of radionuclides in groundwater include transverse dispersion of the contaminant plume and radioactive decay. Radionuclide transport in the fractured medium of the volcanic tuffs is characterized by smaller effective porosity relative to the porous medium of the alluvium. Note that red indicates radionuclide concentration. ....	F8-1
Figure 8 - 2.	Summary of inputs and outputs from the SZ flow and transport component of the TSPA-VA analysis. Site characterization information that forms the basis of saturated zone flow and transport modeling is also indicated. ....	F8-2
Figure 8 - 3	Geological framework model for the USGS regional-scale SZ flow model (from D'Agnese et al. 1997a, Figure 21, 41). ....	F8-3
Figure 8 - 4.	Regional map and the SZ flow system. Blue arrows indicate general directions of groundwater flow in the saturated zone on a regional scale. Light yellow shading indicates major areas of groundwater discharge by a combination of spring discharge and evapotranspiration. ....	F8-4
Figure 8 - 5.	Map showing the estimated potentiometric surface of the Death Valley region (from D'Agnese et al. 1997a, Figure 27, 60). ....	F8-5
Figure 8 - 6.	Regional map showing topography, groundwater sub-basins, and general directions of groundwater flow (from D'Agnese et al. 1997a, Figure 30, 64). ....	F8-6
Figure 8 - 7.	Generalized geologic cross-section along the flowpath in the SZ from the repository to Amargosa Valley. ....	F8-7
Figure 8 - 8.	Regional map showing boundaries and grid of USGS regional-scale flow model (D'Agnese et al., 1997a). ....	F8-8
Figure 8 - 9.	Regional map showing evapotranspiration areas in the Death Valley Region (from D'Agnese et al. 1997a, Figure 23, 45). ....	F8-9
Figure 8 - 10.	Regional map showing recharge zones in the Death Valley Region (from D'Agnese et al. 1997a, Figure 25, p. 54). ....	F8-10
Figure 8 - 11.	Regional map showing model calibration of simulated heads and residuals (observed minus simulated) for the USGS regional-scale flow model (from D'Agnese et al. 1997a, Figure 48, 96). ....	F8-11
Figure 8 - 12.	Regional map showing simulated discharge locations under pluvial conditions (long-term-average climatic conditions) of USGS regional-scale flow model. (from D'Agnese et al. 1997b). ....	F8-12
Figure 8 - 13.	Sub regional map showing boundaries of the USGS site-scale flow model and wells with observations of hydraulic head (from Czarnecki et al. 1998, Figure 1). ....	F8-13

Figure 8 - 14. Perspective block diagram showing the numerical grid and geologic framework of the USGS site-scale flow model. The upper surface conforms to the assumed water table and the thickness is 1,250 m. Color scale corresponds to the unit numbers of the hydrostratigraphic units in the USGS site-scale model (see Table 8-8) (from Czarnecki et al., 1998 Figure 9).	F8-14
Figure 8 - 15. Locations of nodes for recharge in upper Fortymile Wash, the north-south oriented barrier in Solitario Canyon, and the east-west oriented barrier in the USGS site-scale flow model (from Czarnecki et al. 1998, Figure 8).	F8-15
Figure 8 - 16. Regional map showing model calibration (simulated heads and residuals) of USGS site-scale flow model (from Czarnecki et al. 1998, Figure 17).	F8-16
Figure 8 - 17. Normalized vectors indicating the direction and magnitude of groundwater flow in the USGS site-scale flow model (from Czarnecki et al. 1998, Figure 20).	F8-17
Figure 8 - 18. Map showing topography, the repository footprint, and the TSPA 3-D SZ model boundaries and grid. Low-permeability features corresponding to the moderate- and high-hydraulic gradient regions are shown in yellow. Reaches of Fortymile Wash along which recharge is specified are shown by different colors.	F8-18
Figure 8 - 19. Perspective block diagram of the distribution of permeability in the TSPA 3-D SZ flow model. Colors correspond to hydrogeologic unit numbers (Table 8-11). Low-permeability features shown in Figure 8-18 are not included in this figure. Note that unit 13 is missing.	F8-19
Figure 8 - 20. Map showing simulated hydraulic head and residuals for the TSPA 3-D SZ flow model. Symbols in the upper image indicate the magnitude of the difference between simulated hydraulic head and measurements in wells. The upper image shows a shaded relief map of the surface topography while the outline of the repository is shown in red. The lower image shows a perspective view of the simulated hydraulic head over the same domain.	F8-20
Figure 8 - 21. Simulated particle paths from the TSPA 3-D SZ flow model. The simulated pathlines are superimposed on a shaded relief map of the surface topography. The transport model results shown are for a hypothetical release of a nonsorbing radionuclide at 10,000 years following the introduction of a source evenly distributed over the footprint of the potential repository at the water table.	F8-21
Figure 8 - 22. Schematic diagram showing the conceptual basis of the TSPA 1-D SZ transport model from below the repository to 20 km south. The six source sub regions at the water table beneath the repository correspond to the six streamtubes in the SZ. The cross-sectional area of each streamtube (e.g., $A_{sz}(5)$ ) is proportional to the volumetric groundwater flux through that streamtube. The total volumetric groundwater flux in the UZ through the repository horizon is $Q_{UZ}$ and the specific discharge for ground water in the saturated zone is $q_{sz}$ .	F8-22
Figure 8 - 23. Flow chart illustrating the convolution integral method in SZ flow and transport calculations in TSPA-VA.	F8-23



Figure 8 - 24.	Validation test case showing the simulated concentration-breakthrough curves calculated by the convolution integral method and calculated by explicit transient simulation using the FEHMN model. The simulations include a variable solute mass source from the UZ and five climate states summarized in Table 8-15.....	F8-24
Figure 8 - 25.	Map view of the potential repository footprint at the water table (shown in red). The six radionuclide source sub regions used in transport simulation are labeled . The eastern extensions of zones 2, 5, and 6 were added to account for lateral diversion of groundwater flow and radionuclide transport in the UZ. ....	F8-25
Figure 8 - 26.	Distributions of volcanic confining-unit permeabilities based on aquifer tests and the expert distributions from the SZ Expert Elicitation for hydrogeologic model units. The dashed line is a log-normal distribution fit to the data.....	F8-26
Figure 8 - 27.	Distributions of aquifer permeabilities based on aquifer tests and the distributions from the SZ Expert Elicitation for hydrogeologic model units. The dashed line is a log-normal distribution fit to the data.....	F8-27
Figure 8 - 28.	Distributions of porosity based on core data measurements (where data were available) for model units.....	F8-28
Figure 8 - 29.	Simulated radionuclide-concentration breakthrough curves from the TSPA 1-D SZ transport model for the base-case expected-value transport parameter values. Results are shown for the nine radionuclides, assuming a unit mass flux (1 g/y) source at sub region 1.....	F8-29
Figure 8 - 30.	Simulated radionuclide-concentration breakthrough curves from the TSPA 1-D SZ transport model for the 100 base-case realizations of the transport parameter values. Results are shown for the <sup>14</sup> C transport assuming a unit mass flux (1 g/y) source at sub region 1.....	F8-30
Figure 8 - 31.	Simulated radionuclide-concentration breakthrough curves from the TSPA 1-D SZ transport model for the 100 base-case realizations of the transport parameter values. Results are shown for the <sup>129</sup> I transport assuming a unit mass flux (1 g/y) source at sub region 1.....	F8-31
Figure 8 - 32.	Simulated radionuclide-concentration breakthrough curves from the TSPA 1-D SZ transport model for the 100 base-case realizations of the transport parameter values. Results are shown for the <sup>237</sup> Np transport assuming a unit mass flux (1 g/y) source at sub region 1. ....	F8-32
Figure 8 - 33.	Simulated radionuclide-concentration breakthrough curves from the TSPA 1-D SZ transport model for the 100 base-case realizations of the transport parameter values. Results are shown for the <sup>231</sup> Pa transport assuming a unit mass flux (1 g/y) source at sub region 1. ....	F8-33
Figure 8 - 34.	Simulated radionuclide-concentration breakthrough curves from the TSPA 1-D SZ transport model for the 100 base-case realizations of the transport parameter values. Results are shown for the <sup>239</sup> Pu transport assuming a unit mass flux (1 g/y) source at sub region 1. ....	F8-34

Figure 8 - 35.	Simulated radionuclide-concentration breakthrough curves from the TSPA 1-D SZ transport model for the 100 base-case realizations of the transport parameter values. Results are shown for the $^{239}\text{Pu}$ (irreversible sorption) transport assuming a unit mass flux (1 g/y) source at sub region 1. ....	F8-35
Figure 8 - 36.	Simulated radionuclide-concentration breakthrough curves from the TSPA 1-D SZ transport model for the 100 base-case realizations of the transport parameter values. Results are shown for the $^{242}\text{Pu}$ transport assuming a unit mass flux (1 g/y) source at sub region 1. ....	F8-36
Figure 8 - 37.	Simulated radionuclide-concentration breakthrough curves from the TSPA 1-D SZ transport model for the 100 base-case realizations of the transport parameter values. Results are shown for the $^{242}\text{Pu}$ (irreversible sorption) transport assuming a unit mass flux (1 g/y) source at sub region 1. ....	F8-37
Figure 8 - 38.	Simulated radionuclide-concentration breakthrough curves from the TSPA 1-D SZ transport model for the 100 base-case realizations of the transport parameter values. Results are shown for the $^{79}\text{Se}$ transport assuming a unit mass flux (1 g/y) source at sub region 1. ....	F8-38
Figure 8 - 39.	Simulated radionuclide-concentration breakthrough curves from the TSPA 1-D SZ transport model for the 100 base-case realizations of the transport parameter values. Results are shown for the $^{99}\text{Tc}$ transport assuming a unit mass flux (1 g/y) source at sub region 1. ....	F8-39
Figure 8 - 40.	Simulated radionuclide-concentration breakthrough curves from the TSPA 1-D SZ transport model for the 100 base-case realizations of the transport parameter values. Results are shown for the $^{234}\text{U}$ transport assuming a unit mass flux (1 g/y) source at sub region 1. ....	F8-40
Figure 8 - 41.	Schematic of inlet and solute distribution for a vertical rectangular source in the 3-D solute transport analytical solution, shown centrally located about the origin of the axes. The direction of flow is in the x-direction and the water table is located along the y-axis. Note that a and -a represent locations along the y-axis and b and -b are locations along the z axis (the vertical axis). ....	F8-41
Figure 8 - 42.	Simulated solute plumes using the 3-D analytical solution for two values of vertical transverse dispersivity. The color scale indicates the $\log_{10}$ simulated concentration. ....	F8-42
Figure 8 - 43.	Graph showing the uncertainty distribution of dilution factor used in TSPA-VA SZ transport analyses (solid line) and the relationship between vertical transverse dispersivity and dilution factor (compare lower and upper x-axes). The dashed line shows the uncertainty distribution in vertical transverse dispersivity obtained from Lynn Gelhar for the SZ expert elicitation and the corresponding range in dilution factor derived from the 3-D analytical solution. ....	F8-43

- Figure 8 - 44. Simulated solute plumes using the 3-D analytical solution for six source sub regions. The locations of the source regions are depicted in (a). Relative concentrations along transverse cross-sections at a 20 km distance are shown by the red shading. The cross-section (b), shows the simulated concentrations from a single solute source for the entire repository. The lower cross sections (c), show the simulated concentrations from six separate sources corresponding to the six source sub regions. The maximum simulated relative concentration at a 20 km distance is indicated on each cross-section. ....F8-44
- Figure 8 - 45. Map showing shaded relief image of topography, the TSPA 3-D SZ flow model domain, and the high-permeability faults from the USGS regional-scale hydrogeologic framework model. ....F8-45
- Figure 8 - 46. Map showing the faults from the USGS site-scale flow model. The model domain corresponds to the inner rectangular model boundary indicated in Figure 8-13. ....F8-46
- Figure 8 - 47. Histograms of root-mean-squared error of the head residuals in 100 realizations of the TSPA 3-D SZ flow model with (A) heterogeneous permeability for hydrogeologic units and with (B) heterogeneous permeability for hydrogeologic units and high-permeability faults. The filled circle is the RMSE for the base-case homogenous intra-unit-permeability model. The solid line is the mean of the 100 realizations and the dashed line is the median.....F8-47
- Figure 8 - 48. Histograms of maximum simulated concentrations at a 20 km distance in 100 realizations of the TSPA 3-D SZ flow model with (A) heterogeneous permeability for hydrogeologic units and with (B) heterogeneous permeability for hydrogeologic units and high-permeability faults. The solid line is the mean of the 100 realizations and the dashed line is the median. ....F8-48
- Figure 8 - 49. Histograms of time to reach 95% of simulated peak concentrations at a 20 km distance in 100 realizations of the TSPA 3-D SZ flow model with (A) heterogeneous permeability for hydrogeologic units and with (B) heterogeneous permeability for hydrogeologic units and high-permeability faults. The filled circle is the time for the base-case homogenous intra-unit-permeability flow model. The solid line is the mean of the 100 realizations and the dashed line is the median. ....F8-49
- Figure 8 - 50. Locations of the peak simulated concentrations at a 20 km distance in 100 realizations of the TSPA 3-D SZ flow model with (A) heterogeneous permeability for hydrogeologic units and with (B) heterogeneous permeability for hydrogeologic units and high-permeability faults. The gray circle is the location of peak concentration for the base-case homogenous intra-unit-permeability flow model.....F8-50
- Figure 8 - 51. Schematic diagram of multiple parallel fractures and matrix blocks in fractured medium. ....F8-51
- Figure 8 - 52. Schematic diagram of the 1-D single porosity flow and transport model (effective porosity approach) (a) Conceptualization and (b) Discretization. ....F8-52

Figure 8 - 53. Schematic diagram of the 1-D dual-porosity model as implemented in the FEHMN code, (a) dual-porosity method, (b) two matrix nodes (dual porosity). .....	F8-53
Figure 8 - 54. Diagram of the grid used in the 2-D single-porosity model.....	F8-54
Figure 8 - 55. Concentration breakthrough curves comparing solutions from the 1-D dual-porosity model and the 2-D single-porosity model for different values of fracture spacing, a) at a 15 km distance and (b) at a 20 km distance.....	F8-55
Figure 8 - 56. Simulated concentration breakthrough curves for $^{99}\text{Tc}$ from the 2-D single-porosity model for different values of fracture spacing, at (a) 15 km distance and (b) 20 km distance. ....	F8-56
Figure 8 - 57. Simulated concentration breakthrough curves at a distance of 20 km for $^{99}\text{Tc}$ from the 2-D single-porosity model (fracture spacing of 2 m) for different values of molecular diffusion coefficient. ....	F8-57
Figure 8 - 58. Simulated concentration breakthrough curves at a distance of 20 km for $^{99}\text{Tc}$ from the 2-D single-porosity model with and without radioactive decay for different values of fracture spacing. ....	F8-58
Figure 8 - 59. Simulated concentration breakthrough curves for $^{237}\text{Np}$ from the 2-D single-porosity model and the 1-D single porosity model (fracture spacing of 2 m) for different values of sorption coefficient, (a) at 15 km distance and (b) at 20 km distance. ....	F8-59
Figure 8 - 60. Simulated concentration breakthrough curves at a distance of 20 km for $^{99}\text{Tc}$ from the 2-D single-porosity model (fracture spacing of 2 m) for different values of matrix porosity. ....	F8-60
Figure 8 - 61. Simulated concentration breakthrough curves at a distance of 20 km for $^{99}\text{Tc}$ from the 2-D single-porosity model (fracture spacing of 2 m) for different values of fracture porosity. ....	F8-61
Figure 8 - 62. Simulated concentration breakthrough curves at a distance of 20 km for $^{99}\text{Tc}$ from the 2-D single-porosity model (fracture spacing of 2 m) for different values of longitudinal dispersivity.....	F8-62
Figure 8 - 63. Simulated concentration breakthrough curves at a distance of 20 km for $^{99}\text{TC}$ from the 2-D single-porosity model (fracture spacing of 2 m) for different values of Darcy velocity.....	F8-63
Figure 8 - 64. Simulated concentration breakthrough curves form the 2-D single-porosity model for different values of fracture spacing (shown in blue) and the 1-D single-porosity model for different values of effective porosity in fractured units (shown in red).....	F8-64
Figure 8 - 65. Average dose as a function of critical group size for the Amargosa Valley, estimated for the expected-value case. The solid line indicates average-dose rate per person; the plateau value corresponds to approximately 300 mrem/y maximum dose rate calculated in the base case for the reference person. Approximately 20 people could incur this dose rate based on the calculated amount of radionuclides released to the biosphere and the average water usage per person in the Amargosa Valley. The distribution of these radionuclides among the entire popuulation would reduce the dose rate to an average of approximately 5 mrem/y.....	F8-65

Figure 8 - 66.	Conservative tracer-concentration breakthrough curve at a 4 km distance for the fracture flow model. With no retardation, travel times through the system are only days. ....	F8-66
Figure 8 - 67.	Schematic diagram of the model for 1-D reactive transport of Pu migration. ....	F8-67
Figure 8 - 68.	Base-case simulated breakthrough curves for equilibrium and kinetic formulations of the reactions in Table 8-31. ....	F8-68
Figure 8 - 69.	Sensitivity of Pu(aq) and PuColloid(aq) breakthrough curves to variation in PuColloid formation $K_d$ (as a function of $k_f$ ). $k_r$ is held constant at 1 and $k_f$ is varied as indicated, thus, the $K_d$ ( $k_f/k_r$ ) varies from $10^9$ to $10^4$ . ....	F8-69
Figure 8 - 70.	Sensitivity of Pu(aq) and PuColloid breakthrough curves to variation in $k_f$ and $k_r$ where $K_d$ for PuColloid formation is kept constant at $10^8$ . Value shown is $k_f$ , $k_r = k_f/10^8$ . ....	F8-70
Figure 8 - 71.	Effect of Pu sorption $K_d$ on breakthrough curves of Pu(aq) and PuColloid(aq) when PuColloid formation reaction is equilibrium controlled (see parameters in Table 8-31). Pu sorption $K_d$ varied as indicated. ....	F8-71
Figure 8 - 72.	Effect of Pu sorption $K_d$ on breakthrough curves of Pu(aq) and PuColloid(aq) when PuColloid formation reaction is kinetically controlled (see parameters in Table 8-31). Pu sorption $K_d$ varied as indicated. Note PuColloid (aq) and Pu(aq) curves not as strongly coupled as in the equilibrium case in the previous figure. ....	F8-72
Figure 8 - 73.	Filtration sensitivity on breakthrough curves for equilibrium PuColloid formation reaction. Effect of changing the colloid filtration $K_d$ on the breakthrough curves of Pu(aq) and PuColloid(aq). ....	F8-73
Figure 8 - 74.	Filtration sensitivity on breakthrough curves for kinetic PuColloid formation reaction. Effect of changing the colloid filtration $K_d$ on the breakthrough curves of Pu(aq) and PuColloid(aq). ....	F8-74
Figure 8 - 75.	Effect of decreasing the colloid injection and ambient colloid concentration on Pu(aq) and PuColloid(aq) breakthrough concentrations. The plots show the effects of decreasing the colloid concentration from the base case $6.26 \times 10^{-9}$ M to $6.26 \times 10^{-12}$ M. ....	F8-75
Figure 8 - 76.	Effect of increasing the colloid injection and ambient colloid concentration on Pu[aq] and PuColloid[aq] breakthrough concentrations. The plots show the effects of increasing the colloid concentration from the base case $6.26 \times 10^{-9}$ M to $6.26 \times 10^{-6}$ M. ....	F8-76
Figure 8 - 77.	Comparing the TSPA-VA transport model with the reactive transport model. Cases (b) and (d) from Tables 8-33 and 8-34 are shown for each model formulation. Case (b) has a $K_c$ of 0.1 and is dominated by Pu(aq) transport and its associated sorption. Case (d) has a $K_c$ of 10 and shows the effects of unretarded colloid facilitated transport. PA Pu (total) is equivalent to the TSPA-VA base case analysis and Rxn stands for reaction. ....	F8-77

- Figure 8 - 78. Adding colloid filtration to reactive transport emulation of PA model for  $K_c=10$ . Colloid filtration  $K_d$ s are: a) 0.1, b) 10.0, and c) 1000.0. PA Pu (total) is equivalent to the TSPA-VA base case analysis and Rxn stands for reaction. ....F8-78
- Figure 8 - 79. Kinetic effects of the Pu-Colloid Reaction for  $K_c=0.1$  conditions ( $K_d = 1.59 \times 10^7$ ). a) Equilibrium Pu-Colloid reaction - no filtration, b) Kinetic Pu-Colloid reaction - no filtration ( $k_f=1.59 \times 10^4$ ,  $k_r = 1 \times 10^{-3}$ ), and c) Kinetic Pu-Colloid reaction - modest filtration ( $k_f=1.59 \times 10^4$ ,  $k_r = 1 \times 10^{-3}$ ). PA Pu (total) is equivalent to the TSPA-VA base case analysis and Rxn stands for reaction. ....F8-79
- Figure 8 - 80. Breakthrough curves at 25 km. Pu sorption  $K_d=1.2$ . PuColloid formation  $K_c = 10$ . PuColloid formation rates a)  $k_f = 1.5 \times 10^9$ ,  $k_r = 1$ , b)  $k_f = 1$ ,  $k_r = 1.5 \times 10^{-9}$ , c) same as (b) but with colloid filtration  $K_d = 100$ . PA Pu (total) is equivalent to the TSPA-VA base case analysis and Rxn stands for reaction. ....F8-80
- Figure 8 - 81. Breakthrough curves at (a) 18 km and (b) 25 km. PuColloid formation in disequilibrium ( $k_f = 1$ ,  $k_r = 1.5 \times 10^{-9}$ ), Pu sorption  $K_d= 15$ . Colloid filtration  $K_d = 0.1$ . Note that when the fronts enter the alluvium after 18 km, velocities decrease drastically and reactions come closer to equilibrium. This leads to Pu(aq) forming from the PuColloid(aq), hence the earlier arrival of Pu(aq) at 25 km than at 18 km. Similarly, the PuColloid(aq) concentration increases in the alluvium due to the lower velocities relative to reaction rates. PA Pu (total) is equivalent to the TSPA-VA base case analysis and Rxn stands for reaction. ....F8-81

## TABLES

Table 8 - 1.	Summary of SZ Modeling TSPA Analyses. ....	T8-1
Table 8 - 2.	DTNs For Models and Data in the SZ Base Case Analyses. ....	T8-2
Table 8 - 3.	Computer Codes Used in SZ Analyses. ....	T8-3
Table 8 - 4.	Summary of Codes, Input/Output Files, and DTNs Associated With Technical Figures. ....	T8-4
Table 8 - 5.	Relationship Among Numerical Models Used for the Saturated Zone Analyses. ....	T8-20
Table 8 - 6.	Estimated Hydraulic Conductivity of Regional Hydrogeologic Units (D'Agnese et al. 1997a, Table 1). ....	T8-21
Table 8 - 7.	Water-Budget Components for the Death Valley Regional Groundwater Flow System (D'Agnese et al. 1997a, Table 13) (DTN GS970708312144.003).....	T8-22
Table 8 - 8.	Hydrologic Properties of Hydrogeologic Units in USGS Site-Scale Saturated-Zone Flow Model (from Czarnecki et al. 1998; Table 3)**.....	T8-23
Table 8 - 9.	Estimated Water-Budget Components For the USGS Site-Scale Flow Model Area (from Czarnecki et al. 1998) (DTN GS970808312333.002). ....	T8-24
Table 8 - 10.	High-Priority Issues From the SZ Abstraction/Testing Workshop.....	T8-25
Table 8 - 11.	TSPA 3-D SZ Flow Model Hydrogeologic Units.....	T8-26
Table 8 - 12.	Summary of Permeabilities For the TSPA 3-D SZ Flow Model .....	T8-27
Table 8 - 13.	TSPA 3-D SZ Flow Model Calibration Results.....	T8-28
Table 8 - 14.	Simulated Groundwater Fluxes From the UZ Site-Scale Flow Model For the Source Subregions of the SZ Streamtubes (DTN SNT05091597001.009).....	T8-30
Table 8 - 15.	Climate Changes in the Five-Climate Test Case.....	T8-31
Table 8 - 16.	SZ Flux Factors For Alternative Climate States (e-mail, Pat Tucci, USGS, 12/11/97). ....	T8-32
Table 8 - 17.	Selected Transport Parameters For the 1-D SZ Transport Model.....	T8-33
Table 8 - 18.	Summary of Sorption Coefficients ( $K_d$ ) for the TSPA 1-D SZ Transport Model (DTN SNT05082597001.P05).....	T8-34
Table 8 - 19.	Summary of Stochastic Parameters For the TSPA 1-D SZ Transport Model (DTN SNT05082597001.P05). ....	T8-35
Table 8 - 20.	Stochastic Parameter Values for the 100 Realizations and Expected-Value Case Used in TSPA-VA Base Case SZ Analyses (DTN SNT05082597001.P05).....	T8-37
Table 8 - 21.	Radionuclide Decay and Transport Characteristics (DTN SNT05082597001.P05).....	T8-43
Table 8 - 22.	Input Parameters For Vertical Dispersivity Sensitivity Models.....	T8-44
Table 8 - 23.	Permeability for Major Hydrogeologic Units From model Calibration of the USGS Site-Scale Flow Model and From Hydraulic Testing.....	T8-45

Table 8 - 24.	Permeability Values Obtained Through Calibration of the USGS Site-Scale Flow Model and the TSPA 3-D SZ Flow Model.....	T8-46
Table 8 - 25.	Permeability Values Used in Indicator Geostatistical Simulations of Alluvial Deposits. ....	T8-47
Table 8 - 26.	Parameter Values Used in The Geostatistical Simulations of Permeability in the SZ.....	T8-48
Table 8 - 27.	Porosity of Geologic Units Used in the Dual-Porosity Sensitivity Studies. ....	T8-49
Table 8 - 28.	Fracture Apertures and Fluxes Used for Different Fracture Spacings In the Dual-Porosity Sensitivity Studies.....	T8-50
Table 8 - 29.	Retardation Factors With Matrix Diffusion or Sorption or Both Used In the Dual-Porosity Sensitivity Study.....	T8-51
Table 8 - 30.	Fracture Spacing and Approximate Effective Porosity.....	T8-52
Table 8 - 31.	Reaction Parameters for the Reactive Colloid Transport Sensitivity Analyses. ....	T8-53
Table 8 - 32.	Parameter Ranges for Reactive Colloid-Facilitated Pu transport.....	T8-54
Table 8 - 33.	Relationship Between $K_c$ and TSPA Model Parameters.....	T8-55
Table 8 - 34.	Relationship Between $K_c$ Reaction Transport Model Parameters.....	T8-56
Table 8 - 35.	Reaction Parameters for 25-km Stream Tube Simulations.....	T8-57

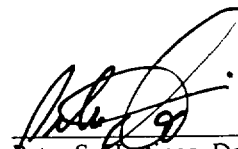


ADDENDUM TO CHAPTER 8 – 8/22/98

Please note that the following figures were inadvertently omitted from this chapter during the reproduction process. They have been included here for technical consistency and to facilitate the review, although they are not formally part of Revision 00.

Figure 8-63. Simulated concentration breakthrough curves at a distance of 20 km for  $^{99}\text{Tc}$  from the 2-D single-porosity model (fracture spacing of 2 m) for different values of Darcy velocity.

A Performance Report (PR) will be issued to correct this chapter. Revision 01 will also include these figures.



21-Aug-98

---

Peter S. Hastings, Deputy Manager  
Performance Assessment Operations

INTENTIONALLY LEFT BLANK

## 8. SATURATED ZONE FLOW AND TRANSPORT

### 8.1 INTRODUCTION

The introductory material in this section explains the significance of the saturated zone to repository performance, gives background on previous performance assessment analyses of the saturated zone, describes the current approach, and comments on data quality and traceability.

#### 8.1.1 Overview

The saturated zone (SZ) flow and transport component of the TSPA-VA analysis evaluates the migration of radionuclides within the SZ at Yucca Mountain, from their introduction at the water table near the repository to the point of release to the biosphere. The SZ is the region beneath the ground surface where rock pores and fractures are completely saturated with groundwater. The repository is located within the unsaturated zone (UZ) approximately 300 meters above the saturated zone. Fractured volcanic rocks, a series of alternating welded and nonwelded tuffs, comprise the shallow volcanic aquifer present in the vicinity of the potential repository. Fractured carbonate rocks are found at much greater depths below the water table and are considered to be the regional carbonate aquifer. Alluvium, a nonfractured, granular porous medium, overlies the volcanic and carbonate aquifers at a distance approximately 10 to 20 km south of the potential repository location (Figure 8-1). Radionuclides escaping a repository are expected to travel downward approximately 300 meters through the unsaturated zone in a dissolved or colloidal form in UZ water to the water table. The radionuclides are assumed to enter the saturated zone and continue 20 km downstream through the groundwater system through the volcanic aquifer and the alluvium to a hypothetical well where they could be a source of contamination of the biosphere (see Figure 8-1).

Important processes that control the movement of radionuclides (i.e., the radionuclide travel time) in the saturated zone include advection, matrix diffusion, and sorption (Figure 8-1). Groundwater movement by advection is the mechanism driving radionuclide migration away from the repository in both fractured and unfractured media. Matrix diffusion is the movement of dissolved radionuclides from groundwater flowing in fractures into the relatively immobile matrix pore water. Matrix diffusion slows radionuclide movement by providing additional solute storage in the system. Sorption of radionuclides on mineral grains slows radionuclide migration in the groundwater in both fractured and porous media. Processes that slow radionuclide migration may reduce potential radiological dose due to relatively longer travel times that allow radioactive decay of radionuclides in transit through the SZ system.

Important processes that affect the concentration of the radionuclide in the groundwater are transverse dispersion of the contaminant plume and radionuclide decay (Figure 8-1). Transverse dispersion causes dilution of radionuclide concentration during SZ transport due to horizontal and/or vertical spreading of the plume along the travel path. In turn, dilution of radionuclides attenuates the potential radiological dose by reducing radionuclide concentrations in groundwater. Radionuclide decay is the natural breakdown of a radionuclide and each radionuclide decays according to a characteristic decay constant, regardless of location. Thus, radionuclide decay is another process that results in a decrease in radionuclide concentration along the entire travel path from the repository to the biosphere.

The SZ flow and transport component of the analysis is coupled to the UZ transport calculations through the spatial and temporal distributions of simulated radionuclide mass flux at the interface between the UZ and the SZ (i.e., the water table). The SZ flow and transport component is linked to the biosphere analysis via the simulated time history of radionuclide concentration in the groundwater produced from a hypothetical well located 20 km from the repository. This hypothetical well is assumed to be located at the point of maximum radionuclide concentration 20 km away from the repository (and in the center of the simulated contaminant plume).

### 8.1.2 Previous TSPA Modeling

Initial modeling efforts reported for a potential repository at Yucca Mountain at the performance assessment of a potential repository at Yucca Mountain (e.g., Sinnock et al. 1984; Sinnock et al. 1985, p. 4.54-4.94; Barnard and Dockery 1991) either completely ignored or gave only cursory attention to the SZ by using simple 1-D approximations to the SZ. At the time, estimates of radionuclide travel times through the UZ were typically over 10,000 years, while the estimates of travel times through the SZ were on the order of 1000 years. Also, the regulation that governed a Yucca Mountain repository (EPA 1985) used a metric of cumulative releases of radionuclides to the accessible environment over a period of 10,000 years. A cumulative release of a radionuclide is the total amount of that radionuclide that crosses a boundary over a given time period. The boundary to the accessible environment was specified at a location 5 km from a repository; the area within the boundary was called the controlled area. Because the travel time in the UZ appeared to be greater than the regulatory period, and the travel time in the SZ appeared to be insignificant compared to the UZ and the regulatory period, any need for an in-depth look at the SZ was obviated.

For the first TSPA, TSPA-1991 (Barnard et al. 1992, 4.51-4.94) it was recognized that fast paths might exist through the UZ, and two alternative conceptual models of flow in the UZ were used: 1) a model that described flow predominately in the matrix, and 2) a new model (the Weeps model) that described flow predominately in the fractures. Because of the possibility that the UZ itself might not provide sufficient delay to meet the EPA 1985 regulation (which had been remanded by then), a more detailed model of the SZ was constructed. This 2-D model of the SZ was based on modeling by Czarnecki (1985) and Czarnecki and Waddell (1984, p. 1-30). The model encompassed the controlled area around the repository: the 5 km distance between the repository and the accessible environment. Boundary conditions for the TSPA model were taken from the Czarnecki model. A particle tracking method was implemented to determine travel times and velocities from the repository to the accessible environment for a conservative tracer. Particles were placed in the repository "footprint" (the area in the SZ immediately below the repository boundary) and travel times to the 5 km boundary were determined. Differences in initial position and path taken produced a distribution of travel times. In general, transport was in a southeasterly direction with travel times varying between 900 and 1500 years (velocities of 3.25 to 5.7 m/y) and a mean travel time of about 1200 years. The results of the 2-D model were abstracted for the TSPA-1991 calculations into 1-D horizontal flow tubes in a single porous medium. For the TSPA abstraction, dispersivities were assumed to be log-uniformly distributed between 50 and 500 m and porosity was set to 17.5%. During the TSPA calculations, the 1-D model was used directly to solve the transport of radionuclides over the 5 km distance to the accessible environment.

By the time of TSPA-1993 (Wilson et al. 1994, pp. 14-4,14-5; Andrews et al. 1994, pp. 3-4 and 3-6), it was becoming apparent that an upcoming regulation for a repository at Yucca Mountain might involve a metric of radiation dose to an individual. Calculation of dose requires a method of accurately determining the concentration of radionuclides at the geosphere/biosphere interface where the biological environment becomes exposed to the contaminants. Cumulative releases can be estimated using only the travel times. A 3-D, confined-aquifer model was constructed for TSPA-1993 to determine whether three dimensions were necessary to properly define the SZ flow system. The analysis concluded that incorporation of 3-D geologic structures was necessary to match observed hydraulic heads (water table heights) because the geologic structures, to a large degree, determined the direction and velocity of groundwater flow.

For TSPA-1993, as with TSPA-1991, travel times and velocities were determined by calculating the transport from various selected locations in each of the three geologic units that intersected the repository footprint to a location 5 km downgradient from the repository of a conservative tracer. Porosity was set to 20%. Two conceptual models were investigated: one that only allowed water to leave and enter the SZ domain from the sides (the non-diversionary model) and another which incorporated a drain out of the volcanic aquifer (the diversionary model). Results showed significant variability as compared to the TSPA-1991 results. Travel times for the various conceptual models and transport paths ranged from 230 to 1700 years (velocities of 3 to 22 m/y), with averages ranging from 500 to 800 years (average velocities of 6 to 10 m/y).

As with TSPA-1991, the detailed model results were used as input to a 1-D, single porosity model for the TSPA-1993 calculations. Longitudinal dispersivity was assumed to be uniformly distributed between 100 and 500 m to match the distribution of velocities and porosity was kept at 20%. Dilution, and thus final concentration, was calculated from an estimate of the cross-sectional area of the transport plume at the boundary to the accessible environment. The estimate was based on assumed transverse dispersivities and mixing depths (typically 50 m) and ranged between 34,000 and 2,200,000 m<sup>2</sup>. Climate change was incorporated in TSPA-1993 as a jump from one steady state condition to another. For the SZ, climate change was only approximated by water table rise; therefore no changes were made to flow or transport parameters. The water table rise was specified with a uniform distribution between 50 and 120 m. The jump in the water table elevation caused radionuclides in transit in the UZ to be immediately introduced to the SZ, resulting sometime later in a pulse of higher releases and doses at the accessible environment. Both cumulative releases and radiation doses (drinking water doses only) were considered as performance metrics in TSPA-1993.

For TSPA-1995 (Atkins et al. 1995), the emphasis was on a more accurate depiction of the engineered barrier system of a potential repository at Yucca Mountain and no new modeling of the SZ was conducted. Velocities from the TSPA-1993 3-D model were used again in 1-D abstractions. A constant longitudinal dispersivity of 500 m was assumed. Various cross-sectional areas of the contaminant plume were estimated as in TSPA-1993. From these cross-sectional areas and the groundwater flux, dilution factors were calculated and the radionuclide concentrations from the 1-D TSPA abstracted model were reduced by these dilution factors. In some calculations, additional dilution was assumed for mixing with other groundwater basins and for mixing with uncontaminated water during well withdrawal. As with TSPA-1993, water table rise was taken from a uniform distribution; however, the rise was more continuous over time.

Sensitivity studies were conducted for both TSPA-1993 and TSPA-1995 to look at how much the uncertainty and variability in parameter distributions influenced the uncertainty and variability of the results. Both TSPAs found repository performance to be sensitive to saturated-zone parameters. For a radiation dose metric in particular, results were sensitive to parameters influencing radionuclide dilution in groundwater. In the simplified TSPA models, these parameters were the groundwater flux and the cross-sectional flow area of the contaminant plume (or the dilution factor). In the actual flow system, these parameters correspond to the groundwater flux, transverse dispersion, transport path lengths, and possible well-withdrawal effects. Parameters primarily affecting radionuclide travel times (sorption coefficients, longitudinal dispersion, etc.) were found to be of lesser importance, although they could be important if the performance period is restricted (e.g., 10,000 years).

A comparison between previous TSPA models of SZ flow and transport and the TSPA-VA model is presented in Table 8-1.

### 8.1.3 Synopsis of Current Approach

As described in Section 8.1.2, past TSPA analyses focused on the biosphere interface located 5 km from the repository. In contrast, the TSPA-VA is now focused on calculating radionuclide dose 20 km downgradient from the repository; this is due to changes in DOE guidance that were based upon recommendations from the National Research Council (1995).

There are several aspects of the SZ analysis described in this chapter. A series of abstraction/testing workshops were conducted to compile a prioritized list of important technical issues related to flow and transport in the SZ to the TSPA-VA (see Section 8.2.3.1). An Expert Elicitation was also conducted to obtain opinions from five experts on groundwater flow and transport regarding significant issues related to the SZ (Section 8.2.3.2). The approach for conducting the TSPA-VA analysis was based upon input from the workshops and the Expert Elicitation. Numerical models were used for the purpose of characterizing and understanding the flow and transport system at Yucca Mountain at the regional- and site-scales (Section 8.2.2) and to perform TSPA-VA calculations (Section 8.3). The characterization models were developed based upon all available data and knowledge about the saturated zone. Likewise, the TSPA flow and transport models were developed based upon site knowledge, input from the workshops and Expert Elicitation, and insights provided by the characterization model results. For TSPA-VA, numerical simulations were performed for the base case (Section 8.4) as well as for sensitivity analyses to study variations of the base case (Section 8.5).

The base-case flow-and-transport component of the TSPA-VA for the saturated zone evaluated the migration of radionuclides from their introduction at the water table below the repository to the release point to the biosphere (**Error! Reference source not found.**). A hierarchy of models was used to simulate the transport of radionuclides in the saturated zone. Explicit, three-dimensional modeling was not used to simulate radionuclide concentrations because it can generate numerical dispersion, which artificially lowers concentration. The TSPA 3-D SZ flow model was used only to determine flowpaths through the SZ (see Section 8.3.2). The TSPA 1-D SZ transport model was developed based on the flowpaths from the three-dimensional flow modeling and used to determine concentration breakthrough curves at a distance of 20 km for unit releases of radionuclides from six streamtubes (see Sections 8.3.3, 8.4.3). The saturated

zone transport component of the analysis was linked to the transport calculations for the unsaturated zone that bring contaminants in downward percolating groundwater from the repository to the water table (e.g., the spatial and temporal distributions of simulated mass flux at the water table) (Figure 8-2). The linking was accomplished by using the convolution integral technique to combine the unit breakthrough curves calculated by the TSPA 1-D SZ transport model with the time-varying radionuclide sources from the unsaturated zone (see Section 8.3.4). Changes in the SZ flow and transport system in response to climatic variations were incorporated for the three discrete climate states (dry, long-term average, and superpluvial) considered in the other components of the TSPA-VA (Section 8.3.5). Specific discharge and volumetric groundwater flow rate in the SZ streamtubes were scaled in transport simulations to reflect climate state. The saturated zone transport results were linked to the biosphere analysis by the simulated time history, or system response as a function of time, of radionuclide concentration in groundwater produced from a hypothetical well located at the biosphere interface. The biosphere was assumed to be located 20 km from the repository (Figure 8-1). Radionuclide concentrations in the hypothetical well water were then used in the biosphere component to calculate doses received by the public.

For the base case, uncertainty in the SZ system was evaluated through Monte Carlo variation in the input parameters (Wilson et al. 1994, pp. 3-19 to 3-21) used in the TSPA 1-D SZ transport model. Primarily, the uncertainty in radionuclide transport parameters was evaluated. The TSPA 1-D SZ transport model calculated 101 unit breakthrough curves (100 Monte Carlo simulations and the expected value case). The results of the one-dimensional SZ transport calculations are located in a "library" of unit radionuclide concentration breakthrough curves. For each TSPA-VA RIP realization (see Section 8.3.7 for an explanation of the overall RIP calculations), a SZ unit breakthrough curve was randomly drawn for use in the convolution integral method.

The TSPA-VA sensitivity studies were designed to examine five of the key issues related to the base case SZ analysis assumptions (see Section 8.4.6). The sensitivity studies were performed to provide information about the importance of these issues with respect to repository performance. The effect of dilution in the saturated zone and vertical transverse dispersivity was investigated to address concerns from the Expert Elicitation panel (Section 8.5.2.1). The impact of including heterogeneity and large-scale flow channelization in a three-dimensional flow and transport model was studied (Section 8.5.2.2). A two-dimensional dual-porosity transport model was used to calculate radionuclide concentrations to examine the effect of the base case assumptions of a single continuum and using effective porosity as a surrogate for the matrix diffusion process (see Section 8.2.3.3 for base case assumptions, and Section 8.5.2.3 for sensitivity analysis description). A study to investigate the effect of calculating average dose to a member of a critical group compared to the dose to an individual calculated for the base case was performed (Section 8.5.2.4). Finally, alternative conceptual models of colloid-facilitated Pu transport were developed and implemented for sensitivity analysis (Section 8.5.2.5).

#### **8.1.4 Chapter Organization**

This chapter of the TSPA-VA report documents the analysis methods used in the base case SZ flow and transport component of the TSPA-VA, the basis for the base case analyses, and the base case results as they relate to performance of the potential repository. In addition, this report

includes a description of sensitivity studies of the base case, and a summary and discussion of all of the results as they pertain to recommendations for repository performance and guidance for licensing. Section 8.2 describes the current understanding of the SZ flow and transport processes at Yucca Mountain and the conceptualization of the SZ system used in the analyses. Section 8.3 explains the approach used for the SZ TSPA-VA base case analyses. Section 8.4 describes the set of base-case analyses of SZ flow and transport, including the assessment of parameter uncertainty and the base-case results. Section 8.5 documents the sensitivity analyses performed to augment the base-case analyses. A summary and discussion of the base case and sensitivity studies performed for TSPA-VA is presented in Section 8.6, focusing on implications related to licensing.

### **8.1.5 Data Quality and Traceability**

Fully qualified data suitable for direct use in modeling of flow and transport in the SZ for TSPA-VA analyses are very limited. Modeling results and inferences regarding parameter values, as incorporated into the TSPA-VA SZ analyses, rely on both qualified (Q) and non-qualified (Non-Q) data and must be considered Non-Q in aggregate. It would be impossible to construct defensible SZ groundwater flow and transport models solely on the basis of Q data. For example, inferences regarding the bulk permeability of several volcanic units from multi-well pump tests (Geldon et al. 1997, pp. ii, B-1-13) rely on water-level data from the C-holes (Q) and water-level measurements from boreholes WT#3, WT#14, p#1, and H-4 (Non-Q). Development of uncertainty distributions of base-case parameters for use in the SZ flow and transport analyses considers primarily Non-Q data, but includes some recently acquired Q data. Assessment of parameter uncertainty also depends heavily on results of the SZ Expert Elicitation (CRWMS M&O, 1998, p. 1-1), which does have Q status. Table 8-2 summarizes the Q-status of each of the components of the TSPA-VA analysis.

Traceability of the models and data used in the SZ analyses is maintained through the Yucca Mountain Project Technical Data Base. The data tracking numbers (DTNs) of the relevant components of the SZ flow and transport calculations for the TSPA-VA base case are given in Table 8-2. Note that these modeling and parameter analysis components represent developed data and are individually comprised of numerous primary data sources.

The computer codes used in the SZ flow and transport portion of the TSPA-VA are summarized in Table 8-3. The various modeling tasks for which each computer code was used, along with the code's quality assurance status is shown in the table. It should be noted that some of these computer codes were used directly in the simulations for the TSPA-VA base case, while others were used indirectly. To assist traceability, the DTNs for data presented in technical figures in this report are given in Table 8-4. The outputs and uses of the models are summarized in Table 8-5. Moving from the most directly used codes to those more indirectly used, the SZ\_CONVOLUTE code was used directly as a subroutine in the RIP simulator to couple the unit concentration breakthrough curves for the SZ to the UZ transport and biosphere components of the TSPA-VA analyses (see Section 8.3.4). The FEHMN code was used to simulate 1-D SZ transport to generate the unit concentration breakthrough curves. The FEHMN code was also used to simulate groundwater flow and particle tracking in the TSPA 3-D SZ flow model to identify the hydrogeologic units within streamtubes downgradient of the repository. In addition, the FEHMN code was used to perform 1-D dual-porosity transport simulations for sensitivity



analyses. The POSTCON computer code was used to reformat output from the TSPA 1-D SZ transport model for storage as a library of simulated concentration breakthrough curves. The RIP code was used to draw the values of sampled parameters for use in the TSPA 1-D SZ transport modeling. The STATISTICA code was used to analyze the uncertainty distributions of various SZ parameters that were sampled in the probabilistic analysis. The MODFLOWP code was used to simulate groundwater flow in the USGS regional-scale flow model and perform parameter optimization for this model. Conclusions regarding the change in specific discharge in the SZ with climate change from the USGS regional-scale flow model were indirectly incorporated into the 1-D transport simulations for the TSPA-VA calculations. The PEST code, in combination with FEHMN, was used as the parameter optimization method for calibration of the USGS site-scale flow model. The GEOMESH code was used to generate the grid used in the USGS site-scale flow model. STRATAMODEL was used to construct the hydrogeologic framework model employed in both the USGS regional-scale flow model, the USGS site-scale flow model, and the TSPA 3-D SZ flow model. The ARC/INFO computer code is a database used for the visualization and organization of geographical information and was employed in construction of the USGS regional-scale flow model and the USGS site-scale flow model. The 3DADE code computes an analytical solution for solute transport and was used in sensitivity studies. The SGSIM and SISIMPDF computer codes perform geostatistical simulation and were used to generate stochastic fields of bulk permeability in the SZ for sensitivity studies.

## **8.2 SZ FLOW AND TRANSPORT CHARACTERIZATION**

Knowledge of the SZ groundwater flow system is incorporated into our conceptual models of flow and transport processes which forms the basis of numerical modeling of the SZ system. A regional-scale flow model, two site-scale flow models, and a transport model were developed and used for different purposes in the SZ analysis. Each model and the inter-relationships between the models is described in Table 8-5. Site knowledge about the flow and transport processes at Yucca Mountain was used to develop these models (Figure 8-2).

This section describes site data and the current understanding of flow and transport processes in the SZ at Yucca Mountain, the development of the flow models used for site characterization of the SZ system, and the conceptualization of the flow and transport system used to develop models used in the TSPA-VA SZ analyses.

### **8.2.1 Description of the SZ System**

Numerous observations and scientific studies have provided both regional-scale and near-site knowledge about the saturated zone groundwater system at Yucca Mountain. Understanding the regional flow system is necessary to understand the site-scale flow system at Yucca Mountain and simulation of regional groundwater flow provides information on boundary conditions for the USGS site-scale flow model (see Table 8-5). A detailed understanding of the site-scale flow and transport system of Yucca Mountain and nearby areas is important to construct a site-scale groundwater flow model which will be used to assess the performance of the potential repository. Understanding of the SZ groundwater flow system near Yucca Mountain is described at the regional scale, and the flow and transport system at Yucca Mountain is described at the site scale.

### 8.2.1.1 Regional Flow System

On a regional scale, the SZ flow system at Yucca Mountain is part of the Alkali Flat-Furnace Creek groundwater subbasin of the larger Death Valley groundwater flow system (Bedinger et al. 1989a; D'Agnese 1994), an area of about 47,000 km<sup>2</sup>. A detailed description of the hydrogeology of the regional flow system is discussed by D'Agnese et al. (1997a) and much of the following sections is taken from that report.

**Geologic Controls** - Regionally, groundwater flows through Quaternary, Tertiary, and Paleozoic aquifers through ten regional hydrogeologic units (D'Agnese et al. 1997a, p. 17-22). These units include Quaternary playa deposits, Quaternary-Tertiary valley fill, Quaternary-Tertiary lava flows, Tertiary volcanic rocks, Tertiary volcanic and volcanoclastic rocks, Tertiary-late Jurassic granitic rocks, Mesozoic sedimentary and metavolcanic rocks, Paleozoic carbonate rocks, Paleozoic-Precambrian clastic rocks, and Precambrian igneous and metamorphic rocks shown in the fence diagram depicted by Figure 8-3. The fence diagram shows east-west vertical slices connected by north-south vertical slices which correspond to traces of geologic cross-sections in the region (D'Agnese et al. 1997a, p.40). This geologic framework was used as the basis for the USGS regional-scale flow model (see Section 8.2.2). Groundwater flow in each of these units is controlled by the relative bulk permeability of the units, which is largely controlled by the degree of fracturing and faulting within the consolidated rocks. Most regional groundwater flow is through the Paleozoic carbonate rocks (Winograd and Thordarson, 1975, p. c-14) (unit B). To the east, the Paleozoic carbonate rocks are quite continuous, while to the west the regional flow is also affected by Quaternary (units Qp, Qtvf) deposits, Tertiary volcanic rocks (unit Tvs), and Paleozoic-Precambrian clastic rocks (unit P1) where the Paleozoic rocks are not as continuous.

Throughout the regional flow system, groundwater movement is controlled by extensive and prevalent structural features that result from regional faulting and fracturing. Such features include NE/SW trending structural zones of potentially high hydraulic conductivity, NW/SE trending faults of potentially low hydraulic conductivity, and anomalously linear surface-water drainage features (such as Fortymile Wash) that may represent buried structural features. D'Agnese et al. (1997a, p. 15) and Faunt (1997) provide a more detailed discussion of geologic controls on regional groundwater flow.

**Hydrologic Characterization** - Hydraulic conductivity of the hydrogeologic units in the region is highly variable, with estimates for individual units ranging over several orders of magnitude (D'Agnese et al. 1997a). The most permeable units generally are the Paleozoic carbonate rocks, the Quaternary-Tertiary valley fill, and the Tertiary volcanic rocks (Table 8-6). It should be noted that the very wide ranges in hydraulic conductivity within hydrogeologic units presented in Table 8-6 represents a variety of measurement methods at various scales and media variability over the entire region.

D'Agnese et al. (1997a, p. 60) present a regional potentiometric surface for the region, which is shown in Figure 8-5. Groundwater flows regionally from recharge areas at higher elevations in mountain ranges, most significantly, the Spring Mountains and Pahute, Mesa where there is more rainfall. Some water may enter the system as subsurface flow from Pahrnagat Valley on the northeast boundary of the basin (Winograd and Thordarson, 1975, p. 110-111) and from other basins to the north. Groundwater discharges at springs and through evapotranspiration at playas

(see Figure 8-4). Significant quantities of groundwater are also currently being discharged from the regional saturated-zone system by pumping in areas such as the Amargosa Valley. Death Valley is the ultimate natural groundwater discharge area and is a closed basin.

On the basis of the potentiometric data, three major subregional flow systems were identified by D'Agnese et al. (1997a, p. 62): the Northern Death Valley subregion, Central Death Valley subregion (which includes Yucca Mountain), and Southern Death Valley subregion (see Figure 8-6). Yucca Mountain is located within the Central Death Valley subregion. The Central Death Valley subregion, is further subdivided into three groundwater basins: the Pahute Mesa-Oasis Valley basin, Ash Meadows basin, and Alkali Flat-Furnace Creek basin (which includes Yucca Mountain). Groundwater in the Pahute Mesa-Oasis Valley basin is derived from infiltration in the Kawich and Belted Ranges and Pahute Mesa, and possibly from underflow from Railroad Valley and Stone Cabin Valley. Discharge in this basin occurs as evapotranspiration in Oasis Valley. Much of the groundwater in the Ash Meadows basin is derived from infiltration in the Spring Mountains to the east. Additional recharge may occur as regional groundwater flows across system boundaries from Sand Spring Valley (Waddell 1982) and Pahrangat Valley (Winograd and Thordarson, 1975, p. 110). Groundwater movement in this basin is influenced by the presence of major NE/SW trending structures, as evidenced by a significant NE trending trough in the potentiometric surface (located to the north of the Spring Mountains in Figure 8-5). This trough is bounded on the south by the Las Vegas Valley shear zone, which may contain low-permeability fault gouge (Winograd and Thordarson, 1975, p. 89-90). Significant quantities of groundwater discharge along a NW/SE trending fault at Ash Meadows. Some groundwater leaves the basin as underflow to the Alkali Flat-Furnace Creek basin. Groundwater in the Alkali Flat-Furnace Creek basin is also derived from infiltration on Pahute Mesa, Timber Mountain, Shoshone Mountains, and the Grapevine and Funeral Mountains. Discharge in this basin is to Alkali Flat (Franklin Lake Playa), as underflow to Death Valley, and as pumpage in the Amargosa Valley.

Because inflow and outflow are poorly defined for many areas in the region, the water budget for the groundwater flow system is difficult to determine. The large size of the region precludes a comprehensive and accurate assessment of all inflows and outflows. Uncertainties in the estimates are large, particularly for pumpage and evapotranspiration estimates for the Death Valley saltpan (D'Agnese et al. 1997a, pp. 2, 11, 69). Generalized water-budget components for the Death Valley flow system are listed in Table 8-7. As tabulated, estimated outflow exceeds estimated inflow by about 30,000 m<sup>3</sup>/d. This difference is probably due to uncertainties in the estimates and, potentially, changes in storage; however, the difference is less than 10 percent of the total estimated flux. Despite potentially large inaccuracies and uncertainties in the budget estimates, the budget permits a general characterization of the flow system.

**Hydrochemical Characterization** - Groundwater composition and isotopic studies can provide insight to the regional groundwater flow system. Hydrochemical data have been used to evaluate the relative contribution of various groundwater sources and pathways to the evolution of the regional flow paths. Groundwater chemistry and isotope data have been used to look at evidence for mixing and compartmentalization of flow domains.

Luckey et al. (1996, p. 42), and Cohen et al. (1997, p. 4.6) provide extensive overviews of previous hydrochemical characterization work which has been conducted in the Yucca Mountain

area beginning in 1971. Winograd and Thordarson (1975, p. 1), White (1979), and Claassen (1985) used hydrochemistry to better understand the flow systems in the Yucca Mountain area. Benson et al. (1983) described lateral variation in SZ water chemistry which they felt was consistent with fracture flow at Yucca Mountain. Chemical and isotopic data collected from boreholes and water supply wells were documented by Benson and McKinley (1985), Matuska and Hess (1989), and La Camera and Westenburg (1994). McKinley et al. (1991) compiled additional data for samples from more than 250 sites in the region. Thomas et al. (1991) compiled new and existing data for 209 sites in southern and eastern Nevada and southeastern California, which includes records of all of the chemical and isotopic data for each site available up to 1989. Meanwhile, regional SZ hydrochemical models were presented by Ogard and Kerrisk (1984), Kerrisk (1987), and Waddell et al. (1984). Stuckless et al. (1991) used stable isotope data to examine evidence of hydrochemical mixing. Peterman and Stuckless (1993, pp. 1559-1560) and Ludwig et al. (1993) discussed regional strontium and uranium isotope data, respectively, including some from Yucca Mountain boreholes and springs. Perfect et al. (1995) compiled data for more than 3000 sites in the area between latitudes 35° and 38° N and longitudes 115° and 118° W. Recently, rare earth data (Johannesson et al. 1997, p. 807) and conservative trace element data (Hodge et al. 1996) of regional discharge sites were used to distinguish between different regional flow pathways and sources. Kremer et al. (1996, pp. 95-102) used a multivariate statistical analysis to group Death Valley groundwaters based upon trace element concentrations in springs.

The available hydrochemical and isotopic data compliment the hydrologic data used to delineate the regional flow system. For example, strontium isotope ( $\delta^{87}\text{Sr}$ ) values measured in boreholes and springs increase from the Pahute Mesa in the north to the southern Amargosa Desert, where the largest values are found in the Amargosa Desert and where groundwater probably encounters alluvial basin fill derived from Precambrian rocks (Peterman and Stuckless, 1993, p.1564). As shown in Figure 8-6, there is a southerly component to the regional groundwater flow system in the Alkali Flat Furnace Creek Groundwater Basin consistent with the increasing isotopic ratios to the south. Another example is the boundary between the Ash Meadows and Alkali Flat groundwater basins. This groundwater basin boundary is fairly similar to the boundary delineated by Winograd and Thordarson (1975, p. 75) based upon different hydrochemical groundwater types.

Previous hydrochemical studies suggested that groundwaters from the central and northwestern Amargosa Desert were a potential source of groundwater to the Furnace Creek Springs in Death Valley (Winograd and Thordarson, 1975, p. 95). However, based upon rare earth element data, Johannesson et al. (1997, p. 807) proposed that the origin of groundwater discharging at the Furnace Creek springs in Death Valley seems to be characteristic of the lower Paleozoic carbonate aquifer beneath Ash Meadows. Dissolved concentrations of rare earth elements are similar between, springs of Ash Meadows and the Furnace Creek, while concentrations in the Amargosa Desert groundwater are lower than both Ash Meadows and Furnace Creek. Thus, discharge from springs in Ash Meadows likely share a common groundwater pathway with the discharge from the Furnace Creek Springs in Death Valley, whereas the contribution of shallow groundwaters from the Amargosa Desert to the Furnace Creek Springs may be minor (Johannesson et al. 1997, pp. 807 and 817). These data support the groundwater transfer from the Ash Meadows Groundwater Basin to the Alkali Flat-Furnace Creek Groundwater Basin in

the southern Amargosa Desert included in the regional groundwater flow system depicted in Figure 8-6.

#### 8.2.1.2 Site Flow System

The site flow system near Yucca Mountain refers to a 1,350 km<sup>2</sup> rectangle (45 km long by 30 km wide), approximately centered on Yucca Mountain. Detailed discussions of the hydrogeology at the site-scale of the Yucca Mountain area are presented by Luckey et al. (1996), and much of the following discussion is taken from this report.

**Geologic Controls** - At the site scale, the rocks in the vicinity of Yucca Mountain were classified into sixteen hydrogeologic units for the purposes of site-scale groundwater flow modeling, primarily based on hydraulic flow properties (Table 8-8). Where possible, hydrogeologic units identified by previous investigators (Luckey et al. 1996; pp. 17-19, Winograd and Thordarson, 1975) were the basis for the USGS site-scale flow model framework. The hydrogeologic units form a series of alternating, but interconnected, volcanic aquifers and confining units overlying the regional carbonate aquifer (Figure 8-7). The volcanic aquifers and confining units interbed with undifferentiated valley-fill and the valley-fill aquifer to the south and structural features delimit the eastern and western edges of Yucca Mountain. Groundwater flow in each of these units is controlled by the relative bulk permeability of the units, which is largely controlled by the degree of fracturing and faulting within the consolidated rocks. Within the tuffs, the degree of welding also influences the bulk permeability, with highly fractured, welded units generally being more permeable than relatively unfractured, non-welded units.

Geologic structures that may influence groundwater flow at Yucca Mountain include normal faults, strike-slip faults, and volcano-tectonic structures (Scott et al. 1983, p. 297). The geometry of the normal faults and strike-slip faults controls much of the topography and drainage patterns at Yucca Mountain (Luckey et al. 1996, p.12). The normal faults generally are oriented north-south, and dip steeply to the west. (A map of the major faults identified by surface mapping is shown in Figure 8-46 in section 8.5.2.2.4.) Displacements on the faults range from less than 1 m to more than 300 m on the Solitario Canyon Fault (Carr, 1984, fig. 30). The Solitario Canyon Fault is believed to be a barrier to east-west groundwater flow, and controls the moderate-hydraulic gradient on the west side of Yucca Mountain (Luckey et al. 1996, p. 25). An east-west trending low permeability zone or a buried graben may be present to the north of Yucca Mountain and may control the large-hydraulic gradient (Fridrich et al. 1994). Yucca Wash is a feature inferred from geologic mapping at the surface, thought to affect the groundwater flow field (Altman et al. 1996, p.139 – 141). Fortymile Wash is an anonymously linear drainage feature that may be a buried structure (Faunt, 1997, p.34). Other north-south trending normal faults have been suggested to provide a zone of enhanced hydraulic conductivity in the vicinity of the C-hole complex, which is located 2 ½ km to the southeast of the potential repository (Geldon et al. 1997, p. H-25). The rock units at Yucca Mountain dip to the east-southeast at about 5 degrees, which partially controls which units are saturated and which lie above the present water table. The effects of these geologic structures on the groundwater flow field were taken into consideration when developing the USGS site-scale flow model and the TSPA 3-D SZ flow model through the incorporation of the hydrogeologic framework model and inclusion of some faults as low-permeability zones.

**Hydrologic Characterization** - The aquifer in volcanic rocks has been hydraulically tested at many of the wells near the Yucca Mountain site. Most of the available data are from single-well tests using constant discharge, fluid injection, pressure injection, and radioactive tracer methods. Estimates of hydraulic conductivity, or the rate at which water can move through a permeable medium, in the fractured volcanic rocks of the saturated zone based on the single-well test results generally range over three orders of magnitude, depending on the depth and the particular hydrogeologic unit. In general, the most permeable units are the carbonate units, the upper and lower volcanic aquifers, and the valley-fill aquifer (Table 8-8). The apparent hydraulic conductivity values determined from multiple-well hydraulic tests at the C-hole complex tend to be much higher, by about two orders of magnitude, than the values from single-well tests for the same intervals (Geldon, 1996, p. 59). Multiple-well hydraulic tests generally yield results that are more representative of large-scale hydraulic conductivity of the aquifer, suggesting that the single-well tests elsewhere at the site may have significantly underestimated the effective hydraulic conductivity (and thus the groundwater flow velocity) at those locations. Surveys of flow in the deeper wells in the saturated zone near Yucca Mountain indicate that groundwater production in most of the wells occurred in a few discrete intervals within the volcanic units (Luckey et al. 1996, p. 38 Figure 15). For performance assessment calculations, these results suggest that most groundwater flow in the fractured volcanic units is through only a small fraction of the saturated thickness.

Faults can act as either preferential conduits or barriers to flow, depending on how the hydrogeologic units are juxtaposed and if those units are more or less permeable than the aquifer. If a fault zone is more permeable than the surrounding aquifers, circulation between two otherwise isolated aquifers can be enhanced, while if the fault zone materials are less permeable than the surrounding rocks then the flow of water will be impeded (Faunt, 1997, p.30). There are not many measurements of fault permeabilities in the Yucca Mountain area. Variability in tidal response in the volcanic and Paleozoic carbonate aquifers at well UE-25 p#1 was analyzed to constrain the possible values of hydraulic conductivity in faults intersecting aquifers at Yucca Mountain (Bredehoeft, 1997, p. 2460). Bredehoeft studied the Fran Ridge Fault and found an upper bound for the fault zone hydraulic conductivity to be on the order of  $10^{-6}$  m/s, slightly higher than the hydraulic conductivity of the overlying tuff aquifer (Bredehoeft, 1997, p. 2463). Based on the results of multi-well aquifer test results, the hydraulic conductivity of the middle volcanic aquifer in the C-holes complex is believed to be structurally controlled (Geldon et al. 1997, p. 40). There seems to be a local high-permeability zone in the C-hole complex vicinity (Geldon et al. 1997, Figure 36). The effects of large-scale permeability variations on the groundwater flow system related to repository performance is discussed in the sensitivity analysis in Section 8.5.2.2.

Variations in water table elevations have been directly monitored for a few decades and inferred on the time scale of 100,000s of years from geological and geochemical data. Water level fluctuations in most wells have been small, on the order of a few decimeters, primarily in response to barometric variations and earth tides (Graves et al. 1997, p.1). Highly transient and longer-term variations in hydraulic head of a few meters to a few decimeters have been observed following earthquakes (Graves et al. 1997, p.59-60). Historical variations have probably been greatest in the Amargosa Valley area because of pumping. Significantly higher water table elevations (80 to 120 m higher than current elevations) at Yucca Mountain have been inferred from the locations of nearby paleospring deposits and from geochemical and mineralogical

evidence from the unsaturated zone at the site (Levy, 1991; Marshall et al. 1993). Higher water table elevations in the geologic past were apparently associated with wetter climatic conditions. From the perspective of performance assessment calculations, fluctuations of this magnitude in water table elevations suggest potentially significant alteration of radionuclide transport pathways in the unsaturated zone on geologic time scales.

Three areas of similar potentiometric gradients have been described at Yucca Mountain (Luckey et al. 1996, pp. 21-27). Measurements of water levels in wells indicate that north of the site there is a region of large hydraulic gradient, potentially 150 m/km (Luckey et al. 1996, p. 21). The cause of the large hydraulic gradient is not known; however, recent results of the saturated zone Expert Elicitation (see Section 8.2.3.2) favor one of two hypotheses: 1) the gradient truly represents the water table, which is held high due to low bulk permeability rocks or some similar barrier, or 2) the gradient is only apparent, that is the high water levels reflect perched water in wells north of Yucca Mountain (CRWMS M&O, 1998, p. 3-6). West of the crest of Yucca Mountain is a region of moderate hydraulic gradient, corresponding to a 45-m increase in water table elevation over a maximum horizontal distance of about 1,000 m (Luckey et al. 1996, p. 25). The water levels in this area are probably controlled by the Solitario Canyon Fault, which acts as a barrier to west-east groundwater flow. Water level data indicate a small horizontal hydraulic gradient (0.1 to 0.3 m/km) immediately southeast of the site (Luckey et al. 1996, p. 26). Ervin et al. (1994, p. 9) state that the small gradient area could result from either groundwater flow through highly transmissive rocks or small groundwater flux or both.

Vertical hydraulic gradients could have an important impact on groundwater movement at the site. Limited information concerning vertical potentiometric gradients is available at 10 sites in the vicinity of Yucca Mountain. Potentiometric levels at Yucca Mountain generally are higher in the lower intervals of the volcanic rocks and in the Paleozoic carbonate rocks, indicating a potential for upward flow (Luckey et al. 1996, pp. 27-28). Potentiometric levels in the carbonates at well UE-25 p#1 are about 21 m higher than levels in the volcanic rocks (Craig and Johnson, 1984, p. 12).

Groundwater flow within the site model area generally is from the north and northwest to the south. Water-level data are very sparse north of Yucca Mountain; thus, the true configuration of the potentiometric surface and direction of groundwater flow from the north are somewhat uncertain. Potentiometric data at Yucca Mountain indicates that groundwater flows from the mountain to the east-southeast, and then to the south near Fortymile Wash (Tucci and Burkhardt, 1995) toward the Amargosa Desert.

Recharge to the site-scale groundwater system in the Yucca Mountain area is believed to occur from: 1) downward and possible lateral recharge from episodic flooding of Fortymile Wash, 2) throughflow resulting from recharge at Pahute and Rainier Mesas, 3) throughflow from the northwestern part of the Amargosa Desert, 4) minor recharge from episodic flooding of the Amargosa River channel, and 5) net infiltration from precipitation events (Czarnecki et al. 1998). Recharge from episodic flooding of Fortymile Wash and throughflow from Pahute and Rainier Mesas is thought to be the dominant source of groundwater flux to the Yucca Mountain area (Czarnecki et al. 1998). Recharge from net infiltration, although relatively small, may play a role in the distribution of heads at Yucca Mountain. No natural discharge from the groundwater system occurs within the USGS site-scale flow model domain. A summary of estimated inflow

and outflow at lateral boundaries, largely based on results of USGS regional-scale flow modeling (D'Agnese et al. 1997a, pp. 2, 69 and 71) for the site-model area is presented in Table 8-9. There is a large degree of uncertainty in the estimates, and any inaccuracies inherent in the regional-flow model are carried through to these estimates. Nearly all of the inflow to the site-model area is by groundwater inflow through the volcanic rocks along the northern, eastern, and western model boundaries. Recharge from precipitation at Yucca Mountain is believed to be small in relation to the boundary inflow (Czarnecki et al. 1998).

Variations in temperature and heat flow measured in boreholes in the saturated zone suggest significant redistribution of heat by vertical groundwater movement in some areas. Different assumptions of average groundwater temperature (20 degrees C and 44 degrees C) have an appreciable effect on viscosity (1.002 centipoise for fresh water at 20 degrees C; 0.6067 centipoise for fresh water at 44 degrees C), which affects groundwater flow calculations. There are linear zones of elevated temperature at the water table to the south of the large gradient (Sass et al. 1988, pp. 31-49) which coincide with the positions of the major north-trending normal fault zones. According to Fridrich et al. (1994, 154-157), Szymanski (1989, p. 3-13 to 3-50) suggests that the hydrostructural fault zones form pathways for upwelling water under Yucca Mountain, and Szymanski invoked a convective origin for the thermal highs. Fridrich et al. (1994, pp. 154-157) agree that the thermal highs probably partly result from upward transport of heat by groundwater flow but they feel the upward groundwater flow is driven by pressure rather than by thermal buoyancy. The tuff aquifer is not thick enough to create observed temperature differences. Hence, upwelling from the deep carbonate aquifer is probably indicated, at least along the Solitario Canyon fault zone (Fridrich et al. 1994, p. 157). Unsaturated-zone processes may also contribute to the ambient groundwater temperature profiles in the area (i.e., evaporative cooling from wind-driven air circulation through the thick unsaturated zones). The temperature profiles provide evidence of interaction between the upper tuff aquifer and the underlying carbonate aquifer. The effects of heat in the groundwater flow system were not accounted for in the base-case analysis, because these effects are assumed to be secondary relative to the effects of other processes (see Section 8.2.3.4).

**Hydrochemical Characterization** - As stated above (Section 8.2.1.1), a significant amount of hydrochemical and isotopic data have been collected in the Yucca Mountain area. Although the previously discussed studies mainly focus on the regional scale, some insights about the site-scale groundwater flow system can be obtained from these studies.

Interaction between the deep carbonate and tuff aquifers beneath Yucca Mountain could be inferred from isotopic data. Stuckless et al. (1991) used the systematic relationship of the  $^{13}\text{C}/^{12}\text{C}$  ratio to the  $\delta^{14}\text{C}$  of the groundwater to suggest that water from at least three sources is mixing in the area beneath Yucca Mountain from: 1) lateral flow from the tuff aquifer to the north where there is long residence time in the tuffs, 2) local recharge probably introduced from flash-flood surface water zones such as Fortymile Wash, and 3) water upwelling from the deep carbonate aquifer into the tuff aquifer south of the large hydraulic gradient. The generally southward increase in  $\delta^{13}\text{C}$  in the tuff aquifer can be interpreted as indication of a southward-increasing contribution from the deep carbonate aquifer (Fridrich et al. 1994, p. 157-160). However, according to Luckey et al. (1996, p. 43), the presence of these three end-member waters is not supported by groundwater flow that can be inferred from potentiometric data, nor



do similar mixing calculations using nonreactive ionic concentrations or hydrogen- or oxygen-isotopic ratios provide support for these three end members.

The chemical characteristics of groundwater in the Yucca Mountain area have evolved mainly from rock/water interactions. Groundwater composition is a function of the chemistry of recharge water and the materials with which it interacts along its travel path. Studies by Benson and McKinley (1985, p. 2), Matuska (1989), and Thomas et al. (1991) indicate the water in the volcanic aquifers and confining units is a relatively dilute sodium bicarbonate type that would be expected to evolve in a volcanic geohydrologic system (Jones, 1966, pp. 193-194).

The calcium to sodium ratio data of Benson and McKinley (1985, p.5) and Matuska (1989) in the water in the Yucca Mountain vicinity increase by an order of magnitude from west to east with the lowest values measured west of and near the Solitario Canyon Fault (Luckey et al. 1996, p. 44). Waters that have evolved over the longest periods of time, by reaction with glassy tuffs, would have the greatest sodium concentrations (White et al. 1980, pp. 10-12). Thus, the small calcium to sodium ratio to the west of Yucca Mountain suggests that the groundwater has chemically evolved more to the west than to the east. This could be due to the combined effect of the Solitario Canyon Fault acting as a barrier to horizontal flow from the west, less-evolved water from the Fortymile Wash vicinity mixing with more-evolved water moving from the west, or a contribution of water from the underlying Paleozoic aquifer to the volcanic system through faults on the east side of Yucca Mountain without substantial upwelling of deeper water through Solitario Canyon Fault (Luckey et al. 1996, p. 44). According to  $^{14}\text{C}$  age data, oldest waters exist beneath the crest of Yucca Mountain and the youngest waters are found beneath Fortymile Wash (Benson and McKinley, 1985, p.14).

**Solute Transport Characterization** - Robinson (1994, pp.86-94) suggested that transport in the vicinity of Yucca Mountain behaves as a dual-porosity system, where matrix permeability is negligible compared to fracture permeability, and the majority of the flow occurs through the fractures. Tracer tests conducted by Los Alamos National Laboratory (LANL) at the C-well complex support the assumption that transport through the volcanic units can be described by a dual-porosity model (CRWMS M&O, 1997).

Geldon et al. (1997, p. TT-1) describe three long-term, forced-gradient, cross-hole tracer tests conducted by the USGS from February 1996 through the present. For each test, one tracer (iodide, 2,6 difluorobenzoic acid [DFBA], or pyridone) was injected into a well while a nearby well was pumped and the solute recovery curve through time was measured. Geldon et al. (1997, pp. TT8 and TT9) used the Moench (1989) dual-porosity analytical solution coupled to a parameter estimation method to analyze the data. The method assumed steady-state, radial 2-D flow conditions through homogeneous, isotropic media. Longitudinal dispersivity, flow porosity, and matrix porosity were estimated for the Bullfrog and Tram tuff intervals (middle volcanic aquifer). If fractures are considered to be the only flow pathway, then the resulting flow porosity values (0.072 to 0.099) are high (typical maximum fracture porosity values are on the order of 0.001). These tracer test results suggest that the fracture network between the C-holes is not well-connected and the actual tracer flow path is a combination of movement through the fractures and the matrix, a result which is not strictly consistent with the dual-porosity conceptual model. However, there is uncertainty in the inferences regarding effective porosity from these tracer tests. In addition, the initial tracer testing in the C-holes was conducted in

high-permeability stratigraphic intervals, which may or may not be representative of the volcanic medium as a whole.

In a different investigation at the C-hole complex, a forced-gradient, cross-hole tracer test involving simultaneous injection of four tracers having different physical and chemical properties (Poly-fluoro Benzoic Acid [PFBA], bromide, lithium, and polystyrene microspheres) was conducted by LANL researchers (CRWMS M&O, 1997). Interpretation of these tracer tests at the C-holes indicates that the transport system can be assumed to behave as a dual-porosity system, where advection is important in the fractures and diffusion occurs into the matrix (CRWMS M&O, 1997). For the TSPA-VA analyses, these tracer test results support matrix diffusion in fractured volcanic units.

Although water flow in the volcanic units below the water table is expected to occur predominantly in fractures, most of the actual water volume in the system is contained in the highly porous tuff matrix, where it is essentially stagnant (Robinson, 1994, p.77). Radionuclide transport is, therefore, expected to be attenuated by diffusive mass transfer between the flowing water in the fractures and the stagnant water in the matrix, a process known as matrix diffusion (Grisak and Pickens 1980). Although matrix diffusion has been discussed and modeled by several investigators (Neretnieks, 1980; Tang et al. 1981), there are limited laboratory data available about the diffusion properties of various radionuclides at Yucca Mountain. Triay et al. (1997, pp. 139-158) discuss some laboratory experiments where a radionuclide solution is placed inside a rock beaker and the decrease in radionuclide concentration through time is measured to gain information about diffusion (Triay et al. 1997, p.9). Diffusion is not a direct input parameter requirement for the base case, which used the effective porosity approach, but it is included in the sensitivity study of dual-porosity transport (Section 8.5.2.3).

Sorption of radionuclides onto rock material is a result of a chemical reaction between the radionuclide in the groundwater and the minerals in the rock. Sorption could occur along fractures or within the matrix if diffusion has occurred. From a mineralogical viewpoint, the volcanic stratigraphy at Yucca Mountain has been divided into three different rock types: devitrified, vitric, and zeolitic. Geochemical properties of the tuffs have been extensively studied. Triay et al. (1997) summarized data from laboratory batch sorption experiments which provide insight to the sorption properties of the tuffs at Yucca Mountain for each of these rock types. Statistical analyses were performed by (Triay et al. 1997) using their sorption data sets and they recommended sorption coefficients for input to the TSPA-VA calculations. CRWMS M&O (1997, p.19) found good agreement between laboratory-derived sorption parameters for lithium compared to the field-derived sorption parameters in the C-wells vicinity, a finding which lends credence to using laboratory-derived sorption parameters to predict transport at a field scale. Although sorption of radionuclides in alluvium is potentially significant to repository performance at a distance of 20 km, no site-specific data are available for mineralogy or sorptive properties of alluvium.

**Colloid Transport Characterization** - Colloids have been found in the groundwaters near Yucca Mountain (Ogard, 1987, p. 117) where colloid transport is most likely to occur through fractures (Tsang and Mangold, 1984, p. 42-43). However, there are large uncertainties related to colloid transport processes. Previous investigators concluded that radionuclides in colloidal form can be transported faster than in dissolved form (Apps et al. 1983; p.70-71, Champ et al. 1982,

p.745-754), causing predicted migration over time scales much smaller than those for models that do not account for colloids. On the other hand, colloids could be retarded by filtration in the porous matrix. Lower recovery of microspheres, a uniformly sized surrogate colloid with a neutral surface charge, suggests significant filtration over the 30-m transport distance in the tracer tests conducted by LANL (CRWMS M&O, 1997). Triay et al. (1997, pp. 173-186) performed laboratory tests to gain insight about colloid stabilities and concentrations which would be expected in Yucca Mountain waters. Measurements of groundwater from well J-13 (approximately 7 km southeast of Yucca Mountain) produced estimates of natural colloid concentrations and colloid size distributions. Laboratory experiments estimated particle aggregation rate constants for silica and kaolinite clay particles as functions of groundwater chemistry, but cannot be used to draw definitive conclusions regarding colloid stability in the SZ.

Groundwater sampling from fractured volcanic tuff in the saturated zone near the Benham underground nuclear test site on Pahute Mesa suggests that colloid-facilitated transport of plutonium in the saturated zone may be relatively rapid. Low concentrations of plutonium, associated with colloidal material in groundwater samples, indicate transport in the saturated zone of at least 1300 m in 28 years. For the TSPA-VA, this observation is used to develop an alternative conceptual model for colloid-facilitated transport of plutonium (see Section 8.5.2.5).

## **8.2.2 Site Characterization Models**

The USGS developed a regional-scale flow model (D'Agnese et al. 1997a) and a site-scale flow model (Czarnecki et al. 1998) for the purpose of better characterizing the SZ flow system at Yucca Mountain. This section describes the two models with an emphasis on their applicability to the TSPA-VA SZ analysis.

### **8.2.2.1 USGS Regional-Scale Flow Model**

A regional-scale three-dimensional numerical groundwater flow model was developed by D'Agnese et al. (1997a, pp. 59-84) to characterize the conditions of the present day groundwater flow system in the Death Valley groundwater flow system (see Table 8-5). Their numerical model was based upon a three-dimensional digital hydrogeologic framework model which described the geometry, composition, and hydraulic properties of the material that control the regional groundwater flow system (D'Agnese et al. 1997a, p.1). The numerical model was also used to evaluate the effects of increased precipitation on the regional groundwater flux rate (e-mail, Pat Tucci, USGS, 12/11/97; D'Agnese et al. 1997b).

From the perspective of the TSPA-VA effort, the most important output from the USGS regional-scale numerical modeling was information to determine a groundwater flux multiplier for the long-term average and super-pluvial climate conditions assumed for the base-case TSPA-VA analysis. The groundwater flux multipliers were used to calculate a groundwater flux for each of the climate states relative to present day conditions which is required as input to the TSPA 1-D SZ transport model (see Section 8.3.3). The USGS regional-scale flow model groundwater fluxes for present day conditions were also used as a consistency check for simulated groundwater flux from the USGS site-scale flow model (Table 8-5).

The numerical code used for the regional flow model was MODFLOWP (Hill 1992). MODFLOWP is an adaptation of the U.S. Geological Survey 3-D, finite-difference modular groundwater flow model, MODFLOW (McDonald and Harbaugh, 1988; Hill 1992) in which nonlinear regression is used to estimate flow-model parameters that result in the best fit to measured hydraulic heads and flows (Cooley and Naff 1990, 232). MODFLOWP (Hill 1992) was used to create a finite-difference model consisting of 163 rows, 153 columns, and three layers for the USGS regional-scale flow model. The grid cells were oriented north-south and were of uniform size, with side dimensions of 1,500 m (Figure 8-8). The layers represented conditions at 0-500 m, 500-1,250 m, and 1,250-2,750 m below the estimated water table. The first and second layers were designed to simulate local and sub regional flow paths mostly within valley-fill alluvium, volcanic rocks, and shallow, carbonate rocks. The third (lowest) layer simulates deep regional flow paths in the volcanic, carbonate, and clastic rocks.

The required regional model parameter values were supplied by discretization of the 3-D hydrogeologic framework model (Faunt 1994) and by digital representations of the remaining conceptual model components (Figure 8-3). The 3-D simulation supported the analysis of interactions between the relatively shallow local and sub regional flow paths and the deeper dominant regional flow paths controlled by the carbonate aquifer.

Similar lateral boundary conditions were imposed on all three layers of the model. All boundaries in the top layer were designated as no-flow except along the western side of the model in Death Valley where constant-head values were selected. No groundwater is believed to enter or exit the Death Valley system at intermediate depths, so all the boundaries in the middle layer were set to no-flow conditions (D'Agnese et al. 1997a, p. 59-69). In layer three, the boundaries were set to no-flow conditions except at four locations along the northern and eastern limits of the model, where the conceptual model suggests interconnections with adjacent systems along buried zones of higher bulk permeability (Faunt 1997, p. 12-13). The upper boundary of the flow model is the water table, and the lower boundary is set at a depth of 2,750 m below the water table, where few fractures are believed to be open to allow significant amounts of groundwater flow (D'Agnese et al. 1997a, p. 59). Vertical conductance between layers in the USGS regional-scale flow model was determined by the values of hydraulic conductivity in adjacent layers at each location.

Model source and sink parameters defining recharge, ET (evapotranspiration), spring-flow discharge, and groundwater pumpage were obtained from the digital geographical information system (GIS) data base. ET estimates were developed from land-surface altitudes, and maximum ET rate maps created within the GIS (Figure 8-9). A recharge-potential map was reclassified to produce a recharge array that contained six zones which range from no recharge potential to high recharge potential (Figure 8-10). For each zone, a parameter could be assigned to represent the percentage of precipitation that infiltrates, and a second array was used to define the variation expected in the recharge rates. Spring discharge rates were obtained from historical records as described by D'Agnese et al. (1997a, p. 86-95). Springs were specified using the general-head boundary package (McDonald and Harbaugh 1988). This required information defining the altitude of the spring orifice and conductance. Because the conductance values were poorly known, springs were grouped by geographic location and a single conductance value was assigned to each group (D'Agnese et al. 1997a). Pumping was simulated using the well package (McDonald and Harbaugh 1988), and all pumping wells were assigned to the first (uppermost)

layer (see D'Agnese et al. 1997a, p. 84-86). Return flows were accounted for by specifying percentages of pumped water that is permanently removed from the system.

Calibration of the regional model using the techniques available in MODFLOWP allowed for estimation of a series of parameters that provide a best fit to observed hydraulic heads (500 observations) and flows (63 observations) (Figure 8-11). Numerous conceptual models were evaluated during calibration to test the validity of various interpretations about the flow system. Conceptual model evaluations focused on testing hypotheses concerning: 1) the location and type of flow system boundaries, 2) the extent and location of recharge areas, and 3) the configuration of hydrogeologic framework features. For each hypothesis tested, a new set of parameters was estimated using MODFLOWP and the resulting new simulated heads and flows were compared to observed values. Only those conceptual model changes contributing to a significant improvement in model fit, as indicated by a reduction in the sum of squared errors, were retained in the final optimized model.

The final model was evaluated to assess the accuracy of simulated results. Model results suggest that even with the limited understanding of fluxes in and out of the regional groundwater flow system, overall budgets are within the expected ranges for the flow system. Because specified-flux boundary conditions were used in the flow model, the optimized model solution is considered to be relatively unique, within the constraints of the conceptual assumptions. The model generally reflected the upward gradient observed at Yucca Mountain; however, within the overall site-model area, the regional model indicated a net downward flow of water to the lowermost layer of the regional model (D'Agnese et al. 1997a).

Problems with the USGS regional-scale flow model are indicated by weighted residuals that are not entirely spatially random, indicating some model inaccuracies. This is related to the occurrence of large, positive, weighted residuals for hydraulic heads, where simulated hydraulic heads are distinctly lower than the observed values, and large, negative, weighted residuals for spring flows, where simulated flows are distinctly less than observed flows. The problem is also related to non-normally distributed, less, extreme, weighted residuals. These results, suggest that additional calibration may significantly improve model accuracy. This analysis suggests that the model is a reasonable representation of the physical system, but evidence of model inaccuracies exists. Inaccuracies in the simulated groundwater fluxes in the flow model are generally proportional to uncertainty in the overall groundwater budget of the region. The model continues to undergo development for future use by the Yucca Mountain Project and the Environmental Restoration Program at the Nevada Test Site.

**Climate Change Modeling** - To assess the effects of climate change at the regional-scale, two simulations were made with the regional groundwater flow model (e-mail, Pat Tucci, USGS, 12/11/97; D'Agnese et al. 1997b). Results from these simulations were used to determine the groundwater flux multiplier for different climate conditions assumed in the TSPA-VA SZ base-case analyses (see Table 8-5). First, as a reasonableness check, a simulation based on past climatic conditions (21,000 years ago, under full glacial conditions) was evaluated by comparing the results of the simulation to observations of paleodischarge sites. Climate changes were simulated with the regional groundwater flow model primarily by changing the distribution and rates of groundwater recharge. Another simulation was conducted to represent a 3-fold increase in rainfall at Yucca Mountain.

Average annual precipitation maps for past-climate conditions were developed and were resampled to the model grid resolution (D'Agnese et al. 1997b). A polynomial function representing the Maxey-Eakin area-altitude relationship was then used to estimate recharge rates and distributions from precipitation for conditions as explained by D'Agnese et al. (1997b). Increased recharge for a tripling of present-day rainfall at Yucca Mountain was assumed to be a simple linear increase over the recharge estimate for past-climate conditions.

Results of climate-change simulations were evaluated through analysis of simulated discharge areas, water level changes, potentiometric surface configurations, and water budgets. During past-climate conditions, recharge increased in most areas to produce a significantly different regional groundwater flow system. Wetter past-climate conditions (i.e., pluvial) provided enough groundwater in the system to maintain paleolake levels in the northern parts of the model domain and at Lake Manley in Death Valley (D'Agnese et al. 1997b). Groundwater discharge occurred at most of the observed paleodischarge sites (Figure 8-12, lower arrow), which indicated that the recharge distribution used in the simulation generally was valid. Large hydraulic gradients in the region were preserved and enhanced under simulated past-climate conditions. Simulated recharge over the region increased by a factor of about five relative to present-day recharge.

Under past-climate conditions (i.e., 21,000 years ago), rainfall at Yucca Mountain was assumed to be about 1.7 times present-day rainfall. Simulated groundwater flux in the SZ beneath Yucca Mountain increased by about 4 times over present-day simulated flux (D'Agnese et al. 1997b). This flux was used as the groundwater flux multiplier for long-term average climate conditions for TSPA 1-D SZ transport modeling.

Analysis of a 3-fold increase (over present conditions) in rainfall at Yucca Mountain was limited in scope to the hydrologic impacts in the immediate vicinity of Yucca Mountain. Recharge at Yucca Mountain was assumed to increase by 1.76 times the recharge rate for past-climate conditions, based on the modified Maxey-Eakin method. The simulated groundwater flux beneath the repository increased by about 6 times the present-day simulated flux (e-mail from Pat Tucci, USGS, 12/11/97; D'Agnese et al. 1997b). This flux was used as the groundwater flux multiplier for superpluvial climate conditions for TSPA 1-D SZ transport modeling.

The limitations to evaluating the effects of climate change on a regional groundwater flow system using numerical modeling are substantial. Therefore, the simulated effects of climate change should be considered conceptual in nature, and only used to describe potential relative impacts to the regional groundwater flow system. Specifically, for the TSPA-VA, these results were used to provide an estimate of the groundwater flux multiplier for different climate conditions. In an approximate sense, inaccuracies in the SZ groundwater flux multiplier derived from the climate change modeling are proportional to inaccuracies in the assumed recharge under alternative climatic conditions.

#### **8.2.2.2 USGS Site-Scale Flow Model**

The USGS developed a 3-D site-scale groundwater flow model for Yucca Mountain for the purpose of site characterization (Czarnecki et al. 1998). In particular, the model was developed to: 1) estimate groundwater flow direction and magnitude from beneath the design repository

area to the accessible environment, 2) characterize the complex three-dimensional behavior of flow through heterogeneous media, 3) provide a means to account for the distribution of groundwater temperature measured within wells within the model area, 4) identify the potential role of faults as barriers or conduits to groundwater flow, and 5) provide a model of the flow system for subsequent flow, heat, and radionuclide-transport modeling. Results from simulations using this model do not directly affect the TSPA-VA SZ analysis because the USGS site-scale flow model was only used for site characterization.

The USGS 3-D flow model covers an area of approximately 1,350 km<sup>2</sup> over a saturated thickness of about 1.5 km (Figure 8-13 and Figure 8-14), delimited by a rectangular box 45 km long and 30 km wide. Development of the model began with the construction of a digital hydrogeologic framework model that was sampled at a plan-view spacing of 1,500 m by 1,500 m with variable thickness (Figure 8-14). This sampling resulted in a gridded data set which was used as input data for the automated generation of a fully 3-D tetrahedral finite-element mesh consisting of 9,279 nodes and 51,461 tetrahedral elements representing 16 different hydrogeologic units. Most faults are represented within the framework model only as offsets of geologic units, not as distinct hydrologic features.

The USGS site-scale flow model was developed using FEHMN (Zyvoloski et al. 1995), a finite-element/finite-volume flow and transport code. The parameter estimation component of the model was achieved through the use of the model independent parameter-estimation software, PEST (Watermark Computing 1994). PEST was used to run FEHMN and to vary user-specified model parameters prior to each run such that the weighted sum of the differences between observed and simulated values of pressure, hydraulic head, or temperature was minimized using nonlinear regression.

Note that the assumptions related to development of the USGS site-scale flow model do not have direct impact on the TSPA-VA SZ results because the USGS model was used for site characterization purposes only. However, many of the same assumptions are inherent in the TSPA 3-D SZ flow model (see Sections 8.3.2 and 8.3.6). The conceptual model represented within the USGS site-scale flow model assumes constant head boundaries along all four boundaries. Constant-head values for the lateral boundaries were obtained from existing potentiometric maps of the area consistent with the USGS regional-scale flow model. No flow was assumed through the bottom of the model. The large-hydraulic gradient area was assumed to be part of the saturated zone, rather than perched water occurrence, and is assumed to be caused by a buried low-permeability fault represented in the model as a low-permeability zone. The moderate-hydraulic gradient area to the west of Yucca Mountain was also assumed to result from a low-permeability fault (Solitario Canyon Fault) (see Figure 8-15).

The water table forms the upper boundary of the flow model. The only recharge applied to this boundary was simulated at upper Fortymile Wash located northeast of Yucca Mountain (Figure 8-15). The recharge rate assigned to these nodes was estimated by PEST during model calibration. Recharge from infiltration of rainfall was not directly applied to Yucca Mountain because the relative amount of such infiltration is believed to be small in relation to groundwater inflow along the lateral boundaries of the model. Pumpage, known to occur south of Yucca Mountain, was not included in this simulation. The model used an automated parameter estimation routine to minimize the difference between 94 observation of hydraulic head and

those simulated by the flow simulator by adjusting selected bulk permeability and flux parameters (Figure 8-16). Because specified-head lateral boundary conditions were used in the flow model, the resulting optimal calibration was relatively non-unique (i.e., approximately the same calibration could be achieved by proportionally scaling bulk permeability values in the model).

Other assumptions that were used in the USGS site-scale flow model are : 1) bulk permeability is uniform within each hydrogeologic unit, 2) the flow system is at steady state, 3) groundwater flow occurs within both the rock matrix and fractures as a single continuum, 4) the volumes associated with the finite-element mesh are sufficiently large so as to exceed the representative elementary volume necessary to simulate fracture flow as single continuum porous-media flow, and 5) the groundwater flow system is isothermal at 44 degrees C. The value of isothermal temperature used in the model corresponds to the approximate average temperature in the upper 1250 m of the SZ near Yucca Mountain.

From Yucca Mountain, the simulated flow path is in a south-southwesterly direction, which is not consistent with the conceptual model of SZ flow. Due to the constant-head boundary configuration, simulated groundwater flow occurs into the model along the northern and southeastern boundaries, and out of the model along the southern, southwestern, and northern portion of the eastern boundaries (Figure 8-17). Comparisons of flux from the USGS regional-scale flow model showed almost twice the amount discharging from the southern end of the USGS site-scale flow model, and substantially different amounts of flux for the north and east sides. The major flux differences between the two models occur in the northeast corner of the USGS site-scale flow model where a large part of the groundwater flow from the north is diverted toward the east, in part because of the interaction of the constant-head boundaries along the northern edges of the site-scale model and the imposed east-west barrier needed to represent the large-hydraulic gradient. Groundwater flux is important to repository performance due to its influence on radionuclide travel time. However, the USGS site-scale flow model was not directly used and thus did not impact TSPA-VA calculations.

During the time that the TSPA-VA base case was performed, the calibrated USGS site-scale flow model was unsuitable to use for TSPA-VA flow and transport calculations because:

- There were strong gradients vertically downward that tended to pull a simulated plume down into the lower carbonate aquifer, a condition unsupported by the hydraulic-head observations. Hydraulic head in the deeper volcanic units and in the lower carbonate aquifer, based on measurements in one well (UE-25 p#1), are generally higher than in the shallower saturated zone, indicating the potential for groundwater to flow upward rather than downward in the vicinity of Yucca Mountain (Luckey et al. 1996, pp. 27-29; Craig and Johnson 1984, p. 12).
- There are known inaccuracies in the geologic framework model portion of the USGS site-scale flow model. The model discretization is coarse (1500 m x 1500 m x variable thickness grid cells), which causes incomplete definition of hydrogeologic units.
- The permeabilities assigned to the hydrogeologic units tended to be low and inconsistent with site data, particularly for the volcanic units. For example, in the case of the middle



volcanic aquifer, values of bulk permeability from large-scale hydraulic testing at the C-hole complex (Geldon et al. 1997), not available during model calibration, were about two orders of magnitude larger than those used in the model.

- There was an unacceptable degree of numerical dispersion that occurred during transport calculations due to the coarse grid.

### **8.2.3 Conceptual Models**

A conceptual model is the set of assumptions and simplifications used to understand and describe a system for an intended purpose. The following sections: 1) describe the procedures used to gain input for developing TSPA-VA SZ conceptual models (e.g., the SZ abstraction/testing workshop and the SZ Expert Elicitation) and 2) provide a description of the processes assumed to be controlling groundwater flow and transport in the saturated zone at Yucca Mountain for the purpose of developing numerical models to perform TSPA-VA SZ calculations (e.g., the TSPA 3-D SZ flow model and the TSPA 1-D transport model). In general, the processes controlling the flow system are at large scales, from 10s to 100s of kilometers, whereas important transport processes occur at much smaller scales, perhaps on the order of centimeters to meters.

#### **8.2.3.1 Issues From the SZ Abstraction/Testing Workshop**

A workshop directed toward TSPA analyses of groundwater flow and transport in the SZ was held on April 1-3, 1997 in Denver, Colorado. The workshop was one of a series of workshops that was designed to integrate current site and design data and models into TSPA-VA analyses. A prioritized list of important technical issues related to groundwater flow and transport in the SZ was developed in this workshop for the purpose of guiding TSPA-VA analyses (Arnold et al. 1997, p. A-19). These issues were prioritized on the basis of specific criteria linked to potential impact to repository performance. The higher priority issues identified in this process are shown in Table 8 - 10.. These issues were, in turn, used to develop a set of abstraction/testing plans for the purpose of addressing these issues in abstracted models for use in TSPA-VA.

The format of the workshop included three major activities. The first was the development of a list of significant issues, which was accomplished through oral presentations and discussion. The second was the prioritization of issues, accomplished in four working groups and through open discussion among all participants. The third activity involved the reorganization of participants into another set of working groups for the development of abstraction/testing analysis plans. Each category of issues was introduced by a presentation from a TSPA representative outlining the ways in which these issues had or had not been addressed in previous TSPA analyses. Oral presentations were made by participants regarding each issue. Prioritization of issues within each category was undertaken at the end of the presentations within that category. Issues were prioritized in individual working groups by consensus or voting.

The final activity consisted of the global prioritization of all issues, presentations on existing workscopes and analysis plans from other workshops, regrouping of participants, and the development of analysis plans. The analysis plans were written to address the key issues and provide abstraction methods for TSPA-VA.

The issue prioritization process in the workshop was guided by a set of five criteria that were designated as performance measures. These criteria were chosen because they were judged to be significant to the long-term performance of the potential repository at Yucca Mountain. The following criteria were formulated within the context of the following guidance question.

Does the process/issue affect the:

- A. Peak radionuclide concentration at 5 km from the repository?
- B. Peak radionuclide concentration at 30 km from the repository?
- C. Time to first arrival (1% of peak)?
- D. Spatial distribution of the plume (both horizontal and vertical)?
- E. Spatial distribution of groundwater flux (e.g., dilution at the UZ-SZ interface)?

Workshop members developed six analysis plans to address uncertainties in the higher priority issues identified within the workshop. These analysis plans were designed to direct modeling activities in the abstraction/testing of process models to be used for SZ flow and transport in the TSPA-VA. The titles and a brief description of the analysis plans are given below:

- A. **Sensitivity Study on Uncertainties in Site-Scale Saturated-Zone Transport Parameters and Models.** This activity was designed to determine the generic sensitivity of SZ flow and transport modeling results to matrix diffusion, dispersivity, matrix and fracture sorption, redox potential in the SZ, and flow through alluvium. The results of this activity have been documented in Zyvoloski et al. (1997).
- B. **Coupling UZ and SZ Transport Models.** The goal of this activity was to evaluate the applicability of the convolution integral method as an abstraction method for coupling UZ and SZ transport in TSPA calculations and to provide a numerical tool for use in TSPA analyses. This activity resulted in the development of the SZ\_CONVOLUTE computer code for use in the TSPA-VA base-case analyses (see Section 8.3.4).
- C. **The Effects of Large-Scale Channelization on Effective Transport Parameters.** The goal of this activity was to evaluate the potential impacts of large-scale hydraulic features on the channelization of radionuclide transport in fractured media in the SZ. Preliminary results of this activity were presented in Arnold and McKenna (1998) and additional results are documented in this report (see Section 8.5.2.2).
- D. **Determination of Effective Field-Scale Transport Parameters Using C-Wells Testing Results.** The objectives of this activity were to determine appropriate values and associated uncertainties for field-scale transport parameters through reanalysis of C-Wells tracer test data. The results of this activity are documented in Geldon et al. (1997).

- E. **Past, Present, and Future Saturated Zone Fluxes.** This activity was designed to evaluate changes in the regional groundwater flow system in response to different climate states and to check for consistency between the USGS site-scale flow model and the USGS regional-scale flow model in terms of groundwater flux. The climate change modeling from this activity is documented in D'Agnese et al. (1997b) and the results concerning changes in specific discharge in the SZ at Yucca Mountain were incorporated into the TSPA-VA analyses (see Section 8.3.5).
- F. **Geologic Structure and Processes Affecting Flow Channelization.** The objective of this activity was to determine the effects of fault offset, fault-zone properties, upwelling from Paleozoic formations, and geothermal heating on horizontal and vertical flow channelization. The results of this activity are documented in Cohen et al. (1997).

### 8.2.3.2 SZ Expert Elicitation

Five panelists participated in an Expert Elicitation to assess the uncertainty in conceptual models of processes and specific parameter values relevant to the saturated zone. The elicitation process consisted of the following:

- A. Written and oral presentation of data to the experts by researchers from the Yucca Mountain Project
- B. Exchange of opinions and assessments among the panel members
- C. Formal interviews with the individual experts to elicit assessments of key issues.

The experts expressed their general opinions about the appropriate conceptual models for flow and transport in the saturated zone and provided probabilistic distributions for some key parameters (CRWMS M&O 1998, pp. 1-1 to 1-7).

The experts generally agreed that groundwater in the saturated zone (volcanic rocks) flows from beneath the repository to the southeast and south primarily through fractured tuffs of the middle volcanic aquifer and the valley fill alluvium. They expected faults and fracture zones to have important impacts on flow in the volcanic units. The panel members offered alternative hypotheses for the large-hydraulic gradient north of Yucca Mountain, and there was disagreement regarding the importance of this feature to repository performance. The panel members did agree that any major transient change in the large-hydraulic gradient is unlikely. The panel members generally concurred with interpretations of geochemical and paleospring data indicating water table rises of 80 to 120 m beneath the repository in response to past climatic variations.

For transport of contaminants in the saturated zone, the experts emphasized the limitations of processes that would cause dilution of contaminant concentrations. The experts believe that transport is by movement in vertically thin plumes through flow tubes beneath the repository. Dilution of contaminants occurs by vertical transverse dispersion and transient fluctuations in the direction of the hydraulic gradient. The experts generally rejected a mixed tank model in which

contaminated flow from the unsaturated zone mixes on a large scale with uncontaminated groundwater in the saturated zone.

The dilution factor distribution developed by the expert elicitation was used to reduce the maximum concentration in the saturated zone beneath the repository to the concentration in the groundwater approximately 20 km downgradient from the repository. The aggregate uncertainty in this parameter ranges from 1 to 100, with a median value of about 10. This range of values for dilution in the saturated zone represents a significant departure from previous TSPA analyses for Yucca Mountain (e.g., Atkins et al. 1995, pp. 7-23 and 7-25; Wilson et al. 1994, pp. 11-35), in which effective values of dilution were typically orders of magnitude higher. The Expert Elicitation provided a median value for specific discharge in the saturated zone (0.6 m/y) that was used in the one-dimensional transport simulations for the TSPA-VA. Finally, the experts discussed what the effective porosity should be, that is, the fraction of the bulk volume of the aquifer that carries flow and solute transport. Some of the panel members believed that effective porosity for radionuclide transport in fractured volcanic rocks in the saturated zone could be as low as conservative estimates of fracture porosity, implying little diffusive interaction with the rock matrix. Consequently, the uncertainty distribution for effective porosity in fractured volcanic units used in the TSPA-VA analyses has a maximum value equivalent to the average matrix porosity and a value of  $1 \times 10^{-5}$  at its lower end.

Information from the SZ Expert Elicitation was used in several different ways in the planning and execution of TSPA-VA analyses. Some information concerning uncertainty in parameter values for use in base-case analyses was incorporated directly into the parameter uncertainty analysis, as described in Section 8.4.2. In addition, results of the SZ Expert Elicitation were considered qualitatively with regard to how reasonable the conceptual model was, when used as a basis for numerical flow and transport modeling in the SZ. Some of the SZ flow and transport issues considered in the abstraction/testing workshop were excluded from explicit evaluation in the base-case TSPA-VA analyses, at least partially based on input from the SZ Expert Elicitation panel (e.g., uncertainty related to the large-hydraulic gradient was not accounted for in the base case, see Section 8.2.3.3).

### **8.2.3.3 Base-Case Conceptual Model**

This section describes the conceptual model of the flow and transport processes in the SZ that are relevant to radionuclide migration from the repository and shows how the TSPA-VA base-case conceptual model was developed. For the base case, conceptual model development included 1) using judgment provided by panelists participating in the Expert Elicitation on processes in the saturated zone (see Section 8.2.3.2), 2) accounting for important issues identified during the SZ abstraction/testing workshop (see Section 8.2.3.1), and 3) assuring consistency with the available data in the SZ and inferences from those data (Section 8.2.1).

Groundwater flow in the saturated zone below and directly down gradient of the repository at Yucca Mountain occurs in fractured, porous volcanic rocks at relatively shallow depths beneath the water table and in fractured carbonate rocks of Paleozoic age at much greater depths. At distances greater than about 10 to 20 km down gradient from the repository where the volcanic rocks thin and disappear under alluvium, groundwater flows either through the alluvium or the deep Paleozoic carbonates. Based on measured water levels in wells, the apparent groundwater

flow direction is generally to the southeast near the repository, with a transition toward the south and southwest farther south of the repository, as shown in Figure 8-4 (D'Agnese et al. 1997a, pp. 64 and 67). Groundwater flow direction could be influenced by horizontal anisotropy in aquifer bulk permeability, especially in fractured volcanic units (Luckey et al. 1996, p. 36). Groundwater flowing beneath Yucca Mountain would probably be pumped at wells 20 km or more to the south in the Amargosa Valley under present conditions (although capture by wells J-13 and J-12 is a possibility). Under predevelopment conditions (before pumping in the Amargosa Valley) and for the current climatic state, natural discharge of groundwater from beneath Yucca Mountain probably occurs further south at Franklin Lake Playa (Czarnecki 1990, pp. 1-12), although spring discharge in Death Valley is a possibility (D'Agnese et al. 1997a, pp. 64 and 69).

Radionuclides migrating from the repository are expected to move approximately 300 m downward in unsaturated zone water to the water table, where they enter the saturated zone. Radionuclides are expected to move through the unsaturated zone below the repository and enter the saturated zone in a well-defined plume, that is, as a flow system distinguishable from the surrounding flow because of differences in chemistry, temperature, concentration, or other parameters. Radionuclides are then carried downstream in the groundwater system. At 20 km, the radionuclides reach a hypothetical water well located near the Amargosa Valley, where they could become a source of contamination in the biosphere (see Figure 8-1).

Flow through the fractured volcanic rocks and the alluvium is assumed to occur as a single-continuum through porous media due to advective forces. The welded and non-welded volcanic units are comprised of a combination of fractures which have relatively high permeabilities, and dense matrix material with permeabilities generally much lower than the fractures (e.g., Geldon 1996, Table 9). Under ambient saturated flow conditions, groundwater tends to flow through the fractures in the volcanic units rather than the matrix. The volcanic units are assumed to contain an interconnected network of fractures over hundreds of meters through which groundwater flow predominantly occurs. This assumption is supported by multi-well hydraulic testing at the C-hole complex and single-well flow surveys where results indicate that groundwater production from wells in the volcanic units occurs primarily through a few discrete intervals (e.g., Luckey et al. 1996, Figure 15) (see Section 8.2.2.2). Once the groundwater enters the unfractured, alluvial units, flow is conceptualized to occur as movement in a classic single-continuum through porous media (see Freeze and Cherry 1979, pp. 15-75).

A combination of the complex hydrogeologic framework and structural controls on the flow system (see Section 8.2.1.2) cause the geometry of the groundwater flow system to be complex, especially at the scale of interest for repository performance (20 km). Therefore, for the TSPA-VA SZ base-case analysis the groundwater flow system was described in three dimensions (see Section 8.3.2).

The groundwater flow system was assumed to be at steady state for current climatic conditions. The steady-state assumption may not be valid in areas in which groundwater withdrawals are occurring, such as south of the repository in the Amargosa Valley region, where the slope of the potentiometric surface toward the southwest may be indicative of groundwater withdrawal (see Figure 8-5). Accounting for pumpage could change the potentiometric surface and hence the radionuclide travel path. However, there is also large uncertainty about which hydrogeologic

units comprise the flow path and the percentage of the flow path occupied by each unit (see Section 8.4.2). The effects of pumpage are probably not significant compared to the effects of uncertainty about the hydrogeologic units.

The groundwater flow system in the SZ is conceptualized to respond to changes in climate by alterations in groundwater flow rates, water table elevations, and the distribution of groundwater discharge. Transient adjustments to the SZ flow system as climatic variations occur are expected to be relatively rapid, at least on the scale of interest (i.e., tens of thousands of years). The SZ flow system is conceptualized to have relatively steady configurations corresponding to discrete climatic states over long time periods.

From the perspective of repository performance, important processes that must be considered in describing radionuclide travel time in the saturated zone include advection, matrix diffusion, and sorption (see Figure 8-1). Processes such as sorption and matrix diffusion increase the residence time for certain radionuclides and allow reduction of dose by radioactive decay. Processes that cause dilution of radionuclides, such as dispersion, contribute directly to the attenuation of radiological dose by reducing radionuclide concentrations in groundwater.

The groundwater transport system in the volcanic units is thought to behave as a dual-porosity system where advection is important in the fractures and diffusion occurs into the matrix, based on the current interpretation of results from tracer tests conducted at the C-hole complex (Section 8.2.1.2). Matrix diffusion is the movement of dissolved radionuclides from groundwater flowing fractures into the relatively immobile through pore water of the matrix, due to differences in concentration. Diffusion probably occurs at a relatively small scale and slows radionuclide movement by providing additional solute storage in the matrix pores (Grisak and Pickens 1980, p. 728). Transport through the alluvial units are assumed to occur as a single-continuum.

For the sake of computational efficiency and lack of data at the site scale in support of modeling a complex dual-porosity system, an effective porosity approach was assumed for the TSPA-VA base-case SZ analysis to describe the transport of radionuclides in the saturated volcanic units at Yucca Mountain. The effective porosity, that is, the porosity that includes the combination of fractures and matrix pores through which the radionuclides are carried, affects how fast the contaminants travel. In porous media (e.g., the alluvium), the effective porosities are greater than in the fractured medium (volcanic units). Because of the smaller effective porosity, travel times tend to be shorter in the fractured media than in the porous media (Figure 8-1). The assumed effective porosity value for each fractured unit was used as a surrogate for the matrix diffusion process which occurs in a dual-porosity system (see Sections 8.4.2 and 8.5.2.3). The much narrower distribution of effective porosity used in the alluvium accounts for uncertainty in flow channelization and bypassing of low-permeability zones in the transport process. In addition, the range of uncertainty in effective porosity is sufficiently large (greater than four orders of magnitude for fractured volcanic units) to encompass the uncertainty in bulk permeability (and thus, specific discharge) in the TSPA 1-D transport analyses (Section 8.3.3).

Hydrodynamic dispersion of radionuclides was assumed to occur using the advection-dispersion model of solute transport (Fetter 1993, p. 51-54). Dispersion is defined in the longitudinal direction relative to groundwater flow. Transverse dispersion, spreading of the plume perpendicular to the travel path, was implicitly approximated using the dilution factor approach,

based on input from the Expert Elicitation panel (Section 8.2.3.2). Also, the transport system was simplified to one dimension based upon the flow path from the three-dimensional groundwater flow system to help minimize numerical dispersion effects.

Nine radionuclides ( $^{14}\text{C}$ ,  $^{129}\text{I}$ ,  $^{237}\text{Np}$ ,  $^{231}\text{Pa}$ ,  $^{239}\text{Pu}$ -reversible,  $^{242}\text{Pu}$ -reversible,  $^{239}\text{Pu}$ -irreversible,  $^{242}\text{Pu}$ -irreversible,  $^{79}\text{Se}$ ,  $^{99}\text{Tc}$ , and  $^{234}\text{U}$ ) were selected as important to account for in the TSPA-VA SZ analysis (see Chapter 6 for discussion of radionuclide selection criteria). These radionuclides are the same as those tracked in the upstream components of the TSPA-VA analyses. All of the radionuclides were assumed to be transported in dissolved form with the exception of the plutonium isotopes.

Significant migration of Pu was conceptualized to occur only by colloid-facilitated transport because of the very high potential for sorption of dissolved Pu onto immobile mineral grains. The conceptual model of colloid-facilitated Pu transport included two modes of migration. In the first mode, Pu is assumed to be in chemical equilibrium among the aqueous phase, sorption onto colloids, and sorption onto mineral grains of the aquifer. In the second mode, Pu is irreversibly attached to colloid particles that do not undergo significant filtration.

Geochemical retardation, through sorption of radionuclides on mineral grains, slows radionuclide migration in groundwater in both fractured and porous media. A linear, equilibrium sorption model ( $K_d$ ) was assumed for those radionuclides which exhibit sorption on mineral grains. All radionuclides in the aqueous phase were assumed to be below the solubility limit (i.e., precipitation of radionuclides into solid phase was assumed to not occur).

#### **8.2.3.4 Alternative Conceptual Models**

Most of the higher-priority issues related to SZ flow and transport that were identified in the SZ abstraction/testing workshop (Section 8.2.3.1) were considered, either explicitly or implicitly, in the base-case TSPA-VA analyses or in sensitivity analyses. The alternative conceptual models described here are other possible conceptualizations of flow and transport processes in the SZ at Yucca Mountain that differ from the base case assumptions. Those issues that have not been considered in the base-case or in sensitivity analyses are listed in this section and qualitative evaluations of their potential effects on the analyses of repository performance are made.

Uncertainty about the amount of transverse dispersivity expected in the saturated zone at Yucca Mountain was discussed at great length during the Expert Elicitation (CRWMS M&O 1998, pp. 3-10 and 3-11). The experts believe that transport is by movement in vertically thin plumes through flow tubes beneath the repository and the consensus was that the transverse dispersivity could be very small, on the scale of millimeters. The experts felt that a plume may have minimal mixing along the flow path, even after traveling kilometers. For the base case, the dilution factor (a surrogate for transverse dispersivity) was treated as a stochastic parameter to account for the uncertainty in the amount of mixing that may occur along the radionuclide travel path. The assumed range and distribution of the dilution factor reflected the expert opinions for the base case analysis (Section 8.4.2). In addition, an analytical solution was used to examine the relationship between vertical transverse dispersion and dilution factor for transport to 20 km (Section 8.5.2.1).

There is uncertainty in the flow field and flow paths, which were assumed to be fixed for the base-case analysis (see Section 8.3.3). Large-scale structural features and spatial heterogeneity in the permeabilities of the volcanic units could channelize or focus flow, creating different flow paths than conceptualized in the base case. Alternative flow paths and fluxes could also be caused by accounting for the large range in permeabilities of the volcanic units and spatial heterogeneity. The sensitivity analysis described in Section 8.5.2.2 discusses the effects of heterogeneity and flow channelization on repository performance.

Alternative conceptual models of the SZ flow system near Yucca Mountain and of the large-hydraulic gradient to the north of the repository location, in particular, have been the subject of considerable debate (Luckey et al. 1996, pp. 21-25). A single conceptual model of the large- and moderate-hydraulic gradient areas, in which vertical zones of lower permeability control these features, is considered in the TSPA-VA base-case analysis. The consensus among the SZ Expert Elicitation panel members was that there is nothing fundamentally unique about the large-hydraulic gradient, that there is very low probability that the large-hydraulic gradient will move, and that alternative conceptual models of this feature would have little impact on predictions of potential repository performance (CRWMS M&O 1998, pp. 3-5 and 3-6). In addition, the results of previous TSPA analyses that have considered two alternative conceptual models of the large-hydraulic gradient (Wilson et al. 1994) found small differences in simulated repository performance relative to these alternatives. The SZ Expert Elicitation panel did feel that alternative conceptual models of the large-hydraulic gradient could be resolved with some additional, carefully collected data and that resolution of alternative conceptual models of the large-hydraulic gradient could be important to the Yucca Mountain Project in terms of demonstrating understanding of the SZ flow system at the site. Thus, alternative conceptual models of the large-hydraulic gradient may be a significant issue from the perspective of site characterization, but probably have a lower priority with regard to performance assessment. It should be noted at this point that, although perched water in the UZ does constitute locally saturated conditions, this issue is not considered in the SZ component of the TSPA-VA analyses and is deferred to the discussion in the UZ section of this report.

Various coupled processes have been proposed as significant issues in SZ flow and transport for consideration in TSPA analyses such as: 1) thermal effects, both from repository-generated heat and from the natural thermal gradient, 2) chemical effects from the introduction of materials in the repository and from thermally induced mineralogic alterations in the SZ medium, and 3) mechanical effects, as caused by thermal expansion around the overlying repository. None of these issues were directly included in TSPA-VA base case or sensitivity analyses of flow and transport in the SZ. In general, these coupled processes would be expected to have less impact on flow and transport in the SZ than in the UZ, simply because of greater distance from the potential repository.

The impacts of repository heat on SZ flow and transport, in terms of thermal perturbations alone, appear to be small based on some preliminary modeling (Ho et al. 1996 7-1; Zyvoloski et al. 1997, pp. 6-51/55). The results in the saturated zone showed a simulated thermal plume that extends at least 5 km down gradient from the potential repository and persists longer than 10,000 years (Ho et al. 1996, p. 7-7). The predicted temperature changes suggest the possibility of mineralogic alteration, including dissolution and precipitation reactions that could permanently alter the bulk permeability structure of the aquifer which could impact groundwater velocities



and hence radionuclide transport (Ho et al. 1996, pp. 7-8). Groundwater fluxes in the SZ were simulated to be somewhat higher in the region downgradient of the repository during the thermal period (i.e., at least out to 10,000 years) and simulated radionuclide concentrations downgradient in the SZ were slightly lower when heat from the repository was coupled with groundwater flow. Analysis of potential free convection indicated that such convection would probably only be possible in the most permeable units and that it would probably be overcome by regional groundwater flow through these units in the SZ (Cohen et al. 1997, p. 62). It has been suggested by the SZ Expert Elicitation panel that thermal buoyancy could limit vertical mixing of the contaminant plume during the thermal period (CRWMS M&O 1998, pp. 3.13 and 3.22, 4.5-4.6). In summary, although uncertainties regarding the thermal impacts on SZ flow and transport remain, these thermal processes are probably secondary to other processes and uncertainties in radionuclide transport in the SZ.

There is considerably greater uncertainty concerning the potential impact of chemical and mineralogical changes in the SZ in response to the presence of the repository. Repository-induced thermal gradients along the groundwater flow paths in the SZ could result in dissolution and precipitation of minerals as well as more complex mineralogical changes to the bedrock medium. It is unknown whether these reactions would increase or decrease the fracture permeability of the medium in zones of dissolution; they would probably tend to decrease bulk permeability in zones of precipitation. It is also unclear what the magnitude of these changes in bulk permeability would be and whether there would be significant changes in groundwater flow patterns in response to the alterations in bulk permeability. These effects could potentially redirect groundwater flow around areas of reduced bulk permeability such that radionuclide travel times would be increased and dispersive mixing would be enhanced. Alternatively, preferential increases in permeability along some fracture zones could potentially reduce radionuclide travel times and decrease dispersive mixing in the SZ. These durable changes to the medium in the SZ would probably affect, at most, the first few thousand meters along the flowpath; the remainder of the flowpath, to a distance of 20 km, would be unaltered. It is also possible that the chemical "signature" of groundwater in the UZ that has been influenced by interaction with repository materials (in particular, cementitious material) could persist into the SZ groundwater system. These chemical changes in the groundwater (e.g., pH) would tend to be buffered by interaction with the bedrock; however, the flowpath length necessary to induce this buffering is unknown. The potential significance of chemically altered groundwater is that radionuclide transport processes, such as sorption, could be very different in this chemical environment relative to ambient conditions.

Finally, mechanical effects of the repository have not been considered in TSPA-VA analyses. The SZ directly below the repository would be subjected to probably small tensional stress due to the thermal perturbation from the repository during the thermal period. This could lead to an increase in fracture permeability and increased groundwater flux in the SZ. This effect has not been quantitatively evaluated, but would probably be small relative to other coupled processes.

### 8.3 ANALYSIS APPROACH TO SZ FLOW AND TRANSPORT FOR TSPA ANALYSES

This section summarizes the approach used for TSPA-VA SZ base-case calculations including details about the numerical models employed, coupling methods utilized to incorporate the SZ work into the overall RIP TSPA-VA assessment, and a summary of all relevant assumptions.

#### 8.3.1 General Approach

For the TSPA-VA, a hierarchy of models was used to simulate the transport of radionuclides in the saturated zone. Explicit, three-dimensional modeling was not used to simulate radionuclide concentrations because it can generate numerical dispersion, which artificially lowers concentration. Three-dimensional modeling was used only to determine flow paths. One-dimensional transport modeling was used, based on the flowpaths from the three-dimensional modeling, to determine concentration breakthrough curves at a distance of 20 km for unit releases of radionuclides. Six 1-D flowpaths, or streamtubes, corresponding to separate radionuclide source regions at the water table beneath the repository, were simulated. Then, within the TSPA-VA calculations, the convolution integral technique described in Section 8.3.4 was used to combine the breakthrough curves with the time-varying radionuclide sources from the unsaturated zone. Finally, the radionuclide concentrations were divided by the dilution factor at 20 km, which was sampled from the distribution suggested by the Expert Elicitation process (Section 8.2.3.2).

For the base case, two models were used in the TSPA-VA saturated zone calculations. First, a deterministic TSPA 3-D flow model was used to simulate the flow model velocity field on which particle tracking was conducted from the repository to a distance of 20 km (see Section 8.3.2). Distribution of the hydrogeologic units along the flowpath was determined using particle tracking in the TSPA 3-D flow model. The TSPA 1-D transport model domain for streamtubes in the SZ was based upon the flowpath simulated in the TSPA 3-D model. The TSPA 1-D transport model was used to calculate the radionuclide concentrations as a function of time at 20 km distance from the repository for a unit step-function mass flux source (i.e., a steady source that was assumed to equal 1 g/y). Uncertainty in the transport of radionuclides was assessed by performing multiple simulations using the TSPA 1-D transport model with varying transport parameter values (Section 8.4.2). Both of the TSPA SZ models were based upon our current understanding of the flow and transport system in the SZ (see Section 8.2).

Because the detailed SZ flow and transport numerical models have relatively long computer run times, the more computationally efficient convolution integral method was chosen to simulate radionuclide transport within the RIP implementation of individual TSPA-VA realizations. Uncertainty in SZ flow and transport was assessed in 100 Monte Carlo realizations of the system, in which the transport parameters were varied, using the TSPA 1-D transport model prior to the actual TSPA-VA runs. These results were stored in a "library" of unit concentration breakthrough curves (DTN # SNT05082597001.P05), which were subsequently accessed during the TSPA-VA realizations. For each realization, the unit concentration breakthrough curve was based upon the sampled input parameters for that realization (see Section 8.4.2). The Monte Carlo approach allows consideration of uncertainty in some parameters, but does not consider conceptual model uncertainty.

The effects of climate change on radionuclide transport in the SZ were incorporated into the analysis by assuming instantaneous change from one steady-state flow condition to another steady-state condition in response to climatic variation. In a manner consistent with the other components of the TSPA-VA analyses, three climate states were utilized: 1) dry climate (present day conditions), 2) long-term average (corresponding to pluvial condition), and 3) super-pluvial (corresponding to glacial maximum conditions). Results from the regional-scale SZ flow model (D'Agnese et al. 1997b) were used to estimate the relative increase in the SZ specific discharge (as a multiplication factor) for each of the alternative climate states. Results from the UZ site-scale flow model (Bodvarsson et al. 1997) were used to estimate the increase in volumetric groundwater flow rate through each SZ streamtubes for each of the alternative climate states. Thus, both the groundwater velocity and the volumetric flow rate of groundwater through each streamtube (i.e., streamtube size) changed for different climatic states. Scaling of radionuclide transport times and concentrations in the SZ for the alternative climate states was performed by the computer code (SZ\_CONVOLUTE) during implementation of the convolution integral method.

The radionuclide concentrations in the six streamtubes were summed at each time step for a given realization to obtain a conservative estimate of the maximum concentration in the saturated zone at 20 km from the repository. For this approximation it is assumed that, in a conceptual sense, implicit spreading of radionuclide mass from individual streamtubes via dilution causes six plumes that essentially overlap. This assumption was examined in more detail in a sensitivity study (Section 8.5.2.1). At each time step, the maximum estimated concentration was compared to the maximum undiluted concentration in the saturated zone. The maximum estimated concentration at a 20 km distance was not allowed to exceed the maximum undiluted concentration in any single streamtube.

The resulting simulated radionuclide concentrations at a 20 km distance were passed to the biosphere model at each time step in the TSPA-VA simulations to calculate total dose. The conservative assumption was made that radionuclide concentrations in discharge from the hypothetical pumping well would be the same as the simulated concentrations in the groundwater, and that no additional dilution occurs due to pumping. This assumption is approximately valid for scenarios in which the pumping discharge rate of the hypothetical well is less than the volumetric groundwater flow rate through the streamtubes used in the TSPA analysis.

### **8.3.2 TSPA 3-D SZ Flow Model**

For the TSPA-VA base case, the TSPA 3-D SZ flow model was developed to determine the flowpath from the repository footprint, or outline, at the water table to a distance 20 km downgradient, the approximate distance to the nearest major public extraction of groundwater. Based on the particle tracking simulation results, the hydrogeologic units that were present along the contaminant travel path were determined, as well as the percentage of the flowpath occupied by each unit. The travel distance through each hydrogeologic unit provided by this analysis was then used to define the travel-path characteristics in the saturated zone for the one-dimensional transport, base-case analysis (see Section 8.3.3).

The TSPA 3-D SZ flow model was developed using FEHMN (Zyvoloski et al. 1995), a finite-element/finite-volume flow and transport code. The basic conservation equations, constitutive relations and numerical methods are described in Zyvoloski (1983, pp. 75-86), Zyvoloski (1986), Zyvoloski and Dash (1990), Reeves et al. (1994), and Zyvoloski et al. (1995).

The three-dimensional flow model used for this analysis incorporated an area of about 20 km by 36 km to a depth of 950 m below the water table. The model grid was a uniform orthogonal mesh with 500-m by 500-m by 50-m elements (Figure 8-18). The hydrogeologic framework in the model was based on a refined version of the regional geologic framework model used by D'Agnese et al. (1997a, pp. 29-35), as shown in Figure 8-19. Sixteen different hydrogeologic units were represented as homogeneous, isotropic units (Table 8-11). Three linear, vertical features with low permeabilities to the west and north of Yucca Mountain were included to simulate the moderate, and large, hydraulic gradient regions. Solitario Canyon Fault was included to simulate the moderate hydraulic-gradient west of Yucca Mountain, while an east-west low permeability barrier and the Yucca Wash extension barrier were included to simulate the large-hydraulic gradient to the north (Figure 8-18).

Flow was modeled as steady state, through a single-continuum, porous medium. Focused recharge along Fortymile Wash, consistent with USGS measurements, was included as a specified flux at the nodes below Fortymile Wash. Specified-pressure boundary conditions were applied to the lateral boundaries based on the interpolation of measured values of hydraulic head (Figure 8-18). Lateral, specified-pressure boundary conditions were specified such that vertical gradients in hydraulic head were zero at the boundaries. Groundwater flow was not allowed to occur across the bottom boundary of the model. Permeability was assumed to be uniform within hydrogeologic units in the model domain (Figure 8-19), and average isothermal (44 degrees C) conditions were applied in the TSPA 3-D SZ flow model.

The model was calibrated by a trial-and-error procedure, and the simulated hydraulic heads were compared with measured head values in the model domain. The calibration criteria used to evaluate the model calibration were: 1) the residuals at all wells and 2) the magnitude and direction of the hydraulic gradient along the potential path of a contaminant plume from the repository. The values of bulk permeability used in the calibrated TSPA 3-D flow model are shown in Table 8-12. There was good agreement between the simulation results and most of the well measurements, particularly in the area downgradient of the repository (Figure 8-20). The differences between simulated and measured hydraulic head values (residuals) were less than 5 m for shallow wells downgradient of the repository, within a 20 km distance. The results of the model calibration are tabulated in Table 8-13. The absolute values of residuals for most wells along the flowpath from the repository were less than 2 m. The simulated direction of groundwater movement in this flow model is consistent with the conceptual model of the system described in Section 8.2.1.2 and is evident in the plot of simulated paths determined by particle tracking at the water table shown in Figure 8-21. Note that the particle tracking method employed in generating this figure did not simulate any transverse dispersion, so the particle pathlines represent advective transport only. The apparent narrowing of the streamtube defined by the particle paths shown in Figure 8-21 is related to a deepening of some particles in the vertical direction and increased groundwater flux toward the south. Solute transport simulations with the TSPA 3-D flow model from beneath the repository to 20 km distance was used to evaluate average groundwater flux and indicated an average simulated specific discharge of 0.61

m/y along the flow path. This value of average specific discharge in the TSPA 3-D flow model was determined by comparing the time at the midpoint of the concentration breakthrough curve simulated with the 3-D model to the midpoint simulated with the TSPA 1-D transport model. This value of simulated groundwater flux is approximately equal to the aggregate expected value from the SZ Expert Elicitation of 0.6 m/y (CRWMS M&O 1998, p. 3-43).

Particle tracking in the 3-D simulated flow field was used to estimate the flowpath lengths in the saturated zone through each of the hydrostratigraphic units downstream from the repository. A swarm of particles was released at the water table and evenly distributed across the repository footprint. Flowpath lengths within the units were then tabulated. Flow was significant in four of the hydrostratigraphic units i.e., the upper volcanic aquifer (fraction of flowpath = 0.143), middle volcanic aquifer (fraction = 0.518), middle volcanic confining unit (fraction = 0.239), and alluvium/undifferentiated valley fill (fraction 0.100). The resulting information was incorporated into the TSPA 1-D SZ transport simulations used in the TSPA-VA analyses (Section 8.3.3).

**Model Limitations** - It was reasonable to use the TSPA 3-D SZ flow model to estimate the radionuclide travel paths in three dimensions. However there were concerns about the model characteristics relative to performing solute transport simulations. The main concern is related to the problem of large numerical dispersion inherent with the use of a relatively coarse grid (cell size is 500 m x 500 m x 50 m) when performing transport calculations. The desire to minimize spurious transverse dispersion for the SZ analyses necessitated the use of 1-D streamtubes for the transport calculations of the SZ analysis, which could be more finely discretized (grids spaced at 5 m intervals).

Some other simplifying assumptions and approaches used in the TSPA 3-D SZ flow model may impact or limit the model effectiveness in representing the physical processes occurring at the site. These limitations are presented from the perspective of what input is passed from the TSPA 3-D SZ flow model into the TSPA-VA SZ base case analysis (i.e., a simulated 3-D flowpath from which the fraction of flowpath through the alluvium is extracted). As already discussed, the model discretization is coarse, which causes incomplete spatial resolution of hydrogeologic features. For example, many of the faults are implicit in the grid through offset of units, hence the exact location for faults will always be approximate, regardless of grid spacing. However, explicit representation of selected faults could be achieved through explicit specification of the fault as a surface within the hydrogeologic framework model, which would cause it to be defined as a set of nodes within the subsequent finite-element mesh, complete with its own set of hydraulic properties. Larger problems include identifying those faults for which hydraulic properties are available or could be anticipated (very little is known) and deciding which faults are most important to represent explicitly within the flow and transport model. Faults, as discrete hydrologic features, were not included in the base case TSPA 3-D SZ flow model because of this lack of data. Potential impacts of high-permeability faults on SZ flow and transport were examined in sensitivity studies in Section 8.5.2.2. For TSPA-VA calculations, these factors influenced the flowpath.

The assumption of uniform bulk permeability within each unit is a simplification of a complex system. Small-scale variations in hydraulic head likely cannot be represented in the model without greater spatial resolution. However, even with a more refined model, bulk permeability data to support spatial variation of bulk permeability generally are lacking. Local areas of high

permeability may exist that would explain estimates of high permeability based on hydraulic tests (for example, within the middle volcanic aquifer), that are not represented in the model. Explicitly accounting for local high permeability zones could possibly change the flowpath assumed for base case calculations.

An average temperature for the entire saturated zone contained within the site model has not been calculated. Different specifications of average groundwater temperature (20 degrees C and 44 degrees C) have an appreciable effect on viscosity (1.002 centipoise for fresh water at 20 degrees C; 0.6067 centipoise for fresh water at 44 degrees C) and therefore hydraulic conductivity (Czarnecki et al. 1998, p. 51) where hydraulic conductivity has an inverse relationship with viscosity. A more appropriate way to address the issue of temperature effects on flow is to simulate coupled groundwater flow and heat transport with appropriate temperature and heat-flow boundary conditions. Using temperature and hydraulic-head data in model calibration would probably constrain simulated results better. However, there are important uncertainties regarding the appropriate thermal (and hydrologic) boundary conditions for the bottom boundary of the flow model that would influence results.

Specified-hydraulic-head boundary conditions were based on interpolation of measured head data. An artifact of that process is the resultant large fluxes that occur in the north-east part of the model. Furthermore, no vertical hydraulic-head data exist at the model boundaries making it difficult to verify the resulting hydraulic-head distribution. Possible inaccuracies of assigned hydraulic-head values at the lateral model boundaries are an important potential source of inaccuracies in groundwater flow simulations. Such inaccuracies probably primarily affect flow directions and flowpaths from the potential repository.

The steady-state assumption may be invalid in areas in which groundwater withdrawals are occurring. The hydraulic-head observation data span almost 50 years of record that results in irregularities in the potentiometric surface. The slope of the potentiometric surface toward the southwest may be indicative of groundwater withdrawals that were not specified in the model. Discharge by pumping wells occurs in the Amargosa Desert in the southwest part of the model domain, but this pumping was not explicitly represented in the model. However, the influence of these well withdrawals is implicitly reflected in the specified-head lateral boundary conditions applied along the southern boundary of the model. Accounting for pumpage could possibly alter the radionuclide flowpath, however, there is also large uncertainty about which hydrogeologic units comprise the flow path and the percentage of the flow path occupied by each unit. Probably the effects of pumpage are not significant compared to the effects of uncertainty about the location of hydrogeologic units.

No-flow boundary conditions were specified along the base of the model. Limitation in the vertical extent of the model (950 m below the water table) results in a lack of spatial continuity of the carbonate aquifer with higher-head areas at the northern end of the model. This limitation may explain the inaccuracy of simulating lower hydraulic-head values than those observed in the deeper observation points within the model. This inaccuracy results in horizontal to vertically downward flow in some regions within the model, a condition unsupported by the hydraulic-head observations.

Finally, the representation of the large-hydraulic gradient remains inconclusive. By specifying an east-west oriented barrier to flow, the observed hydraulic-head data may be better matched, but the resulting flow field is difficult to reconcile. If a buried fault does exist and is a barrier to flow, no data are available to prove or disprove its existence. Furthermore, if the large-hydraulic gradient is actually an artifact of perched-water occurrence, then the resulting flow field in this area would be considerably different. However, the impact of alternatively modeled representations of the large-hydraulic gradient to simulated radionuclide migration on flow direction and radionuclide flowpath downgradient of the repository is expected to be small.

These limitations to the TSPA 3-D flow model, the resulting uncertainties in flow simulations, and the uncertainties in the hydrogeologic framework model suggest that the flowpaths derived from this model should be considered as uncertain in TSPA-VA analyses. The fraction of the flowpath through the alluvium/undifferentiated valley fill is of particular importance to performance assessment calculations with the TSPA 1-D transport model. Because of the significance of this uncertainty, the fraction of the flowpath through the alluvium/undifferentiated valley fill was a stochastic parameter in the TSPA-VA analyses (Section 8.4.2). The relative fractions of the flowpath lengths through the other hydrogeologic units in the TSPA 1-D model simulations were varied in proportion to the flowpath fraction for the alluvium/undifferentiated valley fill for each realization in the TSPA-VA simulations.

It is not possible to quantify the existing uncertainty in the groundwater flow directions or the geologic framework. Conceptually for TSPA-VA calculations, the stochastic nature of the flowpath fraction through the alluvium/undifferentiated valley fill accounts for both our uncertainty in the flow directions in the SZ and our uncertainty in the geology below the water table in the region 10 km to 20 km downgradient of the repository. The degree of this uncertainty is quantified by the distribution assigned to the fraction of flowpath through the alluvium parameter further described in Section 8.4.2, although it is not known if these assumptions are conservative or nonconservative.

### **8.3.3 TSPA 1-D SZ Transport Model**

The TSPA 1-D SZ transport model was developed to simulate the radionuclide concentration breakthrough curves that form the basis of the TSPA-VA calculations performed with the RIP computer program. Each radionuclide was transported separately in the analysis. The 1-D transport simulation method was chosen because of the desire to eliminate spurious dilution of radionuclide concentrations resulting from numerical dispersion, which can occur in coarsely gridded 3-D solute transport simulations. Solute transport simulation using a 1-D numerical model precludes dilution from transverse dispersion, by definition. The dilution from transverse dispersion was explicitly specified in this modeling, as a post-processing step. This dilution factor was treated as a stochastic parameter, as described in Section 8.4.2.

A diagrammatic representation of the conceptual model for 1-D SZ radionuclide transport is shown in Figure 8-22. Flow and transport in the SZ is conceptualized to occur in six streamtubes that originate at the water table below the repository. It should be noted that the diagram shown in Figure 8-22 is conceptual, but indicates a cluster of six streamtubes in the SZ that is approximately 3000 m in width and between 10 m and 20 m in vertical depth. Streamtubes are taken from a concept in classical fluid dynamics that is used to visualize and estimate the

behavior of the elements of a flow system. Each of the six streamtubes is a continuation of a groundwater flow path from the repository in the unsaturated zone. Thus, the volumetric flow rate of groundwater through each streamtube ( $Q_{UZ}$ ) was determined at the water table from flow simulations using the site-scale flow model developed by Bodvarsson et al. (1997) for the unsaturated zone (see Chapter 2) (Table 8-14). The cross-sectional area of each streamtube was specified to be proportional to the volumetric groundwater flow rate. The specific discharge within the streamtubes in the saturated zone ( $q_{SZ}$ ) was 0.6 m/y for current climatic conditions.

Simulations of radionuclide transport in the saturated zone for the TSPA-VA calculations were performed with six, one-dimensional flow tubes using FEHMN (Zyvoloski et al. 1995). The streamtubes were 20 km long, with a regular grid spacing in the tubes of 5 m. The four hydrogeologic units in the streamtubes were the middle volcanic aquifer, the upper volcanic aquifer, the middle volcanic confining unit, and the alluvium/undifferentiated valley fill. The lengths of these units within the streamtubes were defined by particle tracking using the TSPA 3-D flow model for the saturated zone described in Section 8.3.2. The radionuclide transport simulations in the TSPA 1-D transport model were performed assuming a steady, unit (1 g/y) radionuclide mass source at the upstream end of the streamtube (i.e., the water table at the base of the UZ below the water table). Transport of each radionuclide was simulated separately in the TSPA 1-D SZ transport model. Transport simulations with the one-dimensional streamtube approach implicitly assume complete mixing of the radionuclide mass in the volumetric groundwater flow rate specified for each streamtube.

#### 8.3.4 Convolution Integral Method

The convolution integral method was used in the TSPA-VA calculations to determine the radionuclide concentration in the saturated zone, 20 km downgradient of the repository as a function of the transient radionuclide mass flux at the water table beneath the repository. This computationally efficient method combines information about the unit response of the system, as simulated by the TSPA 1-D transport modeling, with the radionuclide source history from the UZ to calculate transient system behavior. The most important assumptions of the convolution method are linear system behavior and steady-state flow conditions in the saturated zone.

The convolution integral method provides an approximation of the transient radionuclide concentration at a specific point downgradient in the SZ in response to the transient radionuclide mass flux from transport in the UZ. This coupling method makes full use of detailed SZ flow and transport simulations for a given realization of the system, without requiring complete numerical simulation of the SZ for the duration of each TSPA-VA realization. The technique is summarized in the flow chart shown in Figure 8-23. The two input functions to the convolution integral method are: 1) a unit concentration breakthrough curve in response to a step-function mass flux source as simulated by the SZ flow and transport model, and 2) the radionuclide mass flux history as simulated by the UZ transport model, resulting in a total of 1111 breakthrough curves for the base case (100 realizations and one expected value realization for all radionuclides included in the analysis). The output function is the radionuclide concentration history downgradient in the SZ.



The mathematical expression for the convolution integral method is written as

(8 - 1)

$$C_{sz}(t) = \int_0^t \dot{m}_{uz}(t-t') \frac{\bar{C}_{sz}(t')}{m_p} dt'$$

where  $C_{sz}(t)$  is the radionuclide concentration downstream in the SZ,  $t$  is time,  $\dot{m}_{uz}(t)$  is the time-dependent radionuclide mass flux entering the SZ from the UZ, and  $\bar{C}_{sz}(t')$  is the derivative of the downstream radionuclide-concentration-time response curve to a step input of mass  $m_p$  (Zyvoloski et al. 1997, p. 6-8).

The effects of climate change on radionuclide transport in the saturated zone were incorporated into the convolution integral analysis by assuming instantaneous change from one steady-state flow condition to another steady-state condition in the saturated zone. Changes in climate state were assumed to affect the magnitude of groundwater flux through the saturated zone system but have a negligible impact on flowpaths. This assumption is supported, in part, by particle tracking analysis for different climate scenarios using the USGS regional-scale flow model (Tucci 1998). These effects were incorporated into the convolution method by scaling the timing of radionuclide concentration breakthrough curves proportionally to the change in saturated zone specific discharge. Also, the concentrations of the radionuclide breakthrough curves were scaled proportionally to the change in volumetric groundwater flow rate from the unsaturated zone into the streamtubes. The USGS regional-scale flow model for the saturated zone provided estimates of the relative change in specific discharge in the saturated zone for future climate states (as summarized in e-mail message from Pat Tucci, 12/11/97). The site-scale flow model for the unsaturated zone (Bodvarsson et al. 1997) provided estimates of changes in the base case volumetric groundwater flow rate through the repository horizon. These estimates are summarized in Table 8-14.

Radioactive decay was also applied to radionuclide concentrations calculated with the convolution integral computer code (SZ\_CONVOLUTE). The convolution integral method consists of numerical integration that accounts for the contributions to the outlet concentration from a series of time intervals. Because the travel time for each contribution to concentration is known, the loss of radionuclide mass (and consequent decrease in concentration) during transport was calculated by first-order decay for that time interval.

There are several important assumptions in the use of the convolution integral method. Groundwater flow in the SZ is assumed to be in steady state as discussed in Section 8.3.2. The transport processes in the SZ are assumed to be linear with respect to the solute source term (i.e., a doubling of the solute mass source results in a doubling of concentration). In addition, the flow and transport processes in the UZ and the SZ are assumed to be independent of one another.

**Verification of the Convolution Integral Method** - The multi-climate convolution code was verified against a 3-D saturated-zone transport simulation run with FEHMN using five consecutive climate states. The base-case, saturated-zone flow field was based on current

conditions. The flow then changed four times throughout the simulations to represent four arbitrary, new climates, as shown in Table 8-15. The flux multiplier updates the flow rate relative to the base-case flow rate.

The FEHMN solution was run on a 3-D 60,720 node rectangular grid having three material types and four permeability barriers to represent flow in the SZ at Yucca Mountain. This 3-D SZ flow and transport example was chosen to be representative of the TSPA-VA base case problem, although the TSPA 3-D SZ flow model and TSPA 1-D transport models used for actual TSPA-VA calculations were not used in this validation exercise. The time-dependent mass flux of tracer from the unsaturated zone was applied to an area having 96 nodes that covers the repository footprint. The differing climates were simulated using restart runs in which the three-dimensional pressure field and tracer distribution were used as initial conditions. To simplify the calculation, the permeability field was adjusted (multiplied by the flow multiplier) to produce the desired flow field rather than modifying the pressure boundary conditions. The breakthrough curve was calculated for a monitoring node that yields the highest concentration at the 5 km fence. This curve is compared to the solution for the convolution code.

The convolution code requires a unit concentration breakthrough curve representing saturated-zone transport resulting from a constant mass flux applied over the repository footprint. This unit breakthrough curve was calculated using FEHMN, (the grid described above, the base-case flow field, and the same monitoring node). The convolution code also requires the time-dependent mass flux of tracer from the unsaturated zone, and the climate change information given in Table 8-15.

Figure 8-24 shows the breakthrough curves calculated with the transient FEHMN simulation and with the convolution integral code. The curves compare well, indicating the accuracy of the convolution integral code. The first two climate changes occur before there is significant breakthrough of solute mass. The convolution integral solution closely matches the small peak in concentration at about 7,000 years, resulting from the transition from climate state 2 to climate state 3. It should be noted that the accuracy of the convolution integral method may be sensitive to the time step employed in the numerical integration procedure implemented by the SZ\_CONVOLUTE code.

### 8.3.5 Alternative Climate States

Three alternative climate states were considered in SZ flow and transport analyses for TSPA-VA. These climate states were: 1) dry (present day conditions), 2) long-term average (corresponding to pluvial conditions), and 3) superpluvial (corresponding to glacial maximum conditions).

An abstraction method for alternative climate states, as they affect flow and transport in the SZ, was developed for utilization with the convolution integral method. A primary simplifying assumption was that groundwater flow in the SZ immediately changes to a new steady state following climate change, a reasonable assumption given the very large time-scale of interest (up to 1,000,000 years). Furthermore, climate change is assumed to proportionately alter groundwater flux throughout the SZ system, without significantly changing groundwater flow directions. This assumption is consistent with regional-scale SZ modeling results which indicate

that simulated climate changes produced only minor changes in groundwater flowpaths in the region near Yucca Mountain (D'Agnese et al. 1997b; Tucci 1998). Change in water table elevation in response to climate change is not considered in this abstraction of SZ flow and transport, in the sense that the model domain is not changed in response to alternative climate states. It is possible that, at the scale of the TSPS 3-D SZ flow model, the water table rise associated with climatic changes could redirect groundwater flow downgradient of the repository. A water table rise of less than 100 m would tend to place generally lower bulk permeability strata of the upper volcanic confining unit (Calico Hills Formation) at the water table beneath the repository, leading to slower movement of contaminants and potentially greater dispersive mixing. Thus, retaining the SZ domain and flow paths for ambient conditions during wetter climate states could be conservative, from the perspective of repository performance.

Changes in the magnitude of SZ groundwater flux were represented by a scaling factor for the three alternative climate states used in the TSPA-VA analyses (i.e., ambient, long-term average, and superpluvial). Scaling factors were employed because they could be derived from regional-scale SZ flow modeling, whereas the magnitude of groundwater flux for present conditions was taken from the SZ Expert Elicitation. These scaling factors were used directly in the convolution integral method to scale the unit concentration breakthrough curves employed in the convolution method. The breakthrough curves were scaled in terms of arrival times, corresponding to changes in groundwater velocity. The values of these SZ groundwater-flux scaling factors for the alternative climate states are given in Table 8-16. These scaling factors were based on the USGS regional-scale flow modeling of climate change (e-mail from Pat Tucci, 12/11/97; D'Agnese et al. 1997b) discussed in Section 8.2.2.1.

Changes in the volumetric groundwater flow rate through each of the 1-D SZ streamtubes for the three alternative climatic states were based on the UZ site-scale flow model simulations (Bodvarsson et al. 1997) for these climatic conditions. These values of volumetric groundwater flow rate are summarized in Table 8-14. Because radionuclide concentration at the inlet of each streamtube is defined by radionuclide mass flux and volumetric groundwater flow rate, the simulated radionuclide concentrations from the convolution integral method are scaled relative to the changes in volumetric groundwater flow rate for alternative climatic states. This approach conserves the average radionuclide concentration from groundwater flowing from the UZ at the inlet of each streamtube in the SZ (i.e., at the water table). This scaling is performed in the SZ\_CONVOLUTE computer code. It is interesting to note that the scaling factor for volumetric groundwater flow rate through the UZ at Yucca Mountain exceeds the scaling factor for specific discharge in the SZ for wetter climatic states. For example, in changing from dry conditions to the long term average climate state, the specific discharge in the SZ is simulated to increase by a factor of about 3.9 and the volumetric groundwater flow rate through the UZ at the water table increases by a factor of about 5.4.

### **8.3.6 Assumptions**

The assumptions used in the base-case analyses of SZ flow and transport implicitly include assumptions employed in the USGS regional-scale flow model and the TSPA flow and transport models (see Sections 8.2.2.1, 8.3.2, 8.3.3), as well as additional assumptions associated with transport modeling and abstraction of results.

Major assumptions in the USGS regional-scale flow model are described in detail in D'Agnese et al. (1997a). The assumptions most relevant to TSPA-VA analyses are summarized here. Groundwater flow was assumed to occur under approximately steady-state conditions, disregarding any transience in the system in response to groundwater pumpage or changing climatic conditions. The spatial distribution of recharge potential was assumed to conform to a modified Maxey-Eakin method (D'Agnese et al. 1997a, pp. 52 – 55). Discharge from the regional-flow system has been estimated from measurements of spring flows, records of well pumpage, and remote sensing methods. The numerical modeling assumes porous-medium behavior of the hydrogeologic units, which are assigned homogeneous hydrologic properties. Underflow out of the regional-scale model domain was assumed to be negligible. Modeling of alternative climate states with the regional-scale SZ flow model (D'Agnese et al. 1997b) included additional assumptions regarding the distributions of recharge and discharge for the system. For the higher values of potential recharge under wetter climatic conditions (particularly the superpluvial case), significant amounts of recharge were rejected in the model at higher elevations because of limitations in hydraulic conductivity in the model. It was assumed that this rejected recharge did not enter the SZ flow system. Redistribution of recharge and discharge by surface water was not included in the model.

The TSPA 3-D SZ flow modeling assumptions are described in Section 8.3.2 of this report. Relevant assumptions include steady-state conditions and single continuum (i.e., equivalent porous medium) behavior. The top boundary (i.e., the water table) was assumed to be no-flow, with the exception of upper Fortymile Wash. The groundwater flux resulting from distributed infiltration and recharge was assumed to be negligible in relation to the magnitudes of lateral groundwater flux in the SZ. Distributed recharge was not included in the model, but focused recharge along upper Fortymile Wash was specified in the model. Well pumpage was not included in the TSPA 3-D SZ flow model. The lateral boundaries are not natural boundaries of the flow system (e.g., no-flow or constant head controlled by surface water features). However, lateral boundaries were assumed as constant head (or pressure), which is acceptable provided that reasonable groundwater flux is simulated to occur in the system. No groundwater flow was assumed to occur across the bottom boundary of the model, at a depth of 950 m below the water table. Hydrogeologic units were designated on the basis of lithology and previous groundwater flow modeling (Czarnecki et al. 1998). The hydrogeology was divided into major aquifer units and confining units, similar to that of Winograd and Thordarson (1975, pp. 13-14) (Section 8.2.1.2). Permeability was assumed to be uniform within hydrogeologic units in the model domain. Three linear, vertical, low-permeability features to the west and north of Yucca Mountain were assumed to control the high- and moderate-hydraulic gradient regions observed near the Yucca Mountain site. Isothermal conditions were assumed in the TSPA SZ flow model.

The TSPA 1-D SZ transport model assumptions related to flow are directly related to the assumptions in the TSPA 3-D SZ flow model. The main difference between the two TSPA models in terms of flow assumptions is that the transport model is only one-dimensional. Due to the geometric differences, the boundary conditions are also different; a constant groundwater flux was applied at the upstream end of the stream tube, and no flow boundaries were implicit on the sides of the stream tube. Four of the hydrogeologic units found in the TSPA 3-D flow model were included in the TSPA 1-D transport model. A unit specified solute-mass-flux continuous-source boundary condition at the upstream end of the stream tube was assumed.

The effective porosity conceptual model employed in the TSPA 1-D SZ transport simulations assumes that the complex processes of fracture flow and matrix diffusion of solutes are approximated by a single continuum, consisting of some fraction of the total volume of the medium. In actuality, the effective porosity of the flow system is a complex function of the groundwater velocity, travel distance, and the degree of channelization of groundwater flow in the system (Zyvoloski et al. 1997, p. 5-2). The effective porosity conceptualization is assumed to apply to solute storage in matrix pore water and to solute retardation by sorption on the aquifer medium.

For radionuclide transport, there is uncertainty about the radionuclide travel path and the groundwater flux. Variations in travel path were accounted for in the TSPA 1-D transport model by assuming that the percentage of travel path through the alluvium is a stochastic parameter (Section 8.4.2). Conversely, the groundwater flux was assumed to be constant. These input parameter assumptions were justified by the fact that in terms of repository performance, travel path (due to different hydrologic properties such as effective porosity among the units), and groundwater flux both affect the radionuclide travel time through the SZ. In porous media (the alluvium), the effective porosities are greater than in the fractured medium (volcanic units). Because of the smaller effective porosity, travel times tend to be shorter in the volcanic units than in the alluvium (Figure 8 - 1). The broad range in the uncertainty in effective porosity considered in the SZ analyses is very large relative to uncertainty in groundwater flux. Therefore, it was decided to treat groundwater flux as a constant.

Hydrodynamic dispersion of radionuclides was assumed to occur using the advection-dispersion model of solute transport (Fetter 1993, pp. 52-54). Dispersivity was defined in the longitudinal direction relative to groundwater flow in the TSPA 1-D transport model. Dispersive dilution of solutes is assumed to occur by molecular diffusion and by hydrodynamic dispersion as a function of groundwater velocity. Transverse dispersion, (spreading of the plume perpendicular to the travel path) was precluded by the one-dimensional nature of the TSPA transport model. Transverse dispersive mixing was implicitly considered through the dilution factor, which was applied to radionuclide concentrations at the 20 km distance.

The linear, equilibrium sorption model was assumed for those radionuclides which exhibit sorption on mineral grains. This model assumes chemical equilibrium between the aqueous phase and sorbed phase of a given species. It also allows effectively unlimited sorptive capacity on the mineral grains. All radionuclides in the aqueous phase are assumed to be below the solubility limit (i.e., precipitation of radionuclides into solid phase is assumed not to occur).

Colloid-facilitated Pu transport in the SZ was assumed to occur by two modes: 1) by equilibrium sorption of Pu onto mobile colloids and 2) by irreversible sorption of Pu onto mobile colloids. An equilibrium colloid-facilitated Pu transport model was employed to simulate transport of Pu by the first mode in the SZ (Robinson et al. 1997, pp. 8-28 and 8-46). This model of colloid-facilitated transport assumes that radionuclides are reversibly sorbed onto colloid particles and also interact with sorptive minerals in the matrix or fracture walls (Sections 8.2.3.3 and 8.4.2). Measurements of the partition coefficients for Pu sorption onto colloids and mineral grains supporting equilibrium sorption behavior are available from laboratory experiments (Triay et al. 1997). Colloid-facilitated Pu transport by the second mode simply means that Pu is either permanently attached to the colloids or incorporated into the colloidal particle. Relatively fast

colloid-facilitated Pu transport by irreversible sorption (or slow desorption) onto colloids is supported by observations in the SZ on Pahute Mesa (Thompson et al. 1998). The fraction of Pu mass associated with each of these two transport modes was a stochastic parameter that was determined in the waste form degradation component (not in the SZ component) of the TSPA-VA analyses. The uncertainty distribution for the fraction of irreversibly sorbed Pu and its basis are described in Chapter 6.

Colloids were assumed to travel at the velocity of groundwater in fractures. Thus, the uncertainty distribution of effective porosity for both colloid-facilitated Pu transport modes was specified to reflect uncertainty in fracture porosity only. The effects of potential colloid filtration were not explicitly included in the base-case model of colloid-facilitated Pu transport. The conservative assumption was made that the effects of colloid filtration were negligible for both modes of colloid-facilitated Pu transport. The implications of the assumptions used in both modes of the colloid-facilitated Pu transport model were examined in sensitivity studies employing an alternative, reactive colloid transport model in Section 8.5.2.5.

In the transport analyses of the TSPA 1-D SZ transport model, it was assumed that radionuclide mass flux from the UZ was uniformly dissolved in the volumetric groundwater flow rate within each of the six streamtubes. This assumption is valid for times during which many (hundreds) of leaking containers contribute to the radionuclide mass flux at the water table and the repository approximately resembles a smeared source. For early simulated times during which only a few containers are leaking, the assumption of a homogeneous, smeared radionuclide source is less valid. In reality, a few discrete contaminant sources would result in significant variability in radionuclide concentrations within a single streamtube that would not be resolved in the TSPA 1-D transport model. However, there could be significant implicit homogenization of radionuclide concentrations within a streamtube from pumping at the hypothetical withdrawal well. If the discharge from the hypothetical withdrawal well exceeds the volumetric groundwater flow rate through a streamtube (about 2000 to 10,000 m<sup>3</sup>/yr for dry climatic conditions), then homogenization of radionuclides within the streamtube is approximately valid.

Several important assumptions are required for application of the convolution integral method in coupling the UZ transport with SZ flow and transport. Groundwater flow in the SZ was assumed to be in steady state, as already assumed by the TSPA flow and transport models. Instantaneous changes from steady state to alternative steady state (based on assumed climate changes) were assumed to occur in the convolution method as described in Section 8.3.4. The response in concentration in the SZ flow and transport model must be linear in relation to the solute source term in the convolution method. A more detailed discussion of the assumptions and limitations of the convolution integral method is presented in Zyvoloski et al. (1997, pp. 6-7 and 8).

### **8.3.7 Implementation With the RIP Computer Code**

Incorporation of the SZ flow and transport component into the TSPA-VA probabilistic analyses occurred in the following way. For a particular TSPA-VA realization implemented by the RIP simulator, the SZ flow and transport realization with the closest value of the  $K_c$  parameter to that used in the UZ transport calculation for the equilibrium colloid-facilitated Pu transport model was selected. This selection was performed to assure consistency between the UZ transport and SZ transport components with regard to the colloid-facilitated Pu transport model. All other

stochastic parameters were considered to be independent between the SZ and other components of the analysis. The results of that particular SZ flow and transport realization were read from the files containing those radionuclide unit-concentration breakthrough curves from the library of all SZ results.

At each time step within the RIP simulation, the current climate state and the radionuclide mass flux at the water table for each of the radionuclides at each of the six source subregions (see Section 8.4.1.3 for description of source subregion designation) were passed to the convolution integral subroutine. The convolution integral subroutine calculated the concentration of each radionuclide for each of the six streamtubes at a 20 km distance from the repository for that time step, including reduction in concentration from the dilution factor. The concentrations for each radionuclide were summed among the six streamtubes. The sum was compared to the maximum undiluted concentration for that radionuclide from among the six streamtubes. If the sum of concentrations from the six streamtubes exceeded the maximum undiluted concentration (a physically unrealistic case), then the maximum undiluted concentration was used as the simulated concentration at that time step for that radionuclide. Otherwise (as usually occurred), the sum of concentrations was less than the maximum undiluted concentration and the sum was used as the simulated concentration at that time step. The simulated radionuclide concentrations were passed by the RIP simulator to the biosphere component of the TSPA-VA at this point for dose calculation.

## **8.4 SZ FLOW AND TRANSPORT BASE CASE**

Base-case analyses of flow and transport in the SZ primarily focused on the uncertainty in transport parameters. Although considerable uncertainty about groundwater fluxes and flowpaths exists, uncertainty in the radionuclide transport properties of the SZ was considered to be of primary importance to repository performance in this component of the system. Multiple realizations of the SZ transport model were constructed to encompass the uncertainty distributions of parameters that define the transport characteristics of the SZ groundwater system. Uncertainty in flowpaths was implicitly considered in the base case by making the fraction of flowpath in the alluvium a stochastic parameter in the TSPA 1-D transport model.

### **8.4.1 Description of the Base Case**

The base case for the SZ flow and transport component of the TSPA-VA, as with other components of the analysis, consisted of a single, expected-value case of the TSPA 1-D transport model and of a suite of multiple, probabilistic realizations of the transport model. The expected-value case was constructed using the expected value for all of the stochastic parameters. The expected value was taken as the mean of some uncertainty distributions; the mean was taken in log space for those parameters that were log transformed to define the distribution. For uncertainty distributions defined by a cumulative distribution function (e.g., the dilution factor from the Expert Elicitation), the expected value was taken as the median of the distribution. The probabilistic realizations consisted of 100 realizations of the stochastic parameters that were randomly sampled using stratified sampling methods (Section 8.4.2). The expected-value case was used for TSPA-VA runs to evaluate the "probable" behavior of the system as a single realization. The probabilistic realizations were used to evaluate the range of uncertainty in the system behavior.

#### 8.4.1.1 Scenarios

The base-case analyses of SZ flow and transport explicitly include some scenarios and implicitly include other scenarios through the ranges of uncertainty in some parameter values. Undisturbed groundwater flow is assumed for ambient climatic conditions. As noted earlier (Section 8.3.5), alternative climatic conditions were simulated by scaling specific discharge and volumetric groundwater flow rate within the streamtubes of the TSPA 1-D transport model. Consequently, climatic variation is a scenario considered in the base case, but only in terms of alterations to the magnitude of groundwater flux. Alteration of SZ groundwater flow paths and potential new sites of groundwater discharge at springs in response to wetter climatic conditions were not considered in the base-case analysis. Exclusion of these possible scenarios was based on results of regional-scale SZ flow modeling (D'Agnese et al. 1997b) that indicated little alteration of flow paths under pluvial conditions. This model also indicated no significant natural groundwater discharge within 20 km downgradient of Yucca Mountain during the long-term average climate, although natural discharge was simulated to occur in lower Fortymile Wash and along the Amargosa River channel just beyond the 20 km limit (Figure 8 - 12).

Colloid-facilitated transport of Pu was implicitly included as a scenario in base case analyses of SZ flow and transport. The range of input parameter values for fracture porosity and Pu colloid partition coefficient, which control Pu transport for the fraction of Pu subject to equilibrium sorption onto colloids (Section 8.4.2), results in Pu transport ranging from relatively rapid Pu breakthrough to very long travel times. The range of input parameters for the irreversibly sorbed Pu fraction results in relatively rapid Pu transport, for varying fractions of the total Pu source. Thus, the two bounding scenarios (and intermediate cases) of 1) relatively rapid colloid-facilitated transport of significant concentrations of Pu and 2) no significant colloid-facilitated transport are included in the base-case analyses.

Similarly, the range of values of effective porosity employed in base-case analyses of SZ flow and transport spans the range for alternative scenarios of matrix diffusion. The lower values of effective porosity used in the simulations correspond to little or no matrix diffusion in fractured tuffs and the higher values of effective porosity correspond to substantially complete solute diffusion into the volcanic rock matrix (Section 8.4.2). The implications of the range of effective porosity are further explored in the sensitivity analysis using the dual-porosity model (Section 8.5.2.3).

There are numerous proposed scenarios relevant to flow and transport in the SZ that have not been evaluated in the base-case analyses. Potential alterations of the bedrock medium in the SZ in response to repository heat and/or chemical output were not considered (see also Section 8.2.3.4). These potential alterations might include changes in bulk permeability and sorptive properties of the medium in response to mineral dissolution/precipitation and mineralogic compositional changes. Also, changes in groundwater flow rates and pathways in response to repository heat were not considered in base-case analyses. Alterations of the SZ flow regime resulting from disruptive volcanic and seismic events are scenarios that were not included in the base case. Transient increases in water table elevation from earthquakes were excluded on the basis of previous modeling studies (Carrigan et al. 1991; Bredehoeft 1992, p. 222). Movement of the large hydraulic gradient from its present location north of Yucca Mountain was excluded as a scenario in the base-case analyses on the basis of the SZ Expert



Elicitation results (CRWMS M&O 1998, pp. 4.2-4.3), indicating that such an event is very unlikely. Scenarios that include anthropogenic alterations to the SZ flow system through future groundwater pumpage were not evaluated in the base case. Exclusion of such scenarios is consistent with biosphere modeling in the TSPA-VA that was based on present-day water usage and population characteristics. Control of groundwater flow by faults or other high-permeability channelization features under ambient or disturbed conditions is not evaluated as a scenario in the base-case analyses, but is evaluated in sensitivity studies (Section 8.5.2.2).

#### **8.4.1.2 Uncertainty**

Uncertainty in radionuclide transport through the saturated zone was incorporated into the analysis by varying key transport parameters. The stochastic parameters used in the one-dimensional transport simulations were: 1) effective porosity in the volcanic units and the alluvium/undifferentiated valley-fill unit, 2) distribution coefficients ( $K_{ds}$ ) for sorbing radionuclides in the volcanic and alluvial units, 3) the ratio of the radionuclide mass in aqueous and colloidal forms ( $K_c$ ) for colloid-facilitated transport of plutonium, 4) longitudinal dispersivity, 5) the fraction of flowpath through the alluvium, and 6) the dilution factor.

Colloid-facilitated transport of plutonium in the saturated zone was simulated using a conceptual model based on both equilibrium, reversible sorption of plutonium onto colloids, and the potential for irreversible sorption of plutonium onto some colloidal particles (see Section 8.2.3.3). These two components of plutonium transport were included in the analysis. A large fraction of the plutonium mass was simulated to move through the saturated zone assuming chemical equilibrium among dissolved plutonium, plutonium sorbed onto colloids, and plutonium sorbed onto the aquifer material. This conceptual model uses the partition coefficient ( $K_c$ ) to define the distribution of plutonium sorbed on colloids relative to the aqueous concentration of plutonium. A small fraction of the plutonium mass was simulated to be irreversibly attached onto colloids and transported relatively rapidly in the saturated zone, without significant retardation. The fraction of Pu subject to irreversible sorption onto colloids was assigned for each realization in the waste form degradation component of the TSPA-VA. The rationale for this stochastic parameter is described in Chapter 6. Colloid transport occurred only within the fracture porosity of the volcanic units, so the uncertainty distribution of effective porosity for colloids varied only over the estimated range of fracture porosity.

The stochastic parameters in the probabilistic analyses for saturated zone flow and transport in the TSPA-VA are summarized in Table 8 - 19. The dilution factor was applied to radionuclide concentrations to implicitly account for transverse dispersion out of the one-dimensional streamtubes. The uncertainty distribution for the dilution factor was a product of the Expert Elicitation described in Section 8.2.3.2. The travel distance through the alluvium/valley fill unit was varied from 0 to 6 km, with a 10-percent probability that no alluvium is present along the 20 km of travel path for radionuclides in the saturated zone.

#### **8.4.1.3 UZ Source Subregions**

Transport of radionuclides in the SZ was simulated to occur from six separate source subregions at the water table below the potential repository (Figure 8 - 25). These subregions were defined on the basis of 1) relative position in the repository (e.g., edge vs. center), 2) variability in UZ

transport characteristics (e.g., spatial distribution of pervasive zeolitic alteration), and 3) geologic variability in the SZ (e.g., location relative to the water table of the welded portion of the Bullfrog Tuff at subregion 1, which may act as a preferential flow pathway). The six subregions correspond to areas at the lower boundary (i.e., the water table) of the UZ transport model. It should be noted that the six source subregions used in the SZ were independent of the zonation of the repository used in the waste-package degradation component of the TSPA-VA. The radionuclide mass flux, as a function of time, was subdivided on the basis of these subregions as output from the UZ transport simulations. Separate unit concentration breakthrough curves were derived using the TSPA 1-D transport model for each radionuclide from each of the six, source subregions for use in the convolution integral method.

Because of eastward lateral diversion of groundwater flow in the UZ, the eastern boundary of subregions 2, 5, 6 were extended as indicated in Figure 8 - 25. The eastern boundary was adjusted so that the total simulated UZ groundwater flux at the water table was approximately equal to the simulated UZ flux through the repository. The volumetric groundwater flow rate for each of the six, source subregions, with the extended eastern boundary, into the six SZ streamtubes was simulated with the UZ site-scale flow model (Bodvarsson et al. 1997; DTN # SNT05091597001.009).

The value of radionuclide concentration in the center of the simulated contaminant plume at 20 km at a given time is calculated by superposition of solutions from the six source subregions. The total concentration is thus the sum of the diluted values of concentration from the six source subregions, as calculated individually by the convolution method, except when the sum exceeded the maximum undiluted concentration from among the streamtubes. This aspect of the TSPA-VA calculations is performed within the RIP code, as explained in Section 8.3.7. This approach, though not an exact physical representation of the system, was chosen as a conservative method for combining the results of the six streamtubes. The approach was chosen from a limited number of options because it is demonstrably conservative, unlike the other available options. This approach was examined relative to other options using an idealized, analytical solution for SZ transport, as presented in the sensitivity studies of Section 8.5.2.1.

#### **8.4.1.4 Transport Modeling**

Radionuclide transport was simulated in the TSPA 1-D SZ transport model by the FEHMN computer code using the finite-element solution method (Zyvoloski et al. 1995) to generate unit breakthrough curves at a distance of 20 km from the repository (Figure 8 - 22). A unit radionuclide specified-flux source (i.e., 1 g/y) was applied at the upstream end of the TSPA 1-D transport model at the beginning of the simulation and was held constant for the duration of the simulation (20,000 to 1,000,000 years, depending on the potential for retardation of a given radionuclide).

The effects of transverse dispersion were implicitly included in the analysis by incorporation of the dilution factor as a post-processing step. The simulated concentrations (as a function of time) were scaled by dividing by the dilution factor for the entire breakthrough curve. The concentrations were also scaled by a geometric factor, which was a function of the volumetric groundwater flow rate (and thus, the cross-sectional area) of each of the six streamtubes. The TSPA 1-D transport model was constructed with a 1 m<sup>2</sup> cross-sectional area. The cross-sectional

areas of the actual SZ streamtubes were calculated as the ratio of volumetric groundwater flow rate for that streamtube divided by the specific discharge. The geometric factor for each streamtube was thus simply the cross-sectional area of that streamtube and the concentrations simulated with the 1 m<sup>2</sup> model divided by the geometric factor to obtain the concentrations in the actual streamtube. These scaling factors were combined and included as a header in the concentration breakthrough curve files by the postprocessing computer code POSTCON. The computer code POSTCON also reformatted the output of simulated concentrations from the FEHMN output files.

For the base-case analyses, transport of nine radionuclides was simulated in the SZ. These radionuclides were chosen on the basis of significance to total radiological dose as demonstrated in previous TSPA calculations. See Chapter 6 of this report for an explanation and justification for the suite of radionuclides considered in the TSPA-VA analyses. These radionuclides are the same as those tracked in the upstream components of the TSPA-VA analyses. The radionuclides are <sup>14</sup>C, <sup>129</sup>I, <sup>237</sup>Np, <sup>231</sup>Pa, <sup>239</sup>Pu-reversible, <sup>242</sup>Pu-reversible, <sup>239</sup>Pu-irreversible, <sup>242</sup>Pu-irreversible, <sup>79</sup>Se, <sup>99</sup>Tc, and <sup>234</sup>U. Radioactive decay was simulated (within the SZ-CONVOLUTE subroutine) for all radionuclides with half lives of less than 1,000,000 years. Ingrowth of radionuclides was not included in the SZ transport calculations. However, the inventories of some radionuclides progeny were adjusted upward to implicitly and conservatively account for ingrowth at the source, as explained in Chapter 6. This method of implicitly accounting for ingrowth at the source is non-conservative (from a repository performance perspective) for cases in which the parent radionuclide is potentially less strongly sorbed than the daughter product (e.g., <sup>235</sup>U decaying to <sup>231</sup>Pa) during transport in the SZ. An improved and conservative method for the analysis would be to simulate transport of the significant parent radionuclides and assume secular equilibrium with progeny at the hypothetical pumping well.

#### **8.4.2 Development of Parameter Distributions and Uncertainty**

Uncertainty in radionuclide transport through the SZ was incorporated into the TSPA-VA by varying key transport parameters for 100 realizations (Section 8.4.1.2). All input parameters required for the TSPA 3-D SZ flow model and the TSPA 1-D SZ transport model were assumed to be either stochastic with an associated distribution or constant. If the parameter was assumed to be stochastic, its distribution was determined and then sampled using the Latin Hypercube Sampling (Wilson et al. 1994, pp. 3-19 to 3-21) module (an efficient type of Monte Carlo sampling) of the RIP code to obtain 100 sets of input parameter values. Latin Hypercube Sampling was performed using RIP prior to performing the TSPA 1-D SZ transport model calculations. This sub section describes the method used to determine the uncertain parameter distributions, and documents all input values for both stochastic and constant parameters used in the TSPA-VA SZ base-case analysis.

Extensive statistical parameter distribution analyses for the volcanic units in the saturated zone have been performed (Schenker et al. 1995, pp. 31-62). Schenker et al. (1995) determined all of the input parameter distributions, including the SZ, for the TSPA-93 analysis. However, the Schenker et al. (1995) work was not directly applicable to the TSPA-VA SZ analysis because the hydrogeologic modeling units assumed for the TSPA-VA base case are different from the previous TSPA hydrogeologic modeling units. For the TSPA-VA, the USGS site-scale flow-model hydrogeologic units, defined by Czarnecki et al. (1998) according to hydraulic flow

properties, were the basis for the TSPA 3-D SZ flow and TSPA 1-D SZ transport model hydrogeologic framework (see Table 8 - 8) and for this parameter development analysis.

The saturated zone Expert Elicitation conducted during the summer of 1997 (see Section 8.2.3.2) also provided information regarding input parameter values and distributions. Input was solicited from five experts (Drs. Allan Freeze, Lynn Gelhar, Don Langmuir, Shlomo Neuman, and Chin-Fu Tsang) about the flow and transport system at Yucca Mountain to assist in the performance assessment process. The experts also assisted in generating parameter uncertainty ranges for the saturated zone, and, if possible, their distributions, with a focus on an assessment of uncertainty (CRWMS M&O, 1998). The experts provided distributions for several parameters based on available site data. All expert distributions for a parameter were then combined into one aggregate distribution (CRWMS M&O, 1998, pp. 2-11 - 2-12).

All available information was used to develop the input parameters for the TSPA-VA SZ base case. The main resource was recommendations about parameter distributions provided during the SZ Expert Elicitation (CRWMS M&O, 1998). However, if the Expert Elicitation did not provide guidance for a particular input parameter, then site data were used in a statistical analysis to either develop parameter distributions or constants. If site data were not available, then other sources from the literature were used to assist in developing the parameters.

For the statistical analysis, the TSPA 1993 data sets of Schenker et al. (1995) were modified to include additional data collected since 1993 (Geldon et al. 1997, pp. B-2, B-5, B-11, B-13; Flint 1998; LeCain 1997) and some data that were not originally included in the 1993 analysis (Montazer et al. 1985). The data were sorted according to hydrogeologic unit, based upon data measurement location within the borehole. Data from field and laboratory tests were available, mainly for the volcanic units. There was limited information about the carbonate units and very few, or no measurements for the alluvium and clastic units in the Yucca Mountain area, depending on the particular hydrogeologic unit and parameter. *STATISTICA*®, a statistical software package (StatSoft, Inc. 1997), was used to calculate the statistical properties for the sub-groups of data (i.e., data for each of the hydrogeologic units) and the type of distribution (i.e., normal, log-normal, etc.) that best fit the data.

The only hydrologic parameter required as input to the TSPA 3-D SZ flow model was bulk permeability. Porosity, bulk density, sorption coefficients ( $K_{ds}$ ),  $K_c$  for plutonium colloids, dilution factor, the fraction of the flow path in alluvium, and dispersivity were the parameters required to perform transport calculations using the TSPA 1-D SZ transport model.

**Permeability** - Permeability has a direct affect on the calculated radionuclide travel time, and could possibly alter the contaminant flow path. As previously discussed in Sections 8.2.3.3 and 8.3.6, flow was assumed to occur as a single continuum in the TSPA-VA base-case SZ analysis. Therefore, bulk permeability, or the combined permeability of fractures and matrix, was used to perform calculations. The bulk permeability was measured by single- and multi-hole aquifer tests (see Section 8.2.1.2) and by air permeability measurements in unsaturated regions of the upper volcanic aquifer.

Aquifer-test data sets from the Yucca Mountain vicinity as well as the aggregate distributions for hydraulic conductivity recommended by the experts (CRWMS M&O 1998, pp. 3.7-3.8) indicate

that bulk permeability is a highly variable parameter and could differ by several orders of magnitude within a modeling unit (Figure 8 - 26 and Figure 8 - 27). For example, permeabilities of the volcanic aquifers range over four orders of magnitude. Although large variability in permeability may affect saturated zone results, bulk permeability was treated as a constant parameter for the base-case analysis, and all units for the base case were assumed to be isotropic (see Section 8.2.3.3).

The constant bulk permeability values used in the TSPA 3-D SZ flow model are listed in Table 8 - 12. The expected value from the aggregate distribution provided by the Expert Elicitation, based on site data, was utilized when possible (i.e., bulk permeability of the 50<sup>th</sup> percentile on the aggregate CDF) (CRWMS M&O 1998, Figures 3-1d, 3-1h, 3-1k, 3-1n). Although the experts did not provide a distribution for the upper carbonate aquifer, it was assumed to be similar to the lower carbonate aquifer with the same bulk permeability. For some of the units that the experts did not specify a permeability distribution, the bulk permeability from the calibrated USGS site-scale flow model was used (i.e., the lava-flow aquifer, lower volcanic confining unit, and granitic confining unit). The remaining units (valley-fill confining unit, middle volcanic confining unit, lower volcanic aquifer, undifferentiated valley fill, upper clastic confining unit, lower clastic confining unit, and faults) were assigned bulk permeability values based upon analyst knowledge of the system and selecting the value which achieved the best TSPA 3-D SZ flow model calibration results (i.e., minimized head residuals) (see Section 8.3.2). The bulk permeability of the middle volcanic aquifer in particular was affected by this model calibration process.

**Fraction of Flow Path In Alluvium** - There is large uncertainty related to the fraction of flow path in the alluvium due to large uncertainties related to the actual location where the volcanic units pinch out and uncertainty related to the flow path simulated by the TSPA 3-D SZ flow model. The fraction of travel path through the alluvium parameter is important due to the different flow and transport properties of the alluvium and volcanic units (Table 8 - 12 and Table 8 - 17). Groundwater fluxes through the alluvium may be higher than through the volcanics due to higher permeabilities. But radionuclide travel times may be slower through the alluvium than through volcanic units due to larger effective porosities (see Section 8.2.3.3) and a larger sorption capacity for neptunium and selenium (Table 8 - 19).

The fraction of the flow path in alluvium was assumed to be a stochastic parameter due to its effect on SZ results and the large uncertainties associated with it. Deterministic output from the TSPA 3-D SZ flow model indicated that the 3-D flow path consisted of about 10% travel through alluvium. The assumed distribution for the fraction of the flow path in alluvium was a piecewise cumulative-distribution function with a range from 0 to 0.3 with an expected value of 0.15. The distribution was defined such that for 10% of the realizations there was no alluvium present along the travel path (e.g., fraction-of-flow path in alluvium equal to 0) (Table 8 - 19). This distribution was chosen to cover the entire range of uncertainty. No radionuclide travel through alluvium is conservative (i.e., faster travel times), although travel through some alluvium is probably more realistic. The low value for the range (0.1) was determined by the TSPA 3-D SZ flow model results, and the high value for the range (0.3) was defined as the largest reasonable value for the fraction, based upon knowledge of the hydrogeologic framework.

**Porosity** - The effective porosity, that portion of the pore space available for contaminant transport, is smaller than the combined total matrix and fracture porosity, and/or greater than or

equal to the fracture porosity. This is primarily due to dead-end pores, entrapped air, or limitations on matrix diffusion due to wide spacing between fractures that carry significant groundwater flow. For transport calculations, the effective porosity rather than matrix porosity was the input parameter used.

Effective porosity was estimated through the interpretation of some of the multi-hole tracer test conducted at the C-wells (Geldon et al. 1997). However, there is large uncertainty about the variability of effective porosity, particularly for the volcanic units. Effective porosity was assumed to be a stochastic parameter for the four units included in the TSPA 1-D SZ transport model (see Table 8 - 17).

Matrix porosity was required to estimate effective porosity values. To determine the matrix porosity values, a statistical analysis was performed using matrix porosity data collected through geophysical techniques in the borehole and laboratory core measurements provided by Flint (1998). Data distributions were developed for each hydrogeologic unit where data were available (Figure 8 - 28). According to the Kalmogorov-Smirnoff categorized test (Statsoft, 1997, p. NON-1617), a normal distribution fit the data best. A normal distribution was used and the mean for each unit was assumed to be the constant matrix porosity value, as shown in Table 8 - 17.

To determine the effective porosity distributions for the alluvium, the Expert Elicitation provided input. The experts suggested a truncated normal distribution with a mean of 0.25 for the alluvial aquifer (CRWMS M&O 1998, pp. 3-20). This distribution was used to sample effective porosities for the undifferentiated valley fill (Table 8 - 19).

The experts did not provide distributions for the effective porosity of the volcanic units. There is information about the matrix porosity from field and laboratory measurements and estimates of fracture porosities available from other analyses, but there are no data that provide insight to the possible distributions for effective porosity. The experts felt specific discharge and kinematic porosity would be lognormally distributed (CRWMS M&O 1998, p. 3-20 input from Freeze and Gelhar), with a lower bound for the fracture porosity of  $10^{-5}$  (CRWMS M&O 1998, p. 3-20 input from Gelhar). Given input from the experts and the large uncertainty about effective porosity, the distributions for the volcanic units were assumed to be triangular distributions in log-space with an upper bound equal to the expected value for matrix porosity (Table 8 - 17) and a lower bound of  $10^{-5}$  equal to the fracture porosity. The most likely value for this distribution was inferred to be 0.02, based upon input from Gelhar about kinematic porosity and distributions for specific discharge and average linear velocity from Freeze (CRWMS M&O 1998, p. 3-20).

**Bulk Density** - The bulk density was not expected to be a sensitive parameter, and for the base case it was assumed to be a constant value for each of the hydrogeologic units (Table 8 - 17). Bulk density is related to transport due to its effect on retardation factor as shown in Equation 8 - 3. The experts did not provide input pertaining to bulk density, and therefore, a statistical analysis was performed using laboratory core measurement data (Flint 1998; Rush et al. 1984; pp. 7-11; Lahoud et al., 1984) to determine the bulk density expected values. To assure consistency among the data measurements, only dry bulk density data were used in this analysis. Data distributions were developed for each hydrogeologic model unit where data were available (i.e., the upper volcanic aquifer, middle volcanic aquifer, and upper volcanic confining unit). A

normal distribution was assumed because the data distributions appeared to fit a normal curve based on results of the Kalmogorov-Smirnoff test (Statsoft, 1997, p. NON-1617). The mean for each unit was assumed to be the constant bulk-density value (Table 8 - 17).

Bulk density for the middle volcanic confining unit was assumed to be the same as the upper-volcanic confining unit, a unit with similar lithology. There were no bulk density data available for the undifferentiated valley fill. In this case, the expected value for bulk density was estimated from the relationship between particle density and matrix porosity (Hillel 1980 p. 14, Equation 2.17)

(8 - 2)

$$\rho_b = (1 - n)\rho_s$$

where  $\rho_b$  is the bulk density ( $\text{g/cm}^3$ ),  $n$  is the matrix porosity, and  $\rho_s$  is the particle density (assumed equal to  $2.65 \text{ g/cm}^3$  [Hillel 1980, p. 10]).

**Sorption Coefficient ( $K_d$ )** - A linear, equilibrium, sorption model ( $K_d$ ) was assumed for those radionuclides which exhibit sorption on mineral grains (neptunium, protactinium, selenium, and uranium). This model assumes chemical equilibrium between the aqueous phase and sorbed phase of a given species. The sorption coefficient is a highly uncertain parameter which can vary by several orders of magnitude. For the transport parameter development, it was assumed that model units were either volcanic or alluvial. Each TSPA 1-D SZ transport model unit was placed into one of these categories. As shown in Table 8-18, the designation "volcanics" includes the upper volcanic aquifer, middle volcanic aquifer, and middle volcanic confining unit while "alluvium" refers to the undifferentiated valley fill.  $K_d$  was assumed to be a stochastic parameter for neptunium, protactinium, selenium, and uranium in the volcanics and alluvium.

The experts did not provide  $K_d$  distributions for the volcanics or alluvium, however, they provided some guidance about sorption coefficient assumptions for neptunium in the volcanic, alluvial, and carbonate units (CRWMS M&O 1998, pp. 3-11-3-13, and 4-5 Langmuir input). The experts cautioned that it may not be appropriate to use laboratory derived  $K_d$  values without knowing how representative they are of field conditions, although it should be possible. They advised that a distribution of  $K_d$  values should be used, rather than taking a "minimum  $K_d$ " approach (CRWMS M&O 1998, pp. 3-22).

Input from Triay et al. (1997, p. 17) was used as the basis for selecting assumed parameter distributions for the volcanic units. Geochemical properties, whether a unit is predominantly devitrified, vitric, or zeolitic, are important to determine sorption characteristics (Triay et al. 1997). The volcanic units in the TSPA 1-D SZ transport model are comprised of a combination of devitrified, vitric, and zeolitic layers. Triay et al. (1997 Table 59) present  $K_d$  distributions for these three tuff types for several radionuclides of concern, based on laboratory batch and column studies performed on tuffs from Yucca Mountain (Triay et al. 1997, Table 59). For each radionuclide, it was assumed that the most conservative distribution (i.e., the distribution which had the lowest mean  $K_d$ ) from among the three types of tuff was assigned to all of the volcanic units (Table 8 - 19).

Information about sorption coefficients for alluvium was provided by a literature survey and analysis conducted by Thibault et al. (1990), where researchers compiled all available measured  $K_d$  data and calculated  $K_d$  distributions for sands, silts, and clays from the data they compiled. The  $K_d$ s for protactinium and selenium in alluvium were assigned a uniform distribution from 0 to an upper limit defined by the expected value for sand, reported by Thibault et al. (1990, Table 4), because there were limited data available (Table 8 - 19). Uniform distributions for neptunium and uranium in alluvium were assumed based upon the presence of oxidizing conditions and an assumption that the alluvium contains at least 5% calcite.

As discussed in Section 8.2.3.3, an effective porosity approach was assumed for the TSPA-VA base-case SZ analysis to describe the dual-porosity transport processes which occur in the saturated volcanic units at Yucca Mountain. The assumed effective porosity value for each unit was used as a surrogate for the matrix diffusion process which occurs in a dual-porosity system. Theoretically, within the FEHMN code the input  $K_d$  value is used to calculate a retardation factor (Zyvoloski et al. 1995, p.45, Equation 92)

(8 - 3)

$$R_f = 1 + \frac{\rho_b \cdot K_d}{n \cdot \rho_f}$$

where  $R_f$  is the retardation factor,  $\rho_b$  is the matrix bulk density ( $\text{g/cm}^3$ ),  $K_d$  is the sorption coefficient ( $\text{ml/g}$ ),  $n$  is the porosity, and  $\rho_f$  is the density of the fluid ( $\text{g/cm}^3$ ). The effective porosity approach assumes that the radionuclide is transported through some fraction of the matrix and likewise, the radionuclides are in contact with only some fraction of the total matrix that would be available for sorption. The effective porosity, a fraction of the matrix porosity, was used as the input porosity value for base case calculations. Mathematically, the  $K_d$  parameter describes the mass of solute on the solid phase per unit mass of solid phase divided by the concentration of solute in solution (Freeze and Cherry 1979, p. 405). If only a fraction of the matrix surface is available to use as sorption sites, then the  $K_d$  value should be scaled accordingly. Therefore, the actual  $K_d$  values were scaled, based upon the assumed effective porosity value that defined the reduced matrix surface area available for sorption.

The actual  $K_d$  values derived from the assumed  $K_d$  parameter distributions for the 100 realizations are shown in Table 8 - 20. Scaled  $K_d$  values were the input parameters for the TSPA 1-D SZ transport model. The scaled  $K_d$  value is equal to the actual  $K_d$  multiplied by a porosity conversion factor (e.g., the ratio between the effective porosity and the matrix porosity)

(8 - 4)

$$\hat{K}_d = K_d \cdot \left( \frac{n_{\text{eff}}}{n} \right)$$



where  $\hat{K}_d$  is the scaled value used as input (ml/g),  $K_d$  is the actual sorption coefficient listed in Table 8 - 19 (ml/g),  $[n_{eff} / n]$  is the porosity conversion factor,  $n_{eff}$  is the effective porosity used as input and  $n$  is the matrix porosity.

For the volcanics, the porosity conversion factor was equal to the average of the three different porosity conversion factors for the volcanics

(8 - 5)

$$n_{CFV} = \frac{(n_{effUVA} / n_{UVA}) + (n_{effMVCU} / n_{MVCU}) + (n_{effMVA} / n_{MVA})}{3}$$

where  $n_{CFV}$  is the porosity conversion factor for volcanic units, the subscript *UVA* represents the upper volcanic aquifer, *MVCU* is the middle volcanic confining unit, and *MVA* is the middle volcanic aquifer. The porosity conversion factor for the alluvium is simply:

(8 - 6)

$$n_{CFA} = \frac{n_{effAL}}{n_{AL}}$$

where  $n_{CFA}$  is the porosity conversion factor for alluvium, and the subscript *AL* indicates alluvium.

**K<sub>c</sub> Parameter** - Plutonium was assumed to be transported only as a colloid for base-case TSPA-VA calculations, where both reversible and irreversible colloids were included. Assumptions about simulating colloid transport in the saturated zone are discussed in Section 8.2.3.3.

The TSPA 1-D SZ transport model did not include an explicit module for accounting for colloid transport at the time of base-case calculations, but Robinson et al. (1997, pp. 8-32 to 8-36) revised the current model to implicitly account for colloid transport through modification of the sorption coefficient parameter. Based upon the methodology described by Robinson et al. (1997), an adjusted sorption coefficient for plutonium in solution ( $\hat{K}_d[Pu]$ ) was the required input parameter for saturated zone colloid calculations. There is great uncertainty about the value for  $\hat{K}_d[Pu]$ , most of which comes from large uncertainty about the  $K_c$  parameter. For the reversible plutonium colloids ( $^{239}Pu$  and  $^{242}Pu$ ),  $K_c$  was assumed to be a stochastic parameter. For the irreversible plutonium colloids ( $^{239}Fm$  and  $^{242}Fm$ ), the  $\hat{K}_d[Pu]$  parameter was assumed to be equal to zero (e.g., that plutonium is always sorbed onto the colloid).

$K_c$  was defined as the ratio of the contaminant mass sorbed onto a mobile colloid versus dissolved contaminant mass present in solution (Robinson et al. 1997, p. 8-35).  $K_c$  is equal to the product of the distribution coefficient for contaminant on colloids and the concentration of colloidal material available for sorption (mass of colloids per unit fluid volume) (Robinson et al. 1997, p. 8-35):

(8 - 7)

$$K_c = K_{dcol} \cdot C_{col}$$

where  $K_{dcol}$  is the sorption coefficient on colloids and  $C_{col}$  is the concentration of colloids in the groundwater.

Colloid sorption data (i.e.,  $K_{dcol}$  and  $C_{col}$ ) were only available for the volcanic units, and the distribution for  $K_c$  was assumed for both the volcanics and the alluvium (Table 8 - 19). It is possible that the types of colloids and their concentrations are different in the alluvium than in the volcanic units, but information from the alluvial aquifer is not available. Any differences in colloid-facilitated Pu transport in the alluvium are probably encompassed in the broad range of the uncertainty distribution for  $K_c$ . For the reversible case, the assumed distribution for  $K_c$  was log-uniform ranging from  $10^{-5}$  to 10 to account for the large range in uncertainties related to both  $K_{dcol}$  and  $C_{col}$  in the saturated zone at Yucca Mountain. The basis for the uncertainty in  $K_c$  is described in Chapter 6.

The effective retardation factor accounting for the presence of colloids is (Robinson et al. 1997, Equation 8-10, p. 8-36):

(8 - 8)

$$\hat{R}_f = \frac{R_f + K_c R_c}{1 + K_c}$$

where  $R_f$  is the retardation factor for aqueous plutonium (see Equation (8 - 3),  $K_c$  is the plutonium colloid partition coefficient, and  $R_c$  is the colloid filtration factor which was assumed to be equal to 1 (i.e., no filtration). A value of 100 ml/g was assumed for the  $K_d$  of aqueous Pu to calculate the value of  $R_f$  using Equation 8 - 3.

By rearranging Equation (8 - 3, the  $\hat{K}_d[Pu]$  parameter was assumed to be equal to:

(8 - 9)

$$\hat{K}_d[Pu] = \frac{n_{eff} \rho_f (\hat{R}_f - 1)}{\rho_b}$$

where  $\hat{K}_d[Pu]$  is the effective sorption coefficient for plutonium considering colloid transport;  $n_{eff}$  is the effective porosity;  $\rho_f$  is the fluid density;  $\hat{R}_f$  is the effective retardation factor for plutonium considering colloid transport, as defined by Equation (8 - 8); and  $\rho_b$  is the bulk density of the medium.

For input to the TSPA 1-D SZ transport model, the  $\hat{K}_d[Pu]$  parameter was scaled in a manner similar to the  $K_d$  parameters described above due to the effective porosity approach assumed in the base case:

(8 - 10)

$$\hat{K}_d[Pu] = \hat{K}_d[Pu] \cdot n_{CFV}$$

where  $\hat{K}_d[Pu]$  is the scaled effective plutonium sorption coefficient accounting for colloid transport, and  $n_{CFV}$  is the volcanic effective porosity. The volcanic effective porosity was used to calculate the scaled  $\hat{K}_d[Pu]$  for the volcanics and alluvium because it was assumed that colloid movement only occurred in the fractures. Although the alluvium was not fractured, it is not known to what degree that colloids would be channelized during transport through the alluvium.

**Longitudinal Dispersivity** - The longitudinal dispersivity is another variable and uncertain parameter which increases with increased contaminant travel distance (Gelhar 1986, pp. 135S-145S). Stochastic parameter values were assumed for each of the hydrogeologic units. All units were assumed to have the same dispersivity value, because there were no data or recommendations to distinguish between the volcanic and alluvial units.

Recommendations from the Expert Elicitation were used as the basis for determining the distribution for longitudinal dispersivity. Gelhar is the recognized expert in this area, and he provided distributions for the longitudinal dispersivity at 5 km and 30 km (CRWMS M&O 1998, p. 3-21). These distributions for longitudinal dispersivity are consistent with his previous work (Gelhar 1986, pp. 135S-145S). Neuman also provided a rough "rule of thumb" for estimating a point dispersivity value. Expected values for longitudinal dispersivity calculated with this rule of thumb are comparable to the mean values presented by Gelhar. The distributions provided by Gelhar for longitudinal dispersivity at 30 km were used for the base-case analysis based on the assumption that his estimates for 30 km would be applicable for the TSPA-VA where a 20 km boundary was used (see Table 8 - 19).

**Dilution Factor** - The dilution factor was used during post-processing to adjust the concentrations in the unit breakthrough curves calculated for the six stream tubes by the TSPA 1-D SZ transport model. This approach implicitly accounts for transverse dispersion. The experts provided an aggregate distribution for dilution factor which was assumed for the base case (CRWMS M&O 1998, p. 3-47). The aggregate uncertainty in this parameter ranges from 1 to 100, with a median value of about 10 (Table 8 - 19). This range of values for dilution in the saturated zone represents a significant departure from previous TSPA analyses for Yucca Mountain (e.g., Atkins et al. 1995, pp. 7-23 and 7-25; Wilson et al. 1994, p. 11-35) in which

effective values of dilution were typically orders of magnitude higher. The effects of transverse vertical dispersivity on performance results is discussed in the dilution and vertical transverse dispersivity sensitivity analysis (Section 8.5.2.1).

### 8.4.3 Analyses

The base-case analyses for SZ flow and transport in TSPA-VA consist of the assessment of uncertainty embodied in the 100 Monte Carlo realizations of the stochastic transport parameters used in the flow and transport realizations. In addition, a single realization using expected values for all of the stochastic parameters in the base case was produced. Variability in transport results in the SZ among radionuclides is a function of the sorptive characteristics and radioactive decay. Table 8 - 20 lists the parameters used for the 100 realizations and the expected-value case. The general characteristics of the radionuclides included in the analyses are given in Table 8 - 21.

### 8.4.4 Results

For the TSPA-VA, the results of the flow and transport analysis for the saturated zone are the radionuclide concentration histories at the geosphere/biosphere interface, which is a well head located 20-km downgradient of the repository in the Amargosa Valley region. These concentrations are directly proportional to the dose calculated for possible future inhabitants.

A steady boundary condition for unit radionuclide mass flux was applied at the inlet of each streamtube for the TSPA 1-D model transport simulations. The resulting unit breakthrough curves of concentration formed the basis for calculating radionuclide concentrations in the TSPA-VA using the convolution integral method. The unit concentration breakthrough curves for the nine radionuclides at 20 km from the repository are shown in Figure 8 - 29. These curves were generated using the expected parameter values and include radioactive decay for illustrative purposes. Differences in the arrival times of different radionuclides are due to variations in sorption among the radionuclides.  $^{237}\text{Np}$  and  $^{234}\text{U}$  experienced a moderate degree of retardation relative to the non-sorbing species for this expected-value case.  $^{79}\text{Se}$  and  $^{231}\text{Pa}$  were highly retarded relative to the non-sorbing species. The  $^{239}\text{Pu}$  and  $^{242}\text{Pu}$  that were subject to the equilibrium colloid-sorption model experienced a moderately high degree of retardation. The  $^{239}\text{Pu}$  and  $^{242}\text{Pu}$  that were subject to the irreversible colloid-sorption model have travel times through the SZ that are somewhat shorter than the non-sorbing species because of a lower effective porosity in the fractured volcanic tuff units. Differences in the maximum concentration among radionuclides are because of radioactive decay during transport through the saturated zone system.  $^{14}\text{C}$  experiences some decay, even for its relatively rapid transport through the SZ system.  $^{239}\text{Pu}$  and  $^{79}\text{Se}$  undergo very significant decay during transport for this expected-value case.

To include parameter uncertainty in the TSPA-VA, 100 breakthrough curves were simulated for each radionuclide by sampling parameter values from their respective probability distributions (Table 8 - 19). The simulated concentration-breakthrough curves for the 100 realizations of SZ transport for all nine radionuclides are shown in Figure 8 - 30 to Figure 8 - 40. Note that these breakthrough curves do not include the effects of radioactive decay, which was incorporated in the convolution integral method. The impact of uncertainty in the one-dimensional transport simulations for a non-sorbing species in the saturated zone is illustrated in Figure 8 - 39. This

figure shows the unit breakthrough curves for  $^{99}\text{Tc}$  concentrations for all 100 realizations used in the base case analyses. Travel times for the non-sorbing  $^{99}\text{Tc}$  vary from a few hundred years to about 4000 years; maximum concentrations, primarily influenced by the dilution factor, vary over two orders of magnitude among these simulations, which are considered equally likely. The uncertainty in longitudinal dispersion is shown by variations in the slopes of the breakthrough curves in Figure 8 - 39.

The probabilistic results of the TSPA 1-D SZ transport model indicate varying degrees of uncertainty in travel times for different radionuclides. Moderate degrees of uncertainty in the travel times for  $^{237}\text{Np}$  and  $^{234}\text{U}$  are indicated in Figure 8 - 32 and Figure 8 - 40, respectively. Simulated travel times in the SZ for  $^{237}\text{Np}$  vary from less than 10,000 years to greater than 200,000 years; simulated travel times for  $^{234}\text{U}$  vary over a similar range. Much greater uncertainty in simulated travel times is indicated for  $^{231}\text{Pa}$ , the reversibly sorbed Pu isotopes, and for  $^{79}\text{Se}$  (see Figure 8 - 33, Figure 8 - 34, Figure 8 - 36, and Figure 8 - 38).

#### 8.4.5 Interpretation

These SZ flow and transport modeling results can be interpreted for their significance to potential repository performance in a general sense. Detailed and quantitative assessments of the significance of simulated flow and transport behavior in the SZ requires the coupling of these results with the other components of the TSPA-VA analyses and formal sensitivity analysis.

Radionuclide migration through the saturated zone affects total system performance in two ways. First, the saturated zone may function as a mechanism for significant delay in releasing radionuclides to the biosphere. Second, there may be significant dilution of radionuclide concentrations that occurs during transport in the saturated zone. Both impacts are functions of the distance between the repository and the point of release to the biosphere, which is assumed for the TSPA-VA to be 20 km from the repository.

Delays in radionuclide migration caused by processes in the saturated zone are potentially important to repository performance if the travel time for a radionuclide through the saturated zone system is long in comparison to its half life. For example, in the expected-value case shown in Figure 8 - 29, the maximum concentrations of  $^{239}\text{Pu}$  (equilibrium colloid sorption) and  $^{79}\text{Se}$  are significantly attenuated relative to the other radionuclides because of radioactive decay. Delay in radionuclide migration in the saturated zone may also be significant if the travel time through the system is long relative to the time period of concern. For example, the travel time of unretarded radionuclides, such as  $^{99}\text{Tc}$  (see Figure 8 - 39), may be relevant to repository performance in a 10,000-year time frame. However, the delay in radionuclide release from the saturated zone for a period of 100,000 years for unretarded radionuclides would be insignificant.

Retardation in the saturated zone for most of the radionuclides that experience sorption is highly uncertain, particularly with regard to sorption characteristics of the alluvium/valley fill material. The delay in migration of  $^{237}\text{Np}$  in the SZ is significant to repository performance within a 10,000-year time frame, even for the least-retarded simulations among the 100 realizations (Figure 8 - 32). The relevance of  $^{237}\text{Np}$  retardation in the SZ, in the context of a 100,000-year time frame, is much more uncertain, based on these simulation results. There is a very broad range in the uncertainty of travel times for  $^{239}\text{Pu}$  and  $^{242}\text{Pu}$  which is simulated to be transported in

the equilibrium, reversible colloid sorption model (Figure 8 - 34 and Figure 8 - 36). Refinement of the colloid-facilitated Pu transport model or narrowing the uncertainty distributions for parameters used in the present model is necessary to draw definitive conclusions regarding the significance of colloid-facilitated Pu transport in the SZ to repository performance.

The dilution of radionuclide concentrations in the saturated zone is handled in a straightforward manner in the TSPA-VA calculations through the dilution-factor parameter. Although there is significant uncertainty in this parameter and complexity in the underlying processes that lead to dilution, the relationship between the dilution factor and dose is a simple linear function for a steady, radionuclide source from the unsaturated zone. Transient peaks in the radionuclide concentration at the source in the saturated zone are also attenuated by longitudinal dispersion during transport in the saturated zone.

#### **8.4.6 Guidance for Sensitivity Studies**

The amount of transverse dispersive mixing and consequent dilution of radionuclide concentrations in the SZ during transport over 20 km remains a highly uncertain and controversial element of the TSPA-VA analysis. Numerical dispersion inherent in 3-D SZ transport model that employs finite-difference and finite-element transport solutions probably prevents accurate simulation of radionuclide transport for cases with small values of longitudinal and transverse dispersivity. Such inaccuracies are generally related to the coarseness of the numerical grid used in the model. However, it is computationally impractical to significantly reduce or eliminate these inaccuracies through grid refinement for the cases with very low values of dispersivity for transport in the SZ to distances of 20 km. In addition, results of the SZ Expert Elicitation (CRWMS M&O 1998, pp. LG-14 – LG-15) indicate that very low values of vertical transverse dispersivity should be considered in TSPA analyses. Alternative analytical methods using an idealized representation of the SZ flow system should be employed in sensitivity studies to evaluate the effects of very low values of vertical transverse dispersivity on simulated dilution in the SZ.

Uncertainty in SZ groundwater flow has not been explicitly incorporated into the base-case analyses for TSPA-VA. There is significant uncertainty in SZ flow both in terms of the magnitude of groundwater flux downgradient of the repository and in terms of the flowpath followed by a contaminant plume. Heterogeneity in hydraulic conductivity, particularly in the form of discrete, highly permeable zones in fractured media, could potentially result in fast radionuclide transport pathways in the SZ with limited transverse mixing. Conceptual and numerical models of the potential heterogeneity in bulk permeability within the media of the SZ should be developed and evaluated for potential impacts on radionuclide transport in the SZ.

The effective porosity approach represents a significant simplification of radionuclide transport by groundwater flow in fractured media. The implications and accuracy of the probabilistic analyses using the effective porosity (single continuum) approach should be examined with the more physically realistic dual-porosity conceptual model. The sensitivity of the dual-porosity transport simulations to fundamental uncertain parameters (particularly, the effective fracture spacing) should be assessed in these sensitivity analyses.

In the base-case analyses, the interface between the SZ and the biosphere is implicitly assumed to be a pumping well with a small discharge rate and the simulated radionuclide concentrations in the SZ were passed directly to the biosphere model. Alternative assumptions regarding dilution of radionuclide concentrations in the pumping well or among multiple pumping wells should be examined in a sensitivity calculation. This analysis can be used to estimate the average dose rate among the critical group as a function of the size of that group. In addition, the cumulative dose among the members of the critical group can be used to estimate population dose.

As shown by the results of the base case transport simulations, there is a great deal of uncertainty in the colloid-facilitated transport of Pu, within the context of the conceptual model of equilibrium, reversible sorption onto colloids. There is considerably less uncertainty in the simulation results for the irreversible sorption model of colloid-facilitated Pu transport. Alternative conceptual models of colloid-facilitated transport should be considered in sensitivity studies. Such alternative conceptual models should be checked for consistency with available field data and should ideally constitute a narrower range of uncertainty than the base case modeling. An obvious choice for an alternative conceptual model of colloid-facilitated Pu transport is a reactive transport model that treats sorption and desorption of Pu on colloids as kinetic processes. A kinetic model could simulate behavior that falls between the bounding cases of equilibrium behavior and totally irreversible sorption, as implemented in the base case SZ transport model. Sensitivity to colloid filtration, which is neglected in the base-case simulations, should also be examined in sensitivity studies.

## **8.5 SENSITIVITY STUDIES**

Sensitivity studies for TSPA-VA consist of two major activities: 1) formal statistical analysis of the response of the TSPA model results to parameter values in the base case (see Chapter 11), and 2) additional process-level modeling and abstraction for alternative conceptual models and/or release scenarios that were not addressed in the base-case analyses. This section describes modeling studies of SZ groundwater flow and transport that fall into the second category mentioned above.

### **8.5.1 Key Issues**

Many of the key technical issues identified in the SZ flow and transport abstraction/testing workshop (Arnold et al. 1997) and in the SZ Expert Elicitation (CRWMS M&O 1998) were addressed in the base case analyses for TSPA-VA. Many of these issues were implicitly incorporated in the calculations through the range of parameter values considered in the Monte Carlo uncertainty distributions.

Key issues that were not covered in the TSPA-VA base case included analysis of the range in the dilution factor, the potential impacts of aquifer heterogeneity, explicit consideration of solute diffusion from fractures into the rock matrix, alternative methods for calculating dose in the critical population group, and alternative conceptual models of colloid-facilitated Pu transport.

## **8.5.2 Analyses**

The sensitivity studies planned to augment base case analyses of SZ flow and transport were primarily motivated by the recognition that base-case analyses did not fully or accurately address some potentially significant issues. The goal of these additional analyses is to assess the influence of these issues using process-level flow and transport modeling and to incorporate the analyses into TSPA-VA calculations if the influence is significant.

### **8.5.2.1 Dilution and Vertical Transverse Dispersivity**

An analytical solution for 3-D solute transport in the SZ from an idealized contaminant source was used to derive the relationship between dilution and vertical-transverse dispersivity. The objective of this vertical-dispersivity model was to evaluate the sensitivity of the maximum concentration downgradient in the SZ to the value of vertical-transverse dispersivity. Results from the SZ Expert Elicitation (CRWMS M&O, 1998) included assessments of the dispersive process in SZ transport in terms of: 1) a dilution factor (from three panel members) and 2) values of vertical transverse dispersivity (from one panel member). The analytical solution for 3-D solute transport was used to relate these two differing assessments of uncertainty in the dispersive process. In addition, this analytical solution was used to investigate alternative methods for calculating maximum concentration in the SZ from the concentrations simulated for the six, 1-D streamtubes used in the TSPA-VA base case. The objective of this streamtube-mixing model was to examine the interaction among the potential contaminant plumes from different source regions at the water table beneath the repository and to assess the potential conservatism associated with the option used to calculate maximum concentration from the results of the six streamtubes.

Analytical solutions for the advection-dispersion equation for solute transport in the SZ have the advantage that they provide accurate solutions for solute concentration as functions of spatial location and time. This is in contrast to numerical solutions to solute transport, which may result in significant numerical dispersion and spurious dilution of solute concentration, especially for cases with small values of dispersivity that are dominated by advection. The disadvantage to analytical solution methods is that they require simplifications or idealizations of the flow system and source geometry which may not be realistic.

#### **8.5.2.1.1 Analytical Solution**

An analytical solution for 3-D solute transport entitled 3DADE (Leij et al. 1991), was used to evaluate the vertical-dispersivity and streamtube-mixing models cited above. This computer code predicts the solute concentration as a function of space and time for specified model parameters in semi-infinite porous media with unidirectional flow. The 3DADE computer code solves the advection-dispersion equation and uses constant concentration (or first-type) boundary conditions at the inlet location of the medium. The transport advection-dispersion equation includes terms to account for advection, dispersion, zero-order production and first-order decay and is described as follows:

(8 - 11)



$$R \frac{\partial C}{\partial t} = D_x \frac{\partial^2 C}{\partial x^2} - v \frac{\partial C}{\partial x} + D_y \frac{\partial^2 C}{\partial y^2} + D_z \frac{\partial^2 C}{\partial z^2} - \mu C + \lambda \quad t > 0, 0 < x < \infty, -\infty < y < \infty, -\infty < z < \infty$$

where  $R$  is the retardation factor;  $C$  is the volume averaged or resident concentration of the solute ( $\text{ML}^{-3}$ );  $t$  is the time (T);  $x$  is the position (L) in the direction of flow;  $y$  and  $z$  are rectangular coordinates, all perpendicular to the flow direction (L);  $D_x$ ,  $D_y$ , and  $D_z$  are dispersion coefficients ( $\text{L}^2\text{t}^{-1}$ ) in the  $x$ ,  $y$ , and  $z$  directions, respectively;  $v$  is the pore-water velocity ( $\text{LT}^{-1}$ );  $\mu$  is a general, first-order, rate coefficient for decay ( $\text{T}^{-1}$ ); and  $\lambda$  is a general, zero-order, rate coefficient for production ( $\text{ML}^{-3}\text{T}^{-1}$ ) (Leij et al. 1991, p. 2720). The general geometry and source location used for the analyses described herein is shown in Figure 8 - 41. Laplace, Fourier, and Hankel transforms are used to derive general solutions for a given initial distribution and solute input and is described in Leij et al. (1991, p. 2720).

#### 8.5.2.1.2 Analytical Solution Models

The 3DADE computer code was used to evaluate the sensitivity of the maximum concentration downgradient in the SZ to the vertical-dispersivity value, referred to above as the vertical-dispersivity model. To accomplish this objective, two sets of analyses were completed using the 3DADE computer code. The analytical solution was calculated for vertical-dispersivity values of 0.5 m and 0.005 m to determine the effect of the vertical dispersivity on the simulated dilution in the SZ at a distance of 20 km downgradient from the repository. The vertical-dispersivity value of 0.5 m is the same value as that suggested for horizontal transverse dispersivity, and 0.005 m is the recommended mean value from Lynn Gelhar, which is a result from the Expert Elicitation (CRWMS M&O 1998, p. 3-21). The other input parameters are shown in Table 8 - 22. A rectangular contaminant source was located at the water table, as shown in Figure 8 - 41, with dimensions of 3000 m by 10 m to reflect the cross-sectional area of the groundwater streamtube from the repository. For both analyses, the analytical solution was solved for the relative maximum concentration in the  $y$ - $x$  and  $z$ - $y$  planes to visualize the contaminant plume. Gelhar did not give values for dilution factor as a result of the Expert Elicitation Project. Instead, he gave values for vertical dispersivity. Since the dilution factor is a direct, input parameter for the base case, a relationship between the dilution factor and vertical dispersivity is of interest as a check on reasonableness of the values used. This was accomplished using the 3DADE computer code by conducting several simulations, using a range of vertical transverse dispersivity values, and calculating the dilution factor by taking the inverse of the maximum relative concentration at 20 km distance.

The second objective includes the streamtube-mixing model, which examines the interaction among the potential contaminant plumes from different source regions at the water table beneath the repository. This objective allows for the investigation of alternative methods for calculating maximum concentration in the SZ from the concentrations simulated for the six 1-D streamtubes used in the TSPA-VA base case. To accomplish this objective, the 3DADE computer code was run for each of the six source regions that were designed to correspond to the six streamtubes that are idealized as rectangular areas, (as will be discussed in Section 8.5.2.1.3 in Figure 8 - 44). These idealized rectangular areas served as the contaminant source for each of the six runs. The geometry of the source regions and their respective cross-sectional areas is consistent with the conceptual model used in the TSPA-VA calculations of SZ transport. The vertical-dispersivity

value used for all six source regions was 0.16 m. The justification for the use of this value will be discussed in the Analytical Solution Model Results Section 8.5.2.1.3. The other input parameters for the streamtube-mixing model are shown in Table 8 - 22. The 3DADE code was run until steady state was reached for each of the source regions. In addition, the 3DADE analytical solution was run to compare the sum of the maximum concentrations from the six individual regions to the maximum concentration from the region as a whole. This was accomplished using the parameters shown in Table 8 - 22 for this model. The rectangular contaminant source is the cross-sectional dimensions of the repository, 3000 m by 10 m.

#### 8.5.2.1.3 Analytical Solution Model Results

Results of the analytical solution for the vertical-dispersivity model are presented in terms of contaminant plumes in plan and cross-sectional view from the repository to approximately 20 km downgradient from the repository. The result of the two sets of analyses illustrate the sensitivity of the maximum concentration downgradient in the SZ to the vertical-dispersivity value as shown in Figure 8 - 42. The influence of the vertical dispersivity on the spreading of the plume in the vertical direction may be examined by comparing Figure 8 - 42a and Figure 8 - 42b. The plume spreads in the vertical direction to more than 300 m below the water table for the vertical dispersivity value of 0.5 m as shown in Figure 8 - 42a. For the vertical-dispersivity value of 0.005 m, the plume spreads in the vertical direction to approximately 50 m below the water table (Figure 8 - 42b).

In addition, Figure 8 - 43 illustrates the relationship determined between the vertical-dispersivity, dilution factor and cumulative probability in the uncertainty of the dilution factor. The upper x-axis of Figure 8 - 43 shows the vertical-dispersivity value that corresponds to the dilution factor based upon results of the analytical solution. The analytical-solution analysis with a vertical-dispersivity value of 0.5 m results in a maximum relative concentration of 0.056, which equates to a dilution factor of about 18. The analytical solution analysis with a vertical dispersivity value of 0.005 m results in a maximum relative maximum concentration of 0.5219, which equates to a dilution factor of about 2, as shown in Figure 8 - 43. The Expert Elicitation panel aggregate-cumulative-distribution-function for uncertainty in the dilution factor ranged from 2 to 100, with a median estimate of about 12, and is represented in Figure 8 - 43 (CRWMS M&O 1998, p. 3-47). Using Lynn Gelhar's recommended values for vertical dispersivity of 0.005m and  $\pm 2\sigma$  values of 0.16 mm - 160 mm (CRWMS M&O 1998, p. 3-21), the analytical solution was used to derive Gelhar's vertical-transverse dispersivity curve shown in Figure 8 - 43. Several simulations, using a range of vertical transverse dispersivity, were used to define this curve. Figure 8 - 43 shows that Gelhar's recommendation for vertical dispersivity results in dilution factors that range from near 1 to approximately 10 (corresponding to  $\pm 2\sigma$  from Gelhar's uncertainty distribution) with a median value of about 2.

These results indicate that Gelhar's assessment of the dispersive process in the SZ is considerably more conservative than the aggregate assessment from the three panel members contributing to the uncertainty distribution of dilution factor. It should be noted that Gelhar's assessment was not included in the TSPA-VA base case because it was not presented in terms of dilution factor. If Gelhar's input were included in the uncertainty distribution based on the analytical solution results presented here, the uncertainty distribution would be shifted to lower

values of the dilution factor and the expected value of dilution factor would decrease from 10 to approximately 8.

Results of the analytical solution for the streamtube-mixing model are presented in cross sections of relative concentration which correspond to individual streamtubes from the six source subregions. The maximum relative concentration for each region is indicated in Figure 8 - 44. The TSPA-VA calculations represent the SZ transport with six independent streamtubes from six, source regions and the radionuclide concentrations are calculated separately for each of the streamtubes used in the analysis of transport of the SZ. Three options were examined to calculate the value of the radionuclide concentration for use in the biosphere component of the TSPA-VA analysis and to evaluate the relative accuracy of these options using the analytical solution for 3-D solute transport (Leij et al. 1991). Option 1 assumes that in a conceptual sense, implicit spreading of radionuclide mass from individual streamtubes (via the dilution factor) results in six essentially overlapping plumes. Based on the assumptions in option 1, the appropriate method to calculate maximum concentration is to use linear superposition and sum the concentrations from the six streamtubes. Option 2 disregards transfer of radionuclide mass among the six streamtubes and uses the maximum diluted concentration from among the six streamtubes. Option 3 represents transport in the SZ with a single streamtube by combining the results for the six streamtubes by taking the volumetrically weighted average of the concentrations in the six streamtubes. Note that option 1 was used in TSPA-VA base case analyses, as described in Section 8.4.1.3. The vertical-dispersivity value for all six source regions was 0.16 m which corresponds to a dilution factor of 10 (see Figure 8 - 43). A dilution factor of 10 was used because this approximates the median dilution factor as per the Expert Elicitation Panel (CRWMS M&O 1998, p. 3-11). The dilution factor is defined as the ratio between the initial contaminant concentration and the highest concentration at a point some distance from the source (CRWMS M&O 1998, p. 3-10).

The relative maximum concentration of all of the source regions as a whole is 0.1493 and is shown in Figure 8 - 44b. This distribution of relative concentration shown in the cross section, 20 km downgradient, represents the "reality" for the idealized analytical solution for the entire solute plume. Option 1 results in a calculated maximum relative concentration of 0.3832, which is 2.6 times greater than the "true" relative maximum concentration of all the source regions as a whole (0.1493). Options 2 and 3 result in calculated maximum relative concentrations of 0.0875 and 0.06608, respectively, which is 1.7 and 2.3 times less than the "true" maximum relative concentration of all the source regions as a whole (0.1493). The results of applying these three options to the concentrations from the separate streamtubes is shown at the bottom of Figure 8 - 44. This analytical-solution analysis provides an estimate of the relative accuracy of the three options and confirms that option 1 overestimates maximum concentration and that options 2 and 3 underestimate maximum concentration. These results indicate that option 1 overestimates the actual maximum concentration, but not by an extreme factor. Options 2 and 3 underestimate the maximum concentrations by factors on the same order as the factor by which option 1 overestimates concentration.

#### **8.5.2.2 Heterogeneity and Flow Channelization**

A requirement of performance assessment modeling for nuclear waste repositories is that the sensitivity of any modeling results be examined with respect to features, events, or processes

(FEPs) that may affect those results. In the absence of any data that would exclude, or "screen out" a FEP, those FEPs that have the potential to most adversely affect performance of the repository must be included in the sensitivity analysis. In the saturated zone (SZ) at Yucca Mountain, well connected, high-permeability pathways through the aquifer from the area beneath the potential repository to the accessible environment constitute a feature that could adversely affect repository performance. In addition to discrete features of high permeability, the general spatially heterogeneous nature of the bulk permeability distribution can cause focusing and channeling of flow within the saturated zone. In the absence of data that can rule out the existence of such features, the potential impact of channeling and high-permeability pathways through the saturated zone must be considered.

This section presents an analysis of the available data, discussion of conceptual models of heterogeneous permeability fields, including discrete, high-permeability pathways along faults, implementation of these conceptual models into a numerical model, and creation of multiple stochastic realizations of permeability for the TSPA 3-D SZ flow model, which is a sub-domain of the USGS site-scale flow model. Results of modeling groundwater flow and radionuclide transport through these multiple three-dimensional, heterogeneous, permeability models are also discussed relative to the base case of homogeneous units and no faulting.

#### **8.5.2.2.1 Available Data**

**Geologic Framework Models** - A three-dimensional depiction of the geology in the saturated zone at Yucca Mountain has been constructed for the USGS site-scale flow model. This geologic model is described in Czarnecki et al. (1998) and is referred to as the "hydrogeologic framework model" (HFM). The HFM reported in Czarnecki et al. (1998) was created on a grid with a regular spacing of 1,500 meters in the X and Y directions. This coarse spacing creates gentle undulations in the surfaces of geologic units that might actually be sharp offsets in a discrete fault. Additionally, this relatively coarse resolution limits the HFM to describing the extent and geometry of the hydrogeologic units in only a general sense (Czarnecki et al. 1998). A total of 18 hydrogeologic units were modeled in the HFM. The top of the HFM is clipped at the water table.

A higher resolution, three-dimensional-stratigraphic-framework model has been developed as the Integrated Site Model (ISM) for the USGS sitescale model domain (Clayton, et al. 1997). In Nov/Dec of 1997, a refined grid was created for the HFM by Claudia Faunt at the USGS. This grid samples the upper surfaces of the hydrogeologic units on a 250 x 250 meter spacing. In the area of the site-scale domain, the extent of the ISM, this resampling produces a better definition of the geologic surfaces. However, in the remainder of the USGS site-scale flow model, the resampling is only interpolating to this more finely discretized points of the underlying 1500 meter grid. This updated set of hydrogeologic unit surfaces, defined on a 250 meter grid spacing, is used to define the three-dimensional distribution of hydrogeologic units described in this sensitivity analysis. These units are then populated with heterogeneous bulk permeability values, or considered to be homogeneous, as discussed below. It is noted that outside of the repository block area there are few data to constrain the position of the geologic surfaces and this may lead to erroneous interpretations of the stratigraphy in those areas. The interpretation of the stratigraphy, whether correct or not, can have profound effects on the calibration of the flow model and the direction of radionuclide migration.

For TSPA-VA sensitivity analyses, a subsection of the USGS site-scale flow model is used. A subdomain covers approximately two-thirds of the area of the full USGS site-scale flow model as shown in Figure 8 - 45. This subdomain is referred to as the "TSPA 3-D SZ flow model". The unit definitions and geometries from the hydrogeologic framework model as described above are retained in the TSPA 3-D SZ flow model.

**Permeability Measurements** - Hydraulic data for fractured bedrock units in the saturated zone are available from several locations in the area of Yucca Mountain. These data were obtained in more than 150 individual aquifer tests at 13 boreholes using a variety of testing methods (Luckey et al. 1996). Hydraulic tests were conducted over both large and small stratigraphic intervals, primarily within the middle volcanic aquifer (Crater Flat Group) and the upper volcanic confining unit (Calico Hills Formation), with varying degrees of reliability and success. Single-borehole testing methods were used in all of the tested boreholes; whereas, multiple-borehole pumping tests have only been conducted at the C-wells complex. In addition, air-permeability tests have been performed in the unsaturated zone near the potential repository in boreholes (LeCain, 1997) and in the heater test alcoves of the Exploratory Studies Facilities (ESF) (Tsang, 1997).

These hydraulic data are probably most useful in formulating our general conceptual model of flow processes and the spatial distribution of bulk permeability in the saturated zone. Because of the sparse nature of these measurements and their questionable reliability, most of these data are not directly applicable in modeling the distribution of permeability for simulating groundwater flow. Hydraulic data from multi-well tests at the C-wells are an exception and probably can be taken as point-specific information about the bulk permeability in the saturated zone.

Taken as a whole, these data suggest a very heterogeneous distribution of bulk permeability in the fractured volcanic units. Average permeabilities in hydrogeologic units designated as aquifers and confining units may be significantly different, but there is probably considerable overlap in the probability distributions of bulk permeability for these different hydrogeologic units. Some of the more stratigraphically variable hydrogeologic units, such as the middle volcanic aquifer, most likely possess greater intra-unit heterogeneity than the more stratigraphically uniform units, such as the upper volcanic confining unit.

Interpretations of pumping test results from the C-wells and the faulted nature of the site suggest that there may be discrete zones of higher bulk permeability associated with tectonic features "overprinted" on stratigraphically controlled heterogeneity. These zones of enhanced bulk permeability correspond to some north-south striking faults and some northwest-southeast striking features in the interpretation of Geldon et al. (1997, pp. 69-70). The implication for groundwater flow in the saturated zone is that flow may be channelized both within higher-permeability stratigraphic intervals and higher-permeability sub-vertical tectonic features (faults or highly fractured zones). The sub-vertical tectonic features may be particularly important flow pathways through the confining units.

**Fault and Fracture Mapping** - Faults defined within the USGS site-scale flow model are taken from a 1:100,000 scale map and various cross sections (Czarnecki et al. 1998). All faults, regardless of length, were included within the USGS SZ site-scale flow model. There is no information on the amount of fault offset for the majority of these mapped faults. In some cases,

the fault lengths and orientations were adjusted from the trace map to the HFM based on cross section interpretations (Czarnecki et al. 1998, pp. 21-28). Due to software constraints and the relatively coarse resolution of the USGS site-scale flow model (1,500 meters in X and Y), almost all faults were considered to be vertical features. In cases where it was thought to be hydrologically significant, thrust faults were included by representing repeated sections of hydrogeologic units. The faults are considered to be "offset only" features, and, as discussed above, the coarse grid discretization of the HFM results in a gently sloping representation of the vertical offset along faults.

It is noted here that the faults included within the USGS site-scale flow model are those mapped on the 1:100,000 scale. In general, only faults mapped in outcrop are included in the USGS site-scale flow model. No interpretations were made to extend either discrete faults or the general nature of faults into the areas of the model covered with alluvium. The definition of faults in areas of outcrop only is readily apparent in the fault trace map shown in Figure 8 - 46. Note that large areas with no mapped faults are covered by alluvium.

The faults within the section of the USGS site-scale flow model that intersects with the ISM of Clayton et al. (1997) are also included as vertical features. These faults are taken from ISM v1.0. The major difference between ISM v1.0 and later versions is the inclusion of a fault structure along Yucca Wash in v1.0. After the construction of the USGS site-scale flow model, faults mapped within the ISM of Clayton et al. (1997) have been defined as three-dimensional features using a dense discretization. Future versions of the USGS site-scale flow model will attempt to incorporate these new fault representations.

#### **8.5.2.2.2 Conceptual Models of Permeability Distribution**

These data from the Yucca Mountain site suggest that the spatial distribution of bulk permeability in the fractured media is influenced by volcanic stratigraphy and by discrete structural features, such as faults. The resulting conceptual model of bulk permeability is one in which these influences are superimposed, resulting in an uncertain, heterogeneous pattern of permeability. A conceptual model of the permeability distribution in the alluvium is based on nearby analog sites, because of the lack of data on alluvial characteristics downgradient of the repository.

**Volcanic Units** – With the exception of work by Barton and Larsen (1985) and Barton (1995), fracture descriptions at Yucca Mountain have focused on the cataloging of properties measured on individual fractures or within fracture sets. These properties (e.g., orientation, length, roughness), are then used to develop univariate statistical descriptions of the fractures at Yucca Mountain. While single, or ensemble descriptions of individual fractures are useful for getting a sense of the types of fractures present at Yucca Mountain (see Sweetkind and Williams-Stroud 1996), it is the characteristics of connected clusters of fractures that control fluid flow and mass transport within the saturated zone. Measurements and detailed descriptions of fracture clusters, or the fracture system *en masse*, are currently lacking at Yucca Mountain.

In the absence of statistical descriptions of fracture groups or clusters, the general relationships between fracture frequency, length, connectivity, and stratigraphic framework are used in conjunction with the local bulk permeability measurements to guide the creation of fracture

permeability models. Fracture permeability models are created for the upper volcanic aquifer, the upper volcanic confining unit, and the middle volcanic aquifer.

For the middle volcanic aquifer, the calibrated bulk permeability value given in Czarnecki et al. (1998) is very close to the mean of the measured values obtained from single-hole tests (Table 8 - 23). The mean value obtained from the multi-well tests at the C-well complex is almost two orders of magnitude larger than the calibrated bulk permeability value for the middle volcanic aquifer. The only data available for the upper volcanic aquifer are from air permeability tests conducted in the unsaturated zone. The log 10 mean of these measurements is approximately 2 orders of magnitude greater than the estimated value for the upper volcanic aquifer from the USGS site-scale flow model. Single and multi-well measurements of bulk permeability for the upper volcanic confining unit give a mean log 10 value that is of similar magnitude to the single-well measurements in the middle volcanic aquifer. For the upper volcanic confining unit, the mean of the measured values is five orders of magnitude greater than the value obtained through inverse parameter-estimation with the USGS site-scale flow model. Based on the differences in the means of the log 10 measured bulk permeability values, the upper volcanic confining unit does not appear to be a confining unit at all. However, when comparing the values obtained through parameter estimation, the upper volcanic confining unit in the USGS site-scale flow model created by Czarnecki et al. (1998) will certainly act as a barrier to flow between aquifers.

Based on synthesis of work by a number of fracture mapping efforts and some air permeability testing, the lateral variations in the background-fracture permeability when defined at the scale of 500 meter grid blocks are felt to be fairly minimal. As a guide to defining variability, the standard deviation of the log 10 permeability data collected in the single-well borehole tests can be used. However, in most cases, these single-well tests interrogated a significantly smaller volume of aquifer than would be within a 500 x 500 x 50 meter grid block in the TSPA 3-D SZ flow model. Measurements of bulk permeability integrated over the larger volume of the grid-blocks would exhibit less variability because the larger sample volume averages out more of the inherent small-scale variability. Additionally, a significant fraction of the variability seen in the single-well tests can most likely be attributed to inconsistencies in the measurement technique (e.g., changes in length of test interval). Therefore, we believe the variability of the permeability values, defined by the standard deviation of the log 10 permeability distribution, at the scale of 500 meter grid blocks, will be considerably less than that seen in the distributions of the single-well permeability tests. For input to the geostatistical simulations, the standard deviation in bulk permeability of the single-well tests for each volcanic unit is reduced by one-half to account for the scale difference between the test volume and the grid-block volume. Most single-well tests in the SZ interrogated the medium on the scale of 10s m, whereas the model grid is on the scale of 500 m. A variety of testing methods was used in the single-well tests, which may have contributed to the apparent variability in the permeability data. These considerations, along with a general lack of data on the variability in permeability, form the basis for this estimate in the reduction in the standard deviation used in the geostatistical modeling.

The vertical continuity of the fractures is unknown. As noted by Sweetkind and Williams-Stroud (1996, p. 64) “. . . there has never been a surface or subsurface data collection effort to characterize the vertical connectivity of the fracture network within the welded flow units.” Measurements of air permeability obtained by LeCain (1997) in borehole UZ-16 were analyzed for vertical spatial correlation by Altman et al. (1996, pp. 44-47). Results of this analysis

showed fracture permeability to be correlated over a distance of approximately 30 meters. Other evidence cited in Sweetkind and Williams-Stroud (1996) suggests that vertical connectivity of the fracture network is fairly high, although lengths of correlation were not stated. Certainly, the fractures within welded units are controlled by the stratigraphy and are generally not pervasive across less-welded units. In some cases, the average stratigraphic thickness of the welded and non-welded units can be used to constrain vertical extent of fracture permeability.

**Alluvium** - In contrast to the volcanic rocks at Yucca Mountain, permeability in the alluvial deposits south and east of the potential repository has not been characterized. Due to this lack of information and the expected similarity of the two alluvial deposits at the grid block scale, the geostatistical model of the Alluvium (Unit Number 19) and Undifferentiated Valley Fill (Unit Number 9) units were created with the same conceptual model of permeability distribution (Table 8 - 24).

The conceptual model of permeability distribution used for the alluvium is generally based on descriptions of alluvial deposits within the southwestern U.S. and specifically on alluvial deposits observed at the Nevada Test Site (McCord et al. 1997). The effective permeability of each unit is controlled by the general grain size and proportion of the facies within the unit. McCord et al. (1997) examined an 8 m by 55 m trench wall dug into alluvial fan deposits at Frenchman Flat on the Nevada Test Site. They found that one-third of the deposits were fine-grained paleosols and debris flow deposits, while the other two-thirds of the sediments were coarse-grained sands deposited in sheets during flood events.

**Faults** - A conceptual model of fault-zone architecture and its relation to permeability has been developed by Caine et al. (1996, p. 213). This conceptual model classifies a fault zone into three distinct materials: fault core, damage zone, and protolith. The fault core may include single slip surfaces, breccia zones, fault gouge and altered zones. In general, the mechanical and geochemical alteration that is associated with faulting is concentrated in the fault core and as a result, the permeability of the fault core is usually lower than the undisturbed protolith (country rock) surrounding the fault zone. The damage zone is characterized by a connected network of fractures surrounding the fault core. Depending on the connectedness of the fractures and the total volume of the damage zone, the damage zone may have enhanced permeability relative to the fault core and the protolith. The area outside of the fault zone is characterized by the representative flow properties of the protolith itself.

The model of fault architecture index proposed by Caine et al. (1996, 213) was originally devised for the deformation of intact protolith. At Yucca Mountain, there is evidence that fault displacement has occurred along pre-existing cooling joints within the protolith. Within the vicinity of mapped fault zones, these joints contain fault gouge (Sweetkind and Williams-Stroud, 1996, p. 76). Fault gouge would act to decrease the permeability of the joints and this area of decreased permeability is analogous with the lower-permeability fault core in the model of Caine et al. (1996).

The damaged zone within the model of Caine et al. (1996) is a zone of enhanced fracturing within the fault zone that surrounds the fault core on both sides. The damaged zone represents an area of enhanced permeability relative to both the fault core and the protolith. Surface observations at Yucca Mountain show well developed damaged zones extending from 50 to over



100 on each side of the fault center (Spengler et al. 1993, 656-658; Sweetkind and Williams-Stroud 1996, p. 12). More recent subsurface mapping within the ESF shows that damaged zones around faults are much less extensive than they are on the surface. An example is the Bow Ridge Fault that has damaged zones of approximately 10 m on each side of the fault center (Sweetkind and Williams-Stroud 1996, p. 76). In the subsurface, the enhancement of the fracture frequency within the damaged zones relative to the protolith is variable and the extent of the damaged zone is dependent on lithology (Sweetkind and Williams-Stroud 1996, p. 11).

#### **8.5.2.2.3 Conceptual Model Implementation**

The conceptual models of bulk permeability distribution within the fractured volcanic rocks, the alluvial deposits, and within the fault zones were implemented into numerical models in two steps. First, the background permeability of several volcanic and alluvial units was modeled using geostatistical simulation. This step results in 100 realizations of bulk permeability for the USGS site-scale, flow model. Second, the faults are added to these 100 realizations.

**Grid Discretization** - The base-case grid discretization used in creating the bulk permeability fields is 250 x 250 x 50 meters. This domain corresponds to the USGS site-scale flow model of Czarnecki et al. (1998, p. 22). The geostatistical model domain is 30,000 x 45,000 x 2,000 meters resulting in a total of 864,000 grid cells ( $n_x = 120$ ,  $n_y = 180$ ,  $n_z = 40$ ). The origin (southwest, bottom corner) of the geostatistical model domain is at Nevada State Plane coordinates of 156,000 easting and 201,000 northing. The elevation of the origin is 500 meters below sea level).

For the TSPA-VA runs, the geostatistical model domain was reconfigured to the smaller-volume TSPA 3-D SZ flow model. The southwest corner of this volume in UTM coordinates is: (542,840 mE, 4,046,780 mN). In the TSPA 3-D flow model, the grid blocks are 500 x 500 x 50 meters and the model extends 950 meters (20 layers) below the water table surface. The larger grid blocks were populated with bulk permeability from the underlying finer discretization created for the USGS site-scale flow model, using the geometric mean of the permeability values in the finer-scale grid blocks. There are a total of 61,320 elements in the TSPA 3-D SZ flow model (42 x 73 x 20).

**Permeability in Fractured Units** - In the base-case run, homogeneous values of bulk permeability were assigned to all of the different hydrogeologic units. These homogeneous values are based on the values obtained through calibration of the USGS site-scale flow model by Czarnecki et al. (1998). A further refinement of the calibration was completed on the TSPA 3-D SZ flow model (Section 8.3.2). This further refinement changed the values of some of the units. The original bulk permeability values for the units given by Czarnecki et al. (1998) and the updated values used in the TSPA 3-D SZ flow model are given in Table 8 - 24. The value of bulk permeability for the middle volcanic aquifer in the TSPA 3-D SZ model is more consistent with multi-well pump test results reported by Geldon et al. (1997) than the value used in the USGS SZ site-scale flow model. Because the values of permeability in the TSPA 3-D flow model are higher than those in the USGS site-scale flow model, the resulting groundwater travel times in the TSPA 3-D SZ flow model would be more conservative (from the perspective of repository performance).

One of the features that may control modeled concentrations at the accessible environment downgradient of the repository is the presence or absence of spatial heterogeneity of bulk permeability of the fractured units. Heterogeneous bulk permeability models were created for the fractured units using sequential-gaussian-geostatistical simulation (the *sgsim* algorithm of Deutsch and Journel 1992, p. 3-7, as implemented in the SGSIM computer code). These multiple realizations of the bulk permeability distribution were conditioned to the mean value of permeability for each unit obtained through calibration of the TSPA 3-D SZ flow model. The parameters defining the spatial correlation of bulk permeability in the fractured units (Table 8 - 26) were derived from information on the spatial continuity in matrix porosity in volcanic units (Istok et al. 1994). The conceptual model assumed that fracture permeability is related to the degree of welding in volcanic units, which is in turn correlated with matrix porosity.

**Permeability in Alluvium** - The units classified as being alluvial deposits are the valley fill aquifer (unit 19), the valley fill confining unit or playa deposits (unit 18) and the undifferentiated valley fill (unit 9). The approximate volume percentages of these units within the geostatistical model domain are 2.6%, 0.017%, and 6.4%, respectively. Permeabilities were assigned to each of these three units by conceptualizing the permeability distribution as bimodal (fine or coarse grained) following the observations made by McCord et al. (1997).

Indicator geostatistical simulation (the *sisim* algorithm of Deutsch and Journel 1992, as implemented in the SISIMPDF computer code) was used to create two, discrete classes of permeability within the alluvial units. Values for each permeability class were chosen such that the geometric mean, weighted by the proportion of each class within the unit (1/3 or 2/3), would equal the mean permeability value determined in the model calibration. The values used in this calculation are given in Table 8 - 25.

The indicator-geostatistical simulation used an anisotropic model of spatial correlation. The fine-grained, lower-permeability class has a spatial correlation of 1000 meters in the north-south and east-west directions and 50 meters in the vertical. The coarser grained, higher-permeability class, has a spatial correlation length of 3,000 meters in the north-south direction and 1,000 meters in the east-west direction. The vertical correlation length of the coarse grained class is 150 meters. The vertical anisotropy of both depositional classes is based on qualitative examination of the map presented in McCord et al. (1997, Figure 2a). The horizontal correlation lengths of grain-size classes were chosen to mimic observed depositional patterns in the southern part of the model where most of the alluvial deposits are located. In this area, sediment transport and deposition occurs mainly in a north-south direction along drainages (e.g., Fortymile Wash).

**Representation of Faults** - Information gained from fault mapping at Yucca Mountain indicates that fault surfaces may have complex shapes, variable thickness, and dip at different angles, as measured from the vertical. Within the geologic framework models, the faults are represented as offset-only features with vertical dips. In the TSPA-VA sensitivity analysis, the faults are represented as discrete zones of enhanced bulk permeability with vertical dip.

In order to represent the faults in a numerical model with an orthogonal grid, the digitized points representing the fault traces in the HFM must be mapped onto the numerical flow-model grid. The 500 x 500 meter grid discretization in the TSPA 3-D SZ flow model is coarse enough that the numerous faults in the HFM cause the majority of the flow model grid blocks to be classified

as faults. In addition to this problem of mapping to a coarse grid, there is also the problem of faults not being mapped in the areas covered by alluvium. Given the density of faults in the areas of outcrop, there are certainly faults under the alluvium; however, it is unclear how they should be represented in the model. A final consideration is the hydrologic significance within the saturated zone of the faults mapped at the ground surface. Many of these mapped faults may not be present in the saturated zone and those that are present at depth may not necessarily be conductive features. Given these uncertainties, there is not an objective way to include the numerous mapped faults in the HFM into the TSPA 3-D SZ flow model.

The main sensitivity analysis of importance to TSPA-VA is the potential presence of a continuous, high-permeability pathway from near the repository to the accessible environment. This type of feature is modeled in the TSPA 3-D SZ flow model by considering only the most significant fault zones that lie within the model domain. Only those faults deemed significant enough to be represented within the USGS regional-scale flow model (Faunt 1997) are retained within the TSPA 3-D SZ flow model. The longest of these faults is the Fortymile Wash structure (Figure 8 - 45). These fault features are assigned a constant permeability of  $1 \times 10^{-11} \text{ m}^2$ . This value of permeability is the same order of magnitude as the value inferred for the faulted interval in the C-holes from multi-well pump tests (Geldon 1996, p. 70) and is applied to the width of the appropriate grid blocks in the TSPA 3-D SZ flow model (i.e., 500 m).

**Summary** - In summary, multiple realizations of bulk permeability were created for the TSPA 3-D SZ flow model domain. The Upper Volcanic Aquifer, Upper Volcanic Confining Unit and the Middle Volcanic Aquifer were considered to be the volcanic units with the greatest influence on the flow field downgradient of the repository. Heterogeneity was modeled in these units with sequential-gaussian-geostatistical simulation, using the SGSIM computer code. All other volcanic units were considered to be homogeneous in the TSPA 3-D SZ flow model. The alluvial units were also modeled as heterogeneous, using a bimodal distribution of bulk permeability. This bimodal distribution was created with indicator-geostatistical simulation. The parameters used in the geostatistical-simulation algorithms are summarized in Table 8 - 26.

Only the faults from the USGS regional-scale flow model that lie within the TSPA 3-D SZ flow model domain were modeled as high permeability features. These faults were all assigned a constant bulk permeability of  $1 \times 10^{-11} \text{ m}^2$ .

The final step of the modeling process was to create a final, three-dimensional domain of permeability data needed as input to the TSPA 3-D SZ flow model. The bulk permeability value assigned to any one grid block is a function of the hydrogeologic unit prevailing at that location and the presence or absence of a fault at that location. The value of protolith permeability assigned to the gridblock may be assigned stochastically through a geostatistical simulation routine (heterogeneous units), or the permeability value derived from parameter estimation may be assigned to all gridblocks within the (homogeneous) units. For the heterogeneous units, the geostatistical simulation algorithm and spatial correlation parameters vary depending on the hydrogeologic unit at that location. If a fault is present at a gridblock, that gridblock is assigned a constant- bulk permeability value.

#### 8.5.2.2.4 Flow and Transport Modeling

The TSPA 3-D SZ flow model was used to simulate groundwater flow and radionuclide transport within the heterogeneous domains described in the previous section. These flow and transport simulations were used to examine the sensitivity of the modeling results to the alternative representations of the spatial distribution of bulk permeability. The TSPA 3-D SZ flow model is summarized here; a complete discussion of the model is provided in Section 8.3.2. Note that the TSPA-3-D flow model encompasses a sub-domain of the USGS site-scale flow model, with western and northern boundaries interior to the USGS site-scale flow model.

The TSPA 3-D SZ flow model used for this analysis incorporated an area of about 20 km by 36 km to a depth of 950 m below the water table. The model grid was a uniform orthogonal mesh with 500-m by 500m X 50m elements. The hydrogeologic framework in the model was based on a refined version of the regional geologic framework model described in the previous section. Sixteen different hydrogeologic units were represented in the model. Three linear, vertical features with low permeabilities to the west and north of Yucca Mountain were included to simulate the moderate and large hydraulic-gradient regions, respectively. Simulations were conducted using the FEHMN computer code (Zyvoloski et al. 1995).

Flow was modeled as steady state through a single-continuum, porous medium. The SZ flow system was represented as a confined system, with the upper boundary at the water table in the TSPA 3-D SZ flow model. Focused recharge along Fortymile Wash, consistent with USGS measurements, was included as a specified flux in corresponding flow model nodes on the upper boundary. Specified-pressure boundary conditions were applied to the lateral boundaries based on the interpolation of measured values of hydraulic head. Groundwater flow was not allowed to occur across the bottom boundary of the model. Permeability was assumed to be uniform within hydrogeologic units in the model domain for which geostatistical simulations were not produced. Average isothermal conditions were applied in the TSPA 3-D SZ flow model.

The TSPA 3-D SZ flow model was calibrated by an iterative procedure, and the simulated hydraulic heads were compared with measured head values in the model domain. There was good agreement between the simulation results and most of the well measurements, particularly in the area downgradient of the repository. The differences between simulated and measured hydraulic head values were less than 5 m for shallow wells downgradient of the repository, within a 10 km distance. The direction of groundwater movement in this flow model is consistent with the conceptual model of the system.

Radionuclide transport simulation in the analyses was performed with the TSPA 3-D SZ flow model results using the finite-element solution method in the FEHMN computer code. A steady-solute mass source totaling 6 g/y was specified to be evenly distributed at the water table over the footprint of the repository in all transport simulations. This radionuclide source term was specified to be consistent with the TSPA 1-D transport simulations in which a unit mass source (1 g/y) was applied to each of the six streamtubes. The expected value of effective porosity (Section 8.4.2) was assigned to each of the hydrogeologic units in the transport simulations.

**Results** - The resulting permeability realizations are broken into two discrete ensembles: 1) those with heterogeneity and faults represented as offset-only features, as defined by the stratigraphic

surfaces in the HFM and 2) those with heterogeneity and faults represented as zones of enhanced permeability. Several metrics are used to compare the results against the base-case system containing homogeneous units and also to compare results across the two ensembles. These metrics are 1) head calibration, 2) a comparison of the peak concentrations, and the time to peak concentration and 3) the focusing of transport results at a boundary 20 km downgradient of the repository.

**Model Calibration to Observed Heads** - The head calibrations for each of the 100 different realizations are summarized by the root mean-squared-error (RMSE) between the modeled heads and the observed heads at 61 wells. The RMSE for the base case TSPA 3-D SZ flow model is 20.1 meters. A histogram of the 100 RMSE values calculated on the heterogeneous permeability realizations is shown in Figure 8 - 47a. The mean of these 100 RMSE values (19.85 meters) is less than the base-case value indicating that, on average, the heterogeneous realizations match the observed head data at least as well, if not better, than the TSPA 3-D SZ flow model.

A histogram of the 100 RMSE values calculated on the heterogeneous-permeability realizations, with the faults defined as enhanced permeability features, is shown in Figure 8 - 47b. The mean of these 100 RMSE values (19.70 meters) is also less than that of the base case indicating that, on average, the heterogeneous realizations match the observed head data at least as well, if not better, than the TSPA 3-D SZ flow model.

The main conclusion that can be drawn from examination of the calibrated heads is that it is possible to reproduce, or even improve, the level of calibration seen in the base-case (homogeneous and no-pathway) model when intra-unit heterogeneity and a continuous high-permeability pathway in the form of a fault are added to the model. The available hydraulic-head data are not sufficient to defend against the presence of either feature examined in this sensitivity analysis. Comparison of the calibrated heads between the two ensembles of realizations indicates that the presence or absence of the high-permeability pathway in the model does not significantly change the calibration.

**Concentrations and Travel Times** - The transport modeling done for the base-case and the sensitivity analyses uses a step-function source term that maintains a constant-solute mass flux from the initiation of the step out to an infinite time. The transport model itself is only run out to 5,000 years at which time most breakthrough curves have reached a concentration plateau, but the concentration continues to rise to the final simulation time. Due to this continual gradual rise in the model concentration, the final concentration for each model is a function of the time to which the model is run. We feel it is more consistent to compare the time to the 95 percent of final concentration and the concentration value that is 95 percent of the final concentration across the model results. This metric captures the time and concentration at which the breakthrough curves have reached a plateau, but is not influenced by the arbitrarily chosen time to the end of the simulation.

Figure 8 - 48A shows a histogram of the 95 percent of final concentrations for the 100 realizations created with intra-unit heterogeneity but without any high permeability connected pathways. The base case value of  $2.82 \times 10^{-9}$  g/l is significantly higher than any of the 100 heterogeneous realizations. In the TSPA 3-D SZ flow model, the radionuclide plume remains very near the water table and the amount of spreading is minimal. When heterogeneous bulk

permeability fields are included in the model, the plume undergoes a greater amount of dispersion and the 95 percent of final concentrations are lower relative to the base case.

Figure 8 - 48B shows a histogram of the 95 percent of final concentrations for the 100 realizations created with intra-unit heterogeneity and also with the faults implemented as high-permeability connected pathways. The base case value of  $2.82 \times 10^{-9}$  is still significantly higher than the mean of the 100 realizations. In general, the 95 percent of final concentrations are larger by a factor of 1.3 in the ensemble containing the faults than in the ensemble without faults.

Histograms showing the times to the 95 percent of final concentrations are shown in Figure 8 - 49 for both ensembles of realizations. A filled circle denoting the base case time to 95 percent of final (915 years) is shown with both ensembles. The longest times to 95 percent of final concentration (Figure 8 - 49A and B) are due to realizations where low permeability zones occur under the repository. In these realizations, a considerable amount of time is necessary for the plume to move out of these regions. The mean travel time to 95 percent of final concentration is shorter for the ensemble that includes the faults as high-permeability connected pathways than in the ensemble of heterogeneous realizations that does not include the high-permeability faults.

**Location of Peak Concentration at 20 Kilometers** - For TSPA-VA the biosphere model is connected to the TSPA 3-D SZ flow model by a hypothetical well that extracts water from the aquifer for potential domestic and agricultural use. The conservative assumption that this well will intersect the highest concentration portion of the radionuclide plume is employed in this connection between models. The location of the highest concentration within the plume is determined along a vertical cross-section through the TSPA 3-D SZ flow model at a distance 20 kilometers downstream of the repository. This cross-section can be viewed as a plane in the X-Z (Easting-Vertical) dimensions. By plotting the locations of the maximum concentration on this plane for each realization in each ensemble, the spatial variability in the location of the maximum concentration can be examined.

Figure 8 - 50A shows the locations of the maximum concentration for the 100 realizations with intra-unit heterogeneity and no high-permeability connected features. For comparison with Figure 8 - 50A, the location of the highest concentration in the base-case run is shown as the gray-filled circle.

Figure 8 - 50B shows the locations of the maximum concentration for the 100 realizations with intra-unit heterogeneity and also high-permeability connected features. The maximum concentration in the base-case plume is at (551840,0) and the vertical fault zone intersects the 20-km plane at an easting coordinate of 551340. From Figure 8 - 50B, it is obvious that the fault zone controls the location of the maximum concentration for the majority of the realizations in this ensemble.

The main effect of the heterogeneity in the realizations is to produce variability in the location of the highest concentration at the 20 km boundary. The location of the highest concentration, as the radionuclide plume crosses the 20 km boundary, is variable from realization to realization when heterogeneity is incorporated into the bulk permeability model. Adding high-permeability pathways tends to produce opposite results by focusing the flow and the radionuclide along the transport path and producing less variability in the location of the highest concentration at the

20 km boundary. It is noted that in this example, the location of the highest concentration in the base-case run happens to be near the location where the fault intersects the 20 km boundary. If the fault crossed the boundary in a different location, the location of maximum concentration could be quite different from the base-case results. The implication for repository performance of this spatial variability in plume location are minor if the analysis assumes the pumping well would be located in the center of the plume. However, if the probability of the pumping well intersecting the plume were to be considered in the analysis, this spatial variability could be significant.

#### **8.5.2.2.5 Conclusions**

Perhaps the most significant conclusion that can be drawn from this sensitivity analysis is an awareness of the difficulty in defending against a connected high-permeability pathway from near the repository to the accessible environment. The data available at Yucca Mountain are not sufficient to rule out the existence of such a pathway. From the results presented in Figure 8 - 47b, steady-state head data alone are not enough to detect the presence or absence of such a feature.

This sensitivity analysis shows that the time to reach 95 percent of final concentration is not significantly affected by the presence or absence of heterogeneous permeability fields or high permeability connected pathways. The 95 percent of final concentration in the base case is higher than in any of the sensitivity analyses considered here. The effect of heterogeneity in the bulk permeability fields is to increase the amount of simulated dispersion and lower the final concentration relative to the TSPA 3-D SZ flow model. Note that these conclusions may be a function of some key assumptions used in the analysis (e.g., the value of permeability used for the high-permeability faults). Heterogeneity in the bulk permeability fields also increases the variability in the location of the peak concentration at the 20 km fence from one realization to the next. Addition of heterogeneity to the TSPA-VA modeling may allow for the elimination of the conservative assumption that the extraction well connected to the biosphere model must always intersect the highest concentration in the radionuclide plume.

#### **8.5.2.3 Dual-Porosity Transport**

The effective-porosity approach for modeling radionuclide transport in fractured media in the saturated zone was used in the TSPA-VA base case analysis. This approach makes the simplifying assumption that some fraction of the total porosity in the fractured tuffs in the saturated zone is available for groundwater flow and radionuclide transport. The resulting analysis used a single-porosity continuum representation of the aquifer, in which uncertainty regarding groundwater flow channelization and/or matrix diffusion was assessed using a range of effective porosity.

In reality, the porosity of the medium that is available for solute transport is a complex function of the fracture network geometry, the bulk permeability distribution, and the solute transport history of the system. Molecular diffusion of radionuclides into and out of the rock matrix plays a key role because of the relatively larger solute storage capacity in the rock matrix in comparison to the fracture network. A dual-porosity model explicitly accounting for the processes influencing radionuclide migration in the fractured medium may be more appropriate.

In the dual-porosity model of solute transport in groundwater, advective transport is conceptualized to occur only in the fractures and the matrix is available for the storage of solute mass by molecular diffusion. Parameters controlling mass transport in a dual-porosity medium may include fracture spacing, fracture and matrix porosities, coefficient of molecular diffusion, sorption coefficient and decay constants of nuclides, dispersivity of geological materials, and Darcy flow velocity.

Understanding the influence of these parameters on the mass transport is very important for the assessment of environmental impact from the migration of radionuclides in the saturated zone under the potential nuclear repository at the Yucca Mountain. A similar sensitivity analysis of parameters and importance under brine-reservoir-breach release condition was performed at the Waste Isolation Pilot Plant (WIPP) site using a regional, double-porosity, solute transport model (Reeves et al. 1987). Although numerous studies have focused on mass transport of contaminants in the fractured media at the site (Peters and Klavetter 1988; Pruess et al. 1990a and 1990b; Robinson 1994), there is no systematic investigation studying the influence of various parameters on the mass transport in the saturated zone using the dual-porosity approach.

The primary objective of the sensitivity studies is to investigate the influence of various parameters on the mass transport in fractured media. At the same time, the potential inaccuracies of the effective-porosity approach in relation to the dual-porosity approach for the saturated zone transport and the approximate relationship between effective fracture spacing and effective porosity for radionuclide transport in the 1-D transport simulations used in TSPA-VA are explored. Simulations of 1-D transport with the alternative approaches were all conducted with the FEHMN code for consistency with the TSPA-VA base case analyses.

#### 8.5.2.3.1 Theory and Model Setup

To simplify the mass transport in the saturated zone, a one-dimensional model may be used to represent the geological system of the volcanic and alluvium units. The geometric factor of a fractured medium may be described by the fracture spacing and aperture size of the fracture (Figure 8 - 51). The fracture porosity is defined by fracture spacing and aperture of the fracture:

(8 - 12)

$$\phi_f = \frac{2b}{s}$$

where  $\phi_f$  is fracture porosity,  $b$  is half of the fracture aperture, and  $s$  is the fracture spacing. The effective fracture porosity ( $1.0 \times 10^{-4}$ ) of three volcanic units (upper volcanic aquifer, middle volcanic aquifer, and middle volcanic confining unit) between 0 to 18 km from the repository is much lower than that of the alluvium deposits (0.25). It is expected that nuclide transport in the fractured volcanic units is potentially much faster than in the alluvium deposits. There are a number of ways to simulate the mass transport in a fractured medium. A simple approach is to consider the fractured medium as a single-porosity continuum, in which the porosity of the continuum is the combination of the fracture and matrix properties (Schwartz and Smith 1988). A second approach is the dual porosity approach, in which each node consists of a fracture node



and a number of matrix nodes. The dual-porosity model can be implemented explicitly (Reeves et al. 1986a and 1986b; Zyvoloski et al. 1997 ) or simulated using a two-dimensional model (Grisak and Pickens 1980; Robinson 1994, pp. 81-84; Lessoff and Konikow 1997). In this study, the three approaches will be compared and one of the approaches will be chosen as the basic approach for sensitivity analysis. Processes affecting the mass transport of radionuclides are advection, dispersion, diffusion, sorption, and radionuclide decay. These processes will be included in the three models.

**One-Dimensional Single-Porosity Continuum Model (Effective-Porosity Approach)** - A single-porosity model may be used to represent a fractured medium if the parameters in the single-porosity model reflect the combination of the matrix and fracture system (Figure 8 - 52a). The mass-transport equation in one dimension may be expressed as

(8 - 13)

$$D_{xx} \frac{\partial^2 C}{\partial x^2} - v_x \frac{\partial C}{\partial x} - R\lambda C = R \frac{\partial C}{\partial t}$$

where  $C$  is the concentration of a radionuclide,  $D_{xx}$  is the dispersion coefficient along the flow direction,  $v_x$  is pore groundwater velocity,  $\lambda$  is the decay constant, and  $R$  is retardation factor. These variables can be expressed as

(8 - 14)

$$D_{xx} = v_x \alpha_x + D_x^*$$

(8 - 15)

$$v_x = \frac{q_x}{\phi_e}$$

(8 - 16)

$$R = 1 + \frac{1 - \phi_e}{\phi_e} K_d \rho_s$$

where  $\alpha_x$  is the longitudinal dispersivity,  $D_x^*$  is effective diffusivity,  $q_x$  is Darcy velocity in the  $x$  direction,  $\phi_e$  is effective porosity,  $K_d$  is the distribution coefficient of contaminant, and  $\rho_s$  is the density of rock. Changes of these parameters will affect mass transport in the system.

The one-dimensional, single-porosity model contains four zones: upper volcanic aquifer (zone 1), middle volcanic aquifer (zone 2), middle volcanic confining unit (zone 3), and undifferentiated valley fill / alluvium (zone 4) (Figure 8 - 52b).

The flow model consists of 5,000 one-dimensional elements and 5,001 nodes with a node spacing of 5 m. Constant pressure is specified at the node 5,001 and a constant flux rate of  $1.9 \times 10^{-5}$  kg/s is assigned at node 1 so that a Darcy velocity of 0.6 m/y will be maintained along the flow path. For mass transport boundary conditions, a constant concentration of  $1.667 \times 10^{-3}$  g/L is applied at node 1 by assuming a source mass flux of 1 g/year coming from the unsaturated zone. The bulk permeability of each zone may change the pressure distribution along the flow path, but it will not change the Darcy velocity. Therefore, a bulk permeability of  $10^{-11}$  m<sup>2</sup> is assigned in each zone. The most important parameters affecting transport are porosity, sorption coefficient, and density of rock, if the sorption coefficient is not zero.

**One-Dimensional Dual-Porosity Model** - The dual-porosity model assumes that each node in a discretized mesh consists of a fractured block and matrix block(s). The fractured block serves as a conduit of fluid while the matrix block acts as a fluid storage mechanism (Figure 8 - 53a). In terms of contaminant transport, mass exchange between the fractured and matrix blocks is by means of molecular diffusion. This approach has been implemented in many codes (Reeves et al. 1986a and 1986b; Zyvoloski et al. 1995). The mass transport equation in the fractures is written as:

(8 - 17)

$$\frac{\partial}{\partial x} \left( D_{xx} \frac{\partial C}{\partial x} \right) - v_x \frac{\partial C}{\partial x} - \frac{\Gamma}{b} - R \lambda C = R \frac{\partial C}{\partial t}$$

where  $\Gamma$  is diffusive flux from fracture to matrix, and  $b$  is half of the fracture aperture. If the flow is in the x-direction and the direction into the matrix is y, the diffusive flux is expressed as:

(8 - 18)

$$\Gamma = -\phi_m D_m \frac{\partial C}{\partial y} \Big|_{y=b}$$

where  $\phi_m$  is the porosity of the matrix, and  $D_m$  is the molecular diffusivity of the matrix. The transport equation in the matrix is characterized by:

(8 - 19)

$$D_m \frac{\partial^2 C'}{\partial y^2} - R_m \lambda C' = R_m \frac{\partial C'}{\partial t}$$

where  $C'$  is the concentration in the matrix, and  $R_m$  is the retardation factor in the matrix.

The geometric specification of the one-dimensional dual-porosity model is the same as that of the one-dimensional single-porosity model. Additional parameters are needed to specify the connection between a fracture node and matrix node(s) (Figure 8 - 53b). As implemented in the dual-porosity option of FEHMN (Zyvoloski et al. 1995), only two matrix nodes are possible. It is assumed that the total volume of a node is the sum of volumes of a fracture node and two

matrix nodes. Percentage of fracture volume defines the porosity of the fractures. Total normalized volume is equal to 1.

(8 - 20)

$$V_f + V_{m1} + V_{m2} = 1$$

where  $V_f$ ,  $V_{m1}$ , and  $V_{m2}$  are volume fractions of fracture, first matrix nodes, and second matrix nodes, respectively. These parameters are related to characteristic lengths of fracture block and two matrix blocks by

(8 - 21)

$$V_f = \frac{L_f}{L_{f0}}$$

and

(8 - 22)

$$V_{m1} = \frac{L_{m1}}{L_{f0}}$$

and

(8 - 23)

$$V_{m2} = \frac{L_{m2}}{L_{f0}}$$

where  $L_f$ ,  $L_{m1}$ , and  $L_{m2}$  are the characteristic lengths of the fracture, first matrix blocks, and second matrix blocks, respectively, and  $L_{f0}$  is a characteristic length scale. In the slab fracture model (Figure 8 - 53),  $L_f$  is equal to half of the fracture aperture ( $b$ ),  $L_{f0}$  is half of the fracture spacing ( $s/2$ ), and  $L_{m1} + L_{m2}$  is equal to  $s/2 - b$  (Figure 8 - 51 and Figure 8 - 53).

**Two-Dimensional Single-Porosity Model** - A one-dimensional fractured medium may also be simulated by a two-dimensional single-porosity continuum (Grisak and Pickens 1980; Robinson 1994, pp. 81-84; Lessoff and Konikow 1997). The two-dimensional transport equation is expressed as

(8 - 24)

$$\Delta(\phi D \Delta C) - \Delta(\phi V C) - R \lambda C = \frac{\partial(R \phi C)}{\partial t}$$

where  $\phi$  is the porosity,  $D$  is the dispersion coefficient tensor, and  $V$  is the groundwater pore velocity. In this approach, a very low bulk permeability is assigned to the matrix nodes so that almost no flow enters into the matrix nodes. The simulation domain consists of mobile regions where fractures exist and immobile regions, which represent matrix nodes. For steady state and saturated conditions, flow exchange between fracture and matrix is not important. For a continuous contaminant source, the most important transport mechanism is the solute mass diffusion from fracture into matrix. In this study, one row denotes fracture nodes and 50 rows represent the matrix nodes (Figure 8 - 54). The ratio of the fracture node width over the matrix nodes width is fracture porosity. A constant pressure was specified at outlet nodes of the simulation domain and a water injection rate was specified at the node corresponding to the inlet of the fracture. This flux rate is proportional to the fracture spacing, thus preserving a constant Darcy flow rate (0.6 m/y) through the bulk medium for different values of fracture spacing. Groundwater will flow in a very narrow channel in the volcanic units and spread out once it reaches the alluvium unit. Because many more nodes are used to represent the matrix in the two-dimensional, single-porosity model than in the one-dimensional, dual-porosity numerical model as implemented by FEHMN with only two matrix nodes, it is assumed that the two-dimensional, single-porosity model yields a more accurate solution for solute transport in the dual-porosity medium.

#### 8.5.2.3.2 Simulation Results

In this study, a finite element heat and mass transfer code, FEHMN (Zyvoloski et al. 1995), was used exclusively for all of the simulations for consistency. Most simulations were based upon the transport of  $^{99}\text{Tc}$ , which is an unretarded, decaying radionuclide. For the sensitivity analysis of sorption coefficients, the transport of  $^{237}\text{Np}$  was simulated. For most of the sensitivity analyses, a fracture spacing of 2 m was used, except where otherwise specified. Some simulation results are shown for both a 15 and 20 km travel distance. Mass transport is in the fractured-volcanic-tuff medium from the source to 17.73 km. The unfractured, porous alluvial unit occurs from 17.73 km to 20 km in the one-dimensional transport model. Thus, the breakthrough curves at 20 km are the combined results of mass transport in both fractured and porous media.

**Comparison of the Two-Dimensional, Single-Porosity Model and the One-Dimensional, Dual-Porosity Model** - One of the arguments that favors the use of the two-dimensional model to simulate one-dimensional, dual-porosity mass transport is that the mass diffusion gradient from fracture to matrix may be more accurately simulated by incorporating a large number of matrix nodes, in the model using the FEHMN code. Hence, the diffusion process is more accurately depicted. In this comparison, the parameters describing dual-porosity mass transport are listed in Table 8 - 27.

Because the alluvium deposit is not fractured, a single porosity of 0.25 is used. A permeability value of  $1.0 \times 10^{-7} \text{ m}^2$  is assigned to fracture and alluvium nodes and a low permeability of  $1.0 \times 10^{-18} \text{ m}^2$  is specified at the matrix nodes of volcanic units for the two-dimensional model. Under this condition, the groundwater will flow through in the first three volcanic units in very narrow channels and spread out in the alluvium unit. Simulation results for fracture spacings of 2, 5, and 10 m are compared for the two models at travel distances of 15 and 20 km (Figure 8 - 55a and Figure 8 - 55b). In the two-dimensional model, the dimension perpendicular to the flow

direction is half of the fracture spacing (Table 8 - 28). Half of the fracture spacing is the same as the characteristic length  $L_{f0}$  in the one-dimensional, dual-porosity model. It was assumed that the volume fraction of the first matrix node is 0.5 in the one-dimensional, dual-porosity model. The simulations showed that the general trend of the two sets of breakthrough curves is very similar in terms of travel times and shapes at both distances, although the two results agree better at 15 km than at 20 km. This may be due to shorter mass transport distance at 15 km. At early times, the concentration from the two-dimensional model is less than that from the one-dimensional model. However, the concentration increases more quickly than the one-dimensional model at late times. It may be concluded that the simulated time to reach diffusion equilibrium is somewhat shorter using the two-dimensional approach than using the one-dimensional approach, but the results from the two approaches are not significantly different. The accuracy of the one-dimensional dual-porosity method is dependent on other model parameter values, in particular, the Darcy flow rate and molecular diffusion coefficient. For the base case parameter values used in the comparison presented here, the one-dimensional dual-porosity model yields an acceptably accurate solution. However, all of following simulations for fractured media use the two-dimensional approach to insure accuracy.

**Comparison of the One-Dimensional (Effective Porosity) and the Two-Dimensional (Single-Porosity) Continuum Models** - A number of simulations were designed to examine the characteristics of concentration breakthrough curves by changing the fracture spacing. These two-dimensional simulations are then compared with two runs of one-dimensional, single-porosity simulation having fracture and matrix porosities, respectively. To maintain a fracture porosity of  $1.0 \times 10^{-4}$  and the same amount of flux for the same cross-sectional area, the fracture aperture and applied flux at node no. 1 are increased as fracture spacing increases (Table 8 - 28). Figure 8 - 56a and Figure 8 - 56b show breakthrough curves at distances of 15 km and 20 km from the repository, respectively. The delay effect of the alluvium unit is evident at 20 km (Figure 8 - 56b) as compared to the early breakthrough times at 15 km (Figure 8 - 56a). Clearly, one-dimensional simulation with the fracture porosity exhibits the earliest breakthrough time while that with the matrix porosity results in the latest breakthrough time in both cases. Results for a smaller fracture spacing ( $s = 0.2$  m) are very similar to the breakthrough curve using the matrix porosity in the one-dimensional simulation, while the breakthrough curve with a larger fracture spacing ( $s = 200$  m) is very close to the simulation using the fracture porosity. If the time is  $t_{0.5}$  for  $C = 0.5C_0$  on the breakthrough curve, the breakthrough curves are asymmetric when they are divided into two parts (early- and late- parts) at time  $t_{0.5}$  for a larger fracture spacing ( $>2$  m). This trend of asymmetry increases as the fracture spacing is increased.

**Sensitivity to Molecular Diffusion Coefficient** - Simulations of transport to a 20 km distance for three different values of molecular diffusion coefficient ( $1.0$ ,  $3.2$ , and  $5.0 \times 10^{-11}$   $\text{m}^2/\text{s}$ ) are shown in Figure 8 - 57. These values of effective-molecular-diffusion coefficient were loosely based upon the range of diffusivity values of  $^{99}\text{Tc}$  from laboratory measurements using volcanic tuff from the Yucca Mountain site (Triay et al. 1997). For a larger molecular-diffusion coefficient ( $5.0 \times 10^{-11}$   $\text{m}^2/\text{s}$ ), a later breakthrough time is expected. Consequently, an early equilibrium is achieved because the diffusion from a fracture to matrix is much quicker than that for a smaller diffusion coefficient value ( $1.0 \times 10^{-11}$   $\text{m}^2/\text{s}$ ). The concentration for a larger diffusivity approaches the input concentration at an earlier time than that for a smaller diffusivity. For the range of diffusivity considered, the difference in the breakthrough curves is not significant.

**Sensitivity to Radionuclide Decay** - The change of decay constants may also affect the transport characteristics of a radionuclide. The net effect of radionuclide decay is to convert the mass of a parent nuclide to that of a daughter product. The half-life of  $^{99}\text{Tc}$  is 213,000 years. Because this half-life is larger than the simulation time (20,000 years), the mass loss is not significant at 20 km distance. This is indicated by comparing the concentration to the initial concentration of  $1.667 \times 10^{-3} \text{ g/L}$ . Three sets of simulations of  $^{99}\text{Tc}$  transport were compared for fracture spacings of 0.2, 2, and 20 m (Figure 8 - 58). For a smaller fracture spacing ( $s = 0.2 \text{ m}$ ), the difference in concentration between simulations with and without decay is relatively larger because of the longer travel times. For the simulation without decay, this maximum concentration is the concentration of the source concentration. For the simulation with decay, this maximum concentration is less than the source concentration by a small factor.

**Sensitivity to Sorption Coefficient** - The input parameters of the simulations so far considered more or less reflected the properties of  $^{99}\text{Tc}$ , a non-sorbing species. The effect of sorption on the mass transport was studied based on the properties of  $^{237}\text{Np}$ .  $^{237}\text{Np}$  exhibits some sorption and is retarded during the transport. A typical value of sorption coefficient for  $^{237}\text{Np}$  is 1 ml/g in the volcanic units and 10 ml/g in alluvium with a decay half-life of  $2.14 \times 10^6$  years. Both the one-dimensional, single-porosity continuum model (effective-porosity approach) and two-dimensional model were set up for this analysis. In the two-dimensional model, the sorption coefficient was assumed to be the same in both the matrix and fracture nodes. In the one-dimensional single-porosity continuum model, the bulk density of the medium was scaled according to the effective porosity when calculating retardation factor by the following equation:

(8 - 25)

$$\rho_b^f = \rho_b \frac{n_{eff}}{n}$$

where  $\rho_b^f$  is the scaled bulk density of fractures,  $\rho_b$  is the bulk density of the fractured medium. In both model setups, sorption coefficient was changed in the volcanic unit ( $K_d = 0, 0.1, 0.5$ , and  $1.0 \text{ ml/g}$ ) while keeping that in the alluvium unit constant ( $K_d = 10 \text{ ml/g}$ ). This range in sorption coefficient corresponds to the lower end of the distribution for  $K_d$  of  $^{237}\text{Np}$  for volcanic units used in the TSPA-VA base-case analyses. Other transport parameter values are given in Table 8 - 27. Simulations at distances of 15 and 20 km, respectively, are shown in Figure 8 - 59a and Figure 8 - 59b. In Figure 8 - 59a, breakthrough curves at  $K_d = 0, 0.1, 0.5$ , and  $1.0 \text{ ml/g}$  for the one-dimensional model fall on the same curve at this display scale. With matrix diffusion in the two-dimensional model, all of the simulations showed late breakthrough times as compared to the one-dimensional simulations. A retardation factor may be defined as

(8 - 26)

$$R = \frac{t_{0.5}^x}{t_{0.5}}$$

where  $t_{0.5}$  is the advective transport time when  $C = 0.5c_0$  for radionuclides in fractures without matrix diffusion and adsorption, and  $t_{0.5}^x$  is the advective transport time for radionuclides in fractures with matrix diffusion or adsorption or both, and  $R$  is the retardation factor for radionuclide transport in fractures with matrix diffusion or adsorption or both. Table 8 - 29 lists the retardation factors for the simulations at 15 km. In the table, simulation "1d-0.1" means one-dimensional simulation with a distribution coefficient of 0.1 ml/g. Columns 2 through 5 are for the one-dimensional simulations and columns 6 through 9 are for the two-dimensional simulations. The results show that retardation due to the matrix diffusion is much more important than the adsorption for radionuclide transport in fractured media. For example, the retardation factor with matrix diffusion and no adsorption ( $R = 2307.7$ ) is more than 700 times higher than that with adsorption ( $K_d = 1.0$ ) and no matrix diffusion ( $R = 2.9$ ).

**Sensitivity to Matrix Porosity** - Matrix porosity characterizes the solute mass storage available to diffusive transfer from the fractures. Large porosity constitutes large storage capacity. For this set of analyses, the value of porosity was changed for three simulations ( $\phi_m = 0.1, 0.25$ , and  $0.4$ ). For a larger matrix porosity ( $0.4$ ), it takes a much longer time to fill the matrix void space. Figure 8 - 60 shows that the simulation with a smaller matrix porosity experiences early breakthrough, whereas the simulation with a larger matrix porosity produces a late breakthrough time.

**Sensitivity to Fracture Porosity** - The values of fracture porosity were changed in a range from  $10^{-5}$  to  $10^{-3}$  for three simulations. Other transport parameter values are given in Table 8 - 27. Very little change was observed in the shapes of breakthrough curves and breakthrough times (Figure 8 - 61) among the simulations.

**Sensitivity to Longitudinal Dispersivity** - Simulations were compared for five values of longitudinal dispersivity ( $\alpha_L = 25, 50, 100, 200$ , and  $400$  m) (Figure 8 - 62). The breakthrough curve for  $\alpha_L = 400$  m exhibits somewhat greater apparent dispersion compared to that for  $\alpha_L = 25$  m. Because the effect of mass diffusion into matrix dominates the response of the system, the five curves differ little, as shown in Figure 8 - 62.

**Sensitivity to Specific Discharge** - Specific discharge changes both the shapes and breakthrough times for the four cases considered ( $q = 0.06, 0.2, 0.6$ , and  $6.0$  m/y.) in the two-dimensional, single-porosity model (Figure 8 - 63). At the simulation time (20000 years), the concentration for  $q = 0.06$  m/year at 20 km is zero. The advective transport times ( $t_{0.5}$ ) are 1000, 7500, and 16000 years for  $q = 6.0, 0.6$ , and  $0.2$  m/y, respectively. Other transport parameter values are given in Table 8 - 27. With a smaller Darcy velocity, the breakthrough is more stretched out than with a larger velocity.

**Comparison of the Effective Porosity Approach and the Two-Dimensional Single-Porosity Continuum Model** - One of the objectives of comparing the mass transport in one-dimensional single-porosity continuum model and the two-dimensional model is to determine the value of the effective porosity that corresponds to a particular value of fracture spacing in a dual-porosity fractured medium. The sorption coefficient and the porosity are the important parameters defining the travel time of a contaminant in the SZ. For this discussion, only porosity was considered because both parameters only affect the advective velocity for equilibrium adsorption. Disregarding differences in the shape of the breakthrough curves, the time  $t_{0.5}$  may

be compared for the one-dimensional model and the two-dimensional model to determine "effective porosity" for the one-dimensional model. Type curves of one-dimensional transport in the single-porosity model were calculated for porosities of 0.0001 (fracture porosity), 0.0005, 0.001, 0.005, 0.01, 0.025, 0.05, 0.075, 0.1, 0.15, and matrix porosity. These type curves were matched by the breakthrough curves in the two-dimensional model for a number of fracture spacings ( $s = 0.2, 2, 5, 10, 20$ , and  $200$  m) (Figure 8 - 64) to determine the "effective porosity" (Table 8 - 30). Matching of these curves was done on the basis of the midpoint (i.e.,  $C/C_0 = 0.5$ ) of the concentration breakthrough curves. The results indicate that the "effective porosity" for  $s = 0.2$  m is almost the same as the matrix porosity and that the effective porosity (0.0005) for  $s = 200$  m is close to the fracture porosity (0.0001). Note that there are significant differences in the shapes of the concentration breakthrough curves for intermediate values of fracture spacing and effective porosity. The implications to performance assessment calculations of the inaccuracies in the effective porosity approach are discussed in the following section.

### 8.5.2.3.3 Discussion and Conclusions

The simulations indicate that changes of breakthrough curves in fractured media are reflected not only in terms of breakthrough time but also the shape of the breakthrough curves. However, varying the porosity value will not change the shape of the breakthrough curves for the one-dimensional, single-porosity model. Therefore, the one-dimensional, single-porosity model may not be able to reproduce the shape of the breakthrough curves for intermediate values of fracture spacing ( $>0.2$ m) under the equilibrium-adsorption assumption. The diffusion from a fracture into its adjacent matrix closely resembles the kinetic adsorption process. In the physically based, kinetic-adsorption model, the flow is divided into two regions: a mobile region between the solid grains, and an immobile region inside the solid grain (van Genuchten and Wierenga 1976, pp. 475-476; van Genuchten 1981; Wood et al. 1990, p. 1569; Zhang et al. 1998, p. 69-71). The mass transfer between the mobile (fractures) and the immobile (matrix) regions are through the process of diffusion. The most striking characteristic in breakthrough curves for transport with the kinetic reaction is the long concentration tail compared to the transport front. This is also true for mass transport in a dual-porosity medium, especially for large fracture spacings. The kinetic adsorption reaction equation is written as (Zhang et al. 1998, p. 71):

(8 - 27)

$$\frac{\partial(n_k R_{ik} c_{ik})}{\partial t} = \alpha(c_i - c_{ik})$$

where  $i$  is the index number of for species  $i$ ,  $\alpha$  is the mass transfer coefficient between the mobile and the immobile regions [ $T^{-1}$ ],  $c_i$  is the concentration in the mobile region, the  $c_{ik}$  is the concentration in the immobile region,  $n_k$  is the intra-grain porosity, and  $R_{ik}$  is the retardation factor in the immobile region. By applying Equations (8 - 18 and (8 - 19 at the boundary between the fracture and the matrix and applying decay terms within the matrix, one obtains:

(8 - 28)



$$\frac{\partial C'}{\partial t} = -\frac{D_m}{R_m \Delta y}(C' - C) = \alpha_f(C - C')$$

where  $\Delta y$  is the distance between the fracture-matrix boundary and the first matrix node near the fracture-matrix boundary in the two-dimensional model, and  $\alpha_f$  is a mass transfer coefficient between the fracture and the matrix. Equation 8 - 28 simply states that mass change in the matrix is a function of average concentration difference in fracture and matrix. In the kinetic adsorption reaction, a smaller mass transfer coefficient,  $\alpha_f$ , creates a longer tail in the breakthrough curve. This is also true for the breakthrough in a dual-porosity fractured medium. However, it should be noted that intra-grain porosity in the kinetic adsorption model is much smaller than the matrix porosity in the dual-porosity model.

Fracture spacing, fracture and matrix porosities, diffusivity, sorption coefficient and decay constant of nuclides, dispersivity of geological materials, and Darcy flow velocity were changed to study the effects of different models on the mass transport of radionuclides in fractured media. All of these parameters exhibit different degrees of influence on the shape and breakthrough time of concentration breakthrough curves in the 1-D transport model for the SZ. The simulations illustrate that matrix diffusion is much more important in retarding the mass transport than the adsorption process in the saturated zone at the Yucca Mountain site. Mathematically, the matrix diffusion process more closely resembles the kinetic adsorption model, and the breakthrough curves exhibit asymmetry in shape and large, apparent dispersion for intermediate values of fracture spacing.

These sensitivity studies also indicate that the effective-porosity approach to simulating radionuclide transport in the saturated zone conservatively approximates solute transport in the fractured volcanic tuff medium for the purposes of the TSPA-VA. Although the effective-porosity, single-continuum conceptual model is a significant simplification of the advective and diffusive processes occurring in fractured media, this approach spans the range of potential transport behavior within the bounds of our uncertainty of the system. For cases in which the dual-porosity conceptual model of radionuclide transport indicates concentration-breakthrough response outside the bounds defined by the effective-porosity model, the effective-porosity model overestimates radionuclide concentration. Therefore, the effective-porosity approach provides a conservative approximation of the system response for the situations in which it results in inaccuracies.

Results of the 1-D transport simulations show that there is relatively good agreement between the effective-porosity model and the dual-porosity model for cases of small effective porosity (the same as fracture porosity), corresponding to large effective fracture spacing (100s of meters). Similarly, there is good agreement between the effective-porosity model and the dual-porosity model for cases of larger effective porosity (the same as matrix porosity), corresponding to small effective-fracture spacing (tenths of a meter). At intermediate values of effective porosity and fracture spacing, the concentration breakthrough curves simulated by the dual-porosity model significantly differ from the results of the effective-porosity model (Figure 8 - 56 and Figure 8 - 64). However, the maximum concentrations from the dual-porosity model are lower than those simulated by the effective-porosity model at longer times, as discussed above.

The results of this sensitivity study are relevant in evaluating the appropriate range of uncertainty in the effective-porosity parameter for use in TSPA-VA analyses. The TSPA-VA base-case analysis of flow and transport in the saturated zone utilizes a relatively broad range in the uncertainty distribution for effective porosity in the fractured volcanic tuff units (Section 8.4.2). The median value for effective porosity in this uncertainty distribution for the volcanic units is approximately 0.003. Examination of Figure 8 - 56 indicates that this value and smaller values of effective porosity correspond to effective fracture spacing in the range of tens to hundreds of meters, based on the dual-porosity modeling results. The reasonableness of effective fracture spacing on the scale of tens to hundreds of meters is supported by flow surveys in boreholes in the saturated zone at Yucca Mountain. Representative surveys in fractured volcanic units indicate relatively wide separation, on the order of tens to hundreds of meters, between zones producing groundwater during pumping of the wells (Luckey et al. 1996, p. 38, Figure 15).

#### **8.5.2.4 Alternative Dilution Assumptions**

Changes in the amount of dilution of radionuclides in the saturated zone have a direct, linear effect on the dose incurred by a receptor 20 km downgradient from Yucca Mountain. The sensitivity study described here addresses how assumptions concerning dilution could influence the results of a dose calculation. If dilution is considered not only in the saturated zone, but also in the biosphere, the assumptions concerning dilution translate into how the choice of a performance measure, based on individual dose (as used in TSPA-VA), could differ from a performance measure based on average dose-rate per person. The sensitivity study presented here is a preliminary scoping estimate; a more accurate analysis would involve actual water-usage data and detailed food-consumption patterns, then calculating and summing the doses incurred by individuals comprising the critical group.

In the TSPA-VA base case, a dilution factor was used to reduce the final concentration of radionuclides in the groundwater. Additionally, several assumptions were made concerning the extraction and use of the groundwater. Some of these assumptions are as follows:

- The individual's water source is always at the point of maximum contamination in the aquifer.
- There is no dilution during withdrawal of water from the aquifer; that is, there is no mixing of contaminated water with uncontaminated water when the water is pumped from the ground or when the water is stored in a tank.
- The locally produced foodstuffs that this individual consumes, as determined by a survey of existing inhabitants of the Amargosa Valley region (Chapter 9), were all grown with this maximally contaminated groundwater. In other words, consumables, possibly grown away from contaminated groundwater, but still in the Amargosa Valley region, were considered to be contaminated.

If the plume of contaminated groundwater is large and dispersed, these assumptions are reasonable. However, the saturated zone modeling allows little dilution of contaminated groundwater with uncontaminated groundwater; the contaminated groundwater travels in flow tubes and is typically diluted by a factor of 10. The original plume has cross-sectional

dimensions of about 3,000 m horizontally and 14 m vertically. With a groundwater flux of 0.6 m/y, the plume would have a volume of approximately 26,000 m<sup>3</sup>/year. The plume at 20 km downgradient has an undefined cross section, but with a dilution factor of 10, it might have dimensions of about 10,000 m horizontally and 42 m vertically, and a volume of approximately 260,000 m<sup>3</sup>/year. Within this plume, concentrations would be variable, so the region of highest concentration might have a much smaller cross section. Together, however, these assumptions may cause an overestimate of the dose received by an individual. Given the size of the plume, these assumptions may be more applicable to a "subsistence-farmer" type of receptor (none of which were found in the YMP survey of local inhabitants) than a receptor defined in guidance from the National Research Council (1995, p. 52) as the "average member of the critical group."

The additional contaminant dispersion that comes with groundwater pumping and multiple food sources can be examined by determining the average dose-rate per person in the critical group. The average dose-rate per person is presented here as an alternative method to the method used in the TSPA-VA base case (Chapter 11) for calculating the dose rate to the average member of the critical group. The primary difference between this method and the method used in the base case is the relaxation of the assumption that all drinking water and all local consumables are produced using well water containing the highest concentration of radionuclides.

The average dose rate per person for the entire Amargosa Valley region is estimated as follows. The peak dose rate for the expected-value base case is approximately 300 mrem/y, occurring at 317,000 years in the future (Chapter 11). This rate defines the maximum average dose rate. The major contributor to this dose rate in the calculation is <sup>237</sup>Np, which reaches 20 km at the peak rate of 12 g/y. These radionuclides can be dissolved in 12 x 10<sup>6</sup> m<sup>3</sup> of groundwater—the estimated current groundwater discharge in the Amargosa Valley. This number is chosen because it represents current conditions and is consistent with biosphere modeling. Also, it might be more than sustainable yield and, therefore, more representative of the long-term average climate. Multiplication by the biosphere dose conversion factors gives the average dose; for <sup>237</sup>Np, the expected value of the biosphere dose conversion factor is 4.6 x 10<sup>6</sup> (mrem/y)/(g/m<sup>3</sup>), resulting in an average peak dose of approximately 4.6 mrem/y. For the entire Amargosa Valley and for all the radionuclides, the average peak dose rate is approximately 5 mrem/y.

The above calculations are applicable if there is sufficient dilution for radionuclides from Yucca Mountain to affect the entire population of Amargosa Valley. Also of interest is the average dose-rate per person for critical groups that might be less than the entire population. Given that an average dose-rate per person for a population of 1,300 is 5 mrem/y, then the average dose for half as many people is 10 mrem/y, and for a fourth as many is 20 mrem/y. Continuing in this manner, the average dose rate for 20 people is found to be 325 mrem/y, which is approximately the maximum dose considered here. Thus, this estimate of 20 people is the maximum that can be exposed at 300 mrem/y or more, and this number can only be achieved if the radionuclide contamination is divided equally among all 20 of them. Over a 70-year life span, the total dose that each person would receive would be about 21 rem.

Figure 8 - 65 presents estimates of average dose per person with respect to the size of the critical group. These results are only for the expected-value base case and are contingent on the

appropriateness of the assumptions concerning population (1300 people) and the total groundwater usage ( $12 \times 10^6 \text{ m}^3/\text{y}$ ) and the average groundwater usage ( $9200 \text{ m}^3/\text{y}$  per person).

#### 8.5.2.5 Reactive Colloid Transport

The TSPA-VA model for radionuclide transport in the saturated zone is based on the assumption that the chemical reactions occur fast, relative to the porewater velocity. Under such conditions, the reactions can be represented with equilibrium reaction formulations. This analysis serves to evaluate the limitations of such an assumption, particularly when one of the reactions of interest is the sorption of plutonium (Pu) onto mobile colloids. The purpose of this analysis is to explore potential implications of reaction processes and formulations that are currently not accounted for in the TSPA-VA model formulation. It is not to prove or disprove the validity of the PA assumptions, rather it is to identify avenues for further investigation between the Viability Assessment (VA) and the License Application (LA) analyses. Such investigations should be comprehensive and indicate which, if any, additional processes and model formulations should be included in the LA performance assessment models. This study provides the framework upon which such an analysis can be performed.

An initial colloid transport model has been developed which incorporates the following reactions:

- Aqueous Pu transport
- Aqueous colloid transport
- Pu sorption onto colloids to form PuColloids
- Filtration of colloids
- Filtration of PuColloids
  - Pu sorption on immobile rock material

In the model, these reactions can be specified as either equilibrium or kinetic. With this model, sensitivity of Pu transport is examined with respect to the reaction formulation and parameters. Laboratory and field-scale experimental data are synthesized here to identify uncertainties and appropriate ranges for the reaction parameters. In this analysis, the parameters are identified that affect the predictions or lead to predictions that vary significantly from the equilibrium-based models. The approach begins by reaction equations at equilibrium formulating kinetic equations and then comparing results. Even with equilibrium formulations, the reaction parameters have wide ranges. The full range of possible parameters is not evaluated here. Rather, starting from a reasonable equilibrium model, this study focuses on examining the significance of kinetic effects. This sensitivity study of Pu transport to sorption, complexation with colloids, and colloid filtration indicates that there may be sets of feasible reaction parameters that lead to a very small component of fast Pu transport on colloids, while sorption retards the migration rate of most of the Pu.

This analysis was initiated very close to the conclusion of the TSPA-VA effort. Although it has been performed independently of those calculations and is not an integral component of the TSPA analysis, an effort has been made to link this approach with the TSPA-VA approach so that comparisons can be made and appropriate analyses identified for the LA.

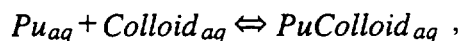
The structure of this section follows the process that was taken in this analysis. Namely, the model was developed and tested on a generic flow system first. Then, processes and parameters were modified for comparison with the TSPA-VA equilibrium model (the  $K_c$  model described in Section 8.4.2). Therefore, the conceptual model, data analysis, and derivation of model reaction parameters are discussed first. Then, model analyses for a generic flow system are presented to highlight the sensitivity to the various reaction parameters. Comparison with the TSPA-VA model is made by identifying a common set of parameters in the two different models, which lead to consistent results. Then, processes in the reactive transport model not incorporated in the current TSPA-VA model are examined with respect to their impact on radionuclide transport. Finally, the reactive transport model is demonstrated on one of the stream tubes used in the TSPA-VA analysis.

#### 8.5.2.5.1 Colloid Transport Model Description

The colloid-transport-model reactions can be represented either with equilibrium or kinetic formulations. The reactions considered here are:

aqueous phase complexation of Pu and colloids

(8 - 29)



sorption of Pu

(8 - 30)



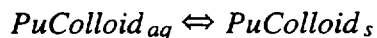
filtration of colloids

(8 - 31)



and filtration of PuColloid complexes

(8 - 32)



where *aq* indicates the aqueous phase and *s* indicates the sorbed phase. All of the reactions are dependent upon the distribution coefficient,  $K_d$ , for both equilibrium and kinetic representations of the reaction. When equilibrium conditions are assumed, then the  $K_d$  is simply

(8 - 33)

$$K_d = \frac{\prod [\text{products}]}{\prod [\text{reactants}]}$$

and when a kinetic formulation is used,

(8 - 34)

$$K_d = \frac{k_f}{k_r}$$

where  $k_f$  and  $k_r$  are the forward and reverse rates of reaction, respectively.

**Relationship Between Equilibrium and Kinetic Parameters** - For a sorption reaction, the relationship between kinetic rates and equilibrium partition coefficients ( $K_d$ s) follows as:

(8 - 35)

$$\frac{dc}{dt} = k_f c - k_r s$$

where *c* is the aqueous concentration, *s* is the sorbed phase concentration, and  $k_f$  and  $k_r$  are the forward and reverse reaction rates. The same applies for Pu-Colloid complexation where *c* is the concentration of Pu(aq) and *s* is the concentration of Pu-Colloid (filtered).

At equilibrium,  $dc/dt$  approaches 0, and the relation becomes:

(8 - 36)

$$k_f c = k_r s$$

which can be rearranged to give the definition of a distribution coefficient:

(8 - 37)

$$\frac{k_f}{k_r} = \frac{s}{c} = K_d$$

Whether a system is in equilibrium or not depends, of course, on the residence time of fluid in the domain in which the reactions take place. Due to practicality, most laboratory experiments are performed in batch mode over long enough time scales to insure that  $dc/dt=0$ . In the transport model evaluations of the impacts of disequilibrium, the ratio of  $k_f/k_r$  is held constant at the desired  $K_d$ , but the magnitude of each rate is varied from large (to insure equilibrium) to small to ensure disequilibrium.

**Data Sources, Ranges, and Conversions to Reactive Transport Model Parameters** - Table 8 - 32 summarizes the estimated ranges on data sets and model parameters for these sensitivity analyses. The next sections describe in more detail the data sources and how the experimental values are converted to model parameters.

**Pu-Colloid Complexation** - Results from batch experiments of Pu complexation with colloid material (Triay et al. 1997) and estimates of ambient colloid concentrations in saturated zone water are used to develop equilibrium and kinetic reaction coefficients for the transport models. Triay et al. measure  $K_d$  for the sorption of Pu onto colloids as:

(8 - 38)

$$K_d(lab) = \frac{\text{Moles of } PuColloid_{aq}}{\text{Grams of } PuColloid_{aq}} \cdot \frac{\text{Kg of } H_2O}{\text{Moles of } Pu_{aq}}$$

The measured  $K_d$ s range from  $10^2$  to  $10^9$  ml/g. The colloid partitioning coefficient,  $K_c$ , is then calculated as:

(8 - 39)

$$K_c = K_d(lab) \cdot \frac{\text{Grams of } Colloid_{aq}}{\text{Kg of } H_2O} = \frac{\text{Moles of } PuColloid_{aq}}{\text{Moles of } Pu_{aq}} = \frac{[PuColloid]}{[Pu]}$$

Since the mass of the colloids in groundwater is on the order of  $10^{-7}$  to  $10^{-8}$  g/ml (Triay et al. 1997), the resulting  $K_c$  range is from  $10^{-5}$  to 10. The reaction term derived from the  $K_c$  that is used in the FEHMN is:

(8 - 40)

$$K_d(fehmn) = \frac{k_f}{k_r} = \frac{[PuColloid]}{[Pu] \cdot [Colloid]} = \frac{K_c}{[Colloid]}$$

This conversion requires an estimate of the colloid site concentration,  $[Colloid]$ . Degueldre (1994, pp. 41-46) estimates that there are 3 reaction sites per  $nm^2$  on each colloid and Degueldre et al. (1997) measured the natural concentration of 100 nm radius colloids in Yucca Mountain water as being between  $10^4$  and  $10^7$  colloids/ml. Assuming the highest colloid concentration in this range,

(8 - 41)

$$\frac{10^{-7.2} \frac{g}{ml}}{10^7 \frac{colloids}{ml}} = 6.3 \times 10^{-15} \frac{g}{colloid}$$

Using an estimated density of 2.65g/cc for colloidal material and assuming spherical colloids, this leads to a colloid radius of 82 nm. Because the mass of colloids per ml varies by almost one half an order of magnitude, a colloidal radius of 100 nm is assumed and sensitivity on that assumption is then tested. With 3 reaction sites per nm<sup>2</sup>, the number of sites on such a colloid is  $3.77 \times 10^5$ , which leads to  $3.77 \times 10^{15}$  sites/L, equivalent to  $6.26 \times 10^{-9}$  moles of sites per liter. Now, with a colloid site concentration of  $6.26 \times 10^{-9}$  M, (8 - 40 becomes:

(8 - 42)

$$K_d(FEHMN) = \frac{K_c}{[Colloid]} = \frac{range[10^{-5} - 10]}{6.26 \times 10^{-9}} \approx [10^3 - 10^8]$$

With a varying colloid diameter, this actually varies, but is certainly within the range given.

**Kinetic Rates** - The  $K_d$  is the ratio of the forward and reverse reaction rates Equation 8 - 34. Experiments are planned at Los Alamos National Laboratory to determine the forward and reverse rates for Pu sorption onto colloids. These experiments will provide initial insight, but additional experiments are necessary to provide a range of values that covers different colloid types and sizes, variations in water chemistry, and different oxidation states of Pu. Preliminary data suggests that the forward rate is relatively fast, but the reverse rate is relatively slow. Therefore, in the modeling exercise, fast rates are used to reproduce equilibrium behavior, and the sensitivity of the results to slower rates is examined by changing the forward and reverse rate constants, but holding the  $K_d$  fixed. Thus, the range used in the modeling covers both equilibrium and kinetic affects.

**Plutonium Sorption to Matrix Material** - Triay et al. (1997) conducted extensive experiments of actinide sorption onto matrix material. The units of their measurements, ml/g (or kg of H<sub>2</sub>O/kg rock), are the same as those used in the FEHMN computer code.

(8 - 43)

$$K_d(sorption) = \frac{\text{Moles of } Pu_s}{\text{kg of Rock}} \cdot \frac{\text{kg of } H_2O}{\text{Moles of } Pu_{aq}}$$

The range of  $K_d$ s measured for Pu is 30 to 300 ml/g. Kinetic rates are chosen such that the values of  $K_d$  remain in this range. The forward rate of the sorption reaction is specified between 0.01 and 10<sup>6</sup>/hr. As with the Pu-Colloid complexation reactions, more data from kinetic experiments would serve to more narrowly bound this range.



**Colloid and PuColloid Filtration** - To address the concern that natural colloids could serve as a vector for contaminant transport, it is important to understand the filtration or removal of colloids from groundwater environments. In a field study by CRWMS M&O (1997, 1), at the C-holes site near Yucca Mountain, hydrophilic latex microspheres were injected as part of a forced-gradient tracer test. A forward rate constant was fit to the breakthrough of the microspheres, assuming there was no matrix diffusion. The forward rate is equivalent to the filtration coefficient used in wastewater treatment (Yao et al. 1971; Herzing et al. 1970) multiplied by the Darcy velocity. For the C-holes experiments, this provides a filtration coefficient of 0.0001 to 0.1/cm. Considerable uncertainty exists in the interpretation of C-holes tracer test results, in particular, with regard to the conceptualization of the flow field. Tracer test results were used in this sensitivity study as guidance for the investigation of a broad range in values of the filtration coefficient. Using the velocities specified in the SZ flow simulations leads to a forward rate of 0.1 to 20 1/hr. The experiments, however, provide no information on the rate of colloid release. Therefore, to represent the uncertainty, a wide range of forward and reverse rates were used, such that the ratio of the two (the filtration  $K_d$ ) varies between 0.001 and 10,000. The base case for these simulations is a filtration  $K_d$  value of 100, so it is on the same order of magnitude as Pu sorption.

#### 8.5.2.5.2 Reactive-Colloid Transport Model Simulation Results

The one-dimensional model used for the extensive parameter sensitivity study represents a 4 km section of fractured tuff. All numerical simulations were conducted using the FEHMN computer code (Zyvoloski et al. 1995). The bulk permeability of the rock is  $5 \times 10^{-13} \text{ m}^2$  and the porosity is  $10^{-4}$ . A head gradient of 4 MPa is specified across the domain resulting in a Darcy velocity of 0.043 m/d (430 m/d pore water velocity). This specific discharge (about 16 m/y) is greater than the value of specific discharge used in the base-case TSPA-VA analyses (0.6 m/y). Thus, the travel time for a conservative solute through the column is only about 10 days (Figure 8 - 66).

Figure 8 - 67 shows a schematic of the flow and transport model used in the sensitivity runs. The reactive transport simulations are based on a constant source of  $10^{-11} \text{ M Pu(aq)}$  added to an ambient system in which colloids are moving, filtering, and resuspending. The Pu can be in the aqueous phase, sorb onto the rock, or react with colloids that can filter or stay suspended. The amount of colloid that can filter is dependent on the specified aqueous concentration and the filtration  $K_d$ . The colloid concentration in these simulations is generally held constant at  $10^7$  colloids/ml ( $6.26 \times 10^{-9} \text{ M colloid sites}$ ). However, a set of simulations which bound Degueudre's et al. (1997) range of  $10^4$  to  $10^7$  colloids/ml examines Pu transport sensitivity to the ambient colloid concentration. As the colloid filtration  $K_d$  changes in the sensitivity simulations, the ambient (initial) sorbed phase colloid concentration needs to be recomputed. This is done with the simple relationship

(8 - 44)

$$[Colloid]_s = K_d \cdot [Colloid]_{aq} .$$

Additional sensitivity analyses examine uncertainty in the Pu concentration entering the SZ and the form in which it arrives. A source of PuColloids is not included in the model and may be a more realistic form coming from the UZ. Once a source term of PuColloids from the UZ is developed, it can be easily incorporated into the model.

**Transport Sensitivity Simulations** - The sensitivity of Pu(aq) and PuColloid(aq) transport to complexation, sorption, and filtration reaction parameters is investigated in this section. The parameters include distribution coefficients and forward and reverse rates. The analysis starts with a base case developed from TSPA-VA parameters. Comparisons are first made between equilibrium and kinetic reaction formulations because the TSPA-VA calculations are based on an assumption of equilibrium. Then, by sampling the ranges for the reaction parameters (see Table 8 - 32), sensitivity of Pu and PuColloid migration to each process is investigated individually, with the primary emphasis being on kinetic effects.

In the base case, all reactions occur fast relative to the flow, resulting in local equilibrium. The PuColloid formation is specified to represent a  $K_c$  value of 1 in the PA model (see (8 - 39)). That is, the ratio of Pu(aq) to PuColloid(aq) should be about 1. The ambient colloid site concentration is held constant at  $6.26 \times 10^{-9}$  M and the Pu(aq) feed concentration is held constant at  $10^{-11}$  M. Therefore, since

(8 - 45)

$$[PuColloid(aq)] = K_d [Pu(aq)][Colloid(aq)]$$

a reaction  $K_d$  of  $10^8$  yields a PuColloid(aq) concentration of  $6.26 \times 10^{-12}$  M, approximately the same as the Pu(aq) concentration. In accordance with the TSPA-VA simulations, Pu sorption onto the rock is also assumed to occur as an equilibrium reaction with a sorption  $K_d$  of 100 L/kg, the expected value from the laboratory sorption experiments.

The TSPA-VA calculations do not explicitly account for filtration of colloids and PuColloids. Therefore, for the base case, a filtration  $K_d$  (see Equation 8 - 44) of 100 is chosen to simulate PuColloid filtration, in order to keep the retardation of PuColloid(aq) similar to that of Pu(aq). Because this base case  $K_d$  value for filtration does not have a basis in laboratory or field experiments, it is chosen with the expectation that the sensitivity analysis must cover a broad range of possible values.

The first set of base-case simulations show the transport rates of the Pu and PuColloids with these equilibrium reactions. They also show that the results are insensitive to whether the reactions are modeled as true equilibrium reactions or as kinetic reactions with fast rates. Table 8 - 31 shows the reaction parameters for both the equilibrium and kinetic formulation of the base case and Figure 8 - 68 shows the Pu(aq) and PuColloid(aq) breakthrough curves. Clearly, with the fast kinetics, there is no difference from the equilibrium case. Table 8 - 31 shows the reaction parameters for all of the subsequent sensitivity simulations which are described in the following sections.

As discussed above, there are three sets of equations for which parameters can be varied. The first set consists of those parameters that govern PuColloid formation; the second set defines Pu

sorption; and the third set describes filtration of colloids and PuColloids. In each of the sensitivity studies that follow, the effect on Pu and PuColloid transport are examined with respect to the magnitude of the  $K_d$  for the reactions and with respect to the magnitude of the reaction rates. Thus, the format is such that the  $K_d$  is held constant, but the reaction rates are varied and then the  $K_d$  is varied by changing only the forward rate of reaction.

**Sensitivity Analyses: PuColloid Formation** - The base-case PuColloid formation  $K_d$  is  $10^8$ . Figure 8 - 69 shows the sensitivity of the Pu(aq) and PuColloid(aq) breakthrough to changes in the PuColloid formation  $K_d$ . Although the  $K_d$  is changing as a function of  $k_f$ , the forward and reverse rates are always fast enough to yield equilibrium conditions. Figure 8 - 69 shows that as  $K_d$  gets larger, more PuColloid is formed, and the breakthrough of PuColloid occurs earlier. When the magnitude of  $K_d$  is larger than  $10^8$ , the concentration of PuColloid(aq) approaches the initial feed concentration of Pu(aq). At that large  $K_d$ , the Pu(aq) breakthrough concentration drops below that of the PuColloid(aq) concentration, making PuColloid the dominant form of mobile Pu. Over the five orders of magnitude in  $K_d$  examined, the maximum change in breakthrough time was 5,000 years.

In contrast, Figure 8 - 70 shows the effect of fixing the PuColloid formation  $K_d$  at  $10^8$ , but varying the forward and reverse rates. There is no effect on the breakthrough of Pu(aq) for this case. However, the breakthrough of aqueous phase PuColloids is affected. For the case in which the forward rate is  $10^6$  and the reverse rate is  $10^{-2}$ , the results are the same as the base case, which indicates that the system is still in equilibrium. However, as the forward rate is further reduced the reaction becomes kinetically controlled. This causes the breakthrough of PuColloid(aq) to occur later in time and the maximum concentration to decrease. It is important to note that the difference in breakthrough time for PuColloid(aq) varies between 4,000 and 60,000 years for these simulations, depending on the magnitude of the forward rate, but the dominant form of total aqueous Pu is always the free ion. Therefore, in this case, an equilibrium assumption would be the most conservative estimate of PuColloid formation.

**Sensitivity Analysis: Pu Sorption** - The sensitivity of Pu(aq) sorption to the solid phase is examined for the case in which PuColloid formation is in equilibrium ( $k_f = 10^8$ ,  $k_r = 1$ ) and kinetically controlled ( $k_f = 10^4$ ,  $k_r = 10^{-4}$ ). Figure 8 - 71 shows the sensitivity of changing the Pu sorption  $K_d$  when the PuColloid(aq) formation is in equilibrium. The case in which the  $K_d = 100$  is the base case shown in the previous figures. The arrival times for the Pu(aq) and PuColloids(aq) are equivalent, but the plateau concentrations for Pu(aq) are slightly higher than for the PuColloid(aq). They are related exactly by Equation 8 - 45, where the Pu(aq) concentration at the model outlet is primarily controlled by sorption when the sorption  $K_d$  is high and by retardation of PuColloid(aq) due to filtration (a fixed value in these simulations) when the Pu sorption  $K_d$  is low. The figure shows that as the  $K_d$  increases, Pu sorption increases and the breakthrough occurs later in time. The breakthrough of PuColloids(aq) follows the same pattern because of the equilibrium condition imposed.

When the formation of PuColloid(aq) is kinetically controlled, the breakthrough curves of Pu(aq) and PuColloid(aq) are less dependent on each other. Figure 8 - 72 shows that for low Pu sorption  $K_d$ , Pu(aq) breaks through sooner than PuColloid(aq), which is retarded by filtration. For high Pu sorption  $K_d$ , however, PuColloid(aq) breaks through sooner than Pu(aq) because it is less retarded and not entirely dependent on the Pu(aq) concentration. For example, in Figure 8 -

72 when the sorption  $K_d$  is 3, Pu(aq) breaks through at approximately 150 years compared to 1,800 years in the equilibrium case. This is because the Pu(aq) concentration is not linked as strongly to the PuColloid(aq) concentration.

There is a very interesting side effect associated with this earlier breakthrough of Pu(aq). Although Pu(aq) and PuColloid(aq) are not coupled by an equilibrium constraint, they are not completely independent either, and the Pu(aq) concentration has some effect on the PuColloid(aq) concentration. Due to the faster Pu(aq) transport, the PuColloid(aq) breakthrough also occurs earlier in time than when equilibrium was specified, but the maximum concentration is lower by over an order of magnitude. In comparing the breakthrough, the Pu(aq) breaks through before the PuColloid(aq) when the  $K_d$  is less than 100. However, when the  $K_d$  is larger than 100, the PuColloid(aq) breaks through first. For example, when the  $K_d$  is 300, the breakthrough of PuColloid(aq) occurs at ~7,000 years compared to ~15,000 years for Pu(aq). This illustrates that when the formation of PuColloid(aq) is kinetically controlled, and the sorption  $K_d$  for Pu(aq) is sufficiently large, then there is a viable source of Pu in the far field as a result of colloid transport. Due to kinetic constraints, the concentration of Pu associated with colloid transport will be less than could be derived under equilibrium conditions.

**Sensitivity Analysis: Colloid and PuColloid Filtration** - Field experiments provide a range of forward colloid filtration rates (Reimus and Turin 1997), yet they provide little indication of the magnitude of the filtration  $K_d$ . Therefore, a range of filtration  $K_d$  values are examined in conjunction with the study range of forward filtration rates. As with the Pu sorption sensitivity studies above, the filtration sensitivity studies begin with cases in which the PuColloid formation reaction is in equilibrium or kinetically controlled. Table 8 - 32 gives the model parameter ranges for this analysis.

When PuColloid formation is in equilibrium, the breakthrough curves of PuColloid(aq) and Pu(aq) (Figure 8 - 73) are virtually identical (the difference can be computed exactly with Equation 8 - 45). As the  $K_d$  for filtration increases, PuColloid(aq) migration is retarded, leading to similar retardation of Pu(aq). When the PuColloid(aq) formation reaction is kinetically controlled, however, the breakthrough curves of Pu(aq) and PuColloid(aq) are not strongly coupled. Figure 8 - 74 shows the breakthrough curves for such conditions. Although the PuColloid(aq) concentrations are never as great as Pu(aq) due to the disequilibrium, there is potential for earlier arrival of PuColloid(aq) than Pu(aq). At low filtration rates, there is less retardation on PuColloid(aq) than Pu(aq). Therefore, it is possible for PuColloids to exist in the aqueous phase even when all Pu(aq) sorbs out of solution because Pu(aq) and PuColloid(aq) are not in equilibrium.

These results highlight a parameter set within the feasible range of values, in which a small component of Pu migrates as PuColloid(aq) when the bulk of the Pu is retarded by sorption. Specifically, when Pu(aq) and PuColloid(aq) are not in equilibrium due to slow reaction rates, and colloid filtration is weak relative to Pu sorption, the Pu migration on colloids can occur at higher velocities than Pu migration in the aqueous phase. In these simulations, the concentration of PuColloid(aq) is several orders of magnitude lower than that of the aqueous Pu feed concentration, but the travel rate is up to two orders of magnitude faster.

In the preceding analyses, the ambient aqueous-colloid concentration has been assumed constant. Now, it is varied to examine the impact on Pu transport (Table 8 - 31) and to compare with parameters used in Figure 8 - 75. Figure 8 - 75 shows the effect of decreasing the ambient colloid concentration. With less available colloid for reaction, less PuColloid is formed. Thus, the breakthrough of total aqueous Plutonium (PuT) is dominated by the free Pu ion. When the colloid concentration is increased, Figure 8 - 76 shows that PuColloid transport begins to dominate the total aqueous Pu (PuT) breakthrough as more and more feed-concentration-limited Pu(aq) reacts to form PuColloid(aq).

### 8.5.2.5.3 Comparison with the TSPA-VA Model

The first step in comparing the reactive transport model with the TSPA 1-D transport model is to ensure that transport is being simulated on the same flow system. In the TSPA-VA analysis, the effects of diffusion from fractures into matrix material are approximated using the effective-porosity approach. Because diffusion from the fracture into the "effective" portion of the matrix leads to a certain amount of retardation, the TSPA-VA base-case analysis uses the following method to account for such diffusion by scaling the  $K_d$  parameter. Starting with the retardation factor,  $R_f$ , for a solute

(8 - 46)

$$R_f = 1 + \frac{\rho_b K_d}{\rho_f n_{frac}}$$

where  $K_d$  is the distribution coefficient for Pu sorption onto rock material (100 kg water/kg rock),  $\rho_b$  is the bulk rock density (~2.5 g/cc),  $\rho_f$  is the fluid density (~1 g/cc), and  $n_{frac}$  is the fracture porosity (0.0001).

When the Pu can react with mobile colloids as well as the immobile rock (the equilibrium  $K_c$  approach), the effective retardation factor becomes:

(8 - 47)

$$\hat{R}_f = \frac{R_f + K_c R_c}{1 + K_c}$$

where  $K_c$  is the Pu colloid partition coefficient (see Table 8 - 33) and  $R_c$  is the colloid retardation factor (assumed equal to 1 - e.g. no colloid filtration).

An effective  $K_d$  can then be calculated that takes into account the effects of both retardation of aqueous Pu and the lack of retardation of colloids to which Pu may sorb:

(8 - 48)

$$\hat{K}_d = \frac{n_{frac}(\hat{R}_f - 1)}{\rho_b}$$

Finally, the effect of diffusion into the matrix is accounted for by scaling Equation (8 - 48 by the ratio of the effective porosity to the matrix porosity to give a "scaled  $K_d$ ",  $\hat{K}_d$ :

(8 - 49)

$$\hat{K}_d = \frac{n_{eff}}{n_{matrix}}(\hat{K}_d)$$

Because the magnitude of  $R_f$  is on the order of  $10^6$ , it is clear that  $\hat{R}_f$  differs significantly only when  $K_c$  is about 1 or greater. In the TSPA-VA base case analysis, the range on  $K_c$  values is 0.00001 to 10. Also, in the TSPA-VA base case analysis, a range of  $K_d$  and  $n_{eff}$  were evaluated. Here we chose an  $n_{eff}$  of 0.003 ( $n_{matrix} = 0.25$ ) to compute the  $\hat{K}_d$ . Table 8 - 33 shows the relationships developed with Equation 8 - 46 to Equation 8 - 49.

**Reactive Transport Model Scaling** - The TSPA-VA base case transport model is based on the assumption of equilibrium-controlled reactions. Unlike the TSPA-VA model Equation 8 - 47, the reactive transport models separate the effects of colloid transport and aqueous phase Pu sorption. Therefore, the effects of diffusion via effective porosity scaling are only factored into the Pu(aq) sorption equation, but not the colloid transport equation because colloids are assumed not to diffuse into the rock matrix. All reactive transport model formulations are initially specified as equilibrium controlled. Further, because colloid filtration is not considered in the TSPA-VA base case model, the colloid filtration terms (Equation 8 - 31 and 8 - 32) are initially turned off. The PuColloid(aq) formation coefficient is computed to match the TSPA-VA base case  $K_c$  model with 8 - 42 and the Pu sorption  $K_d$  is simply scaled by  $n_{eff}/n_{matrix}$ . Thus, for a  $K_c$  value of 1 and a colloid site concentration of  $6.26 \times 10^{-9}$ , Equation 8 - 42 gives a  $K_d$  value for Equation 8 - 29 of  $1.60 \times 10^8$ . To account for diffusion of aqueous phase Pu when the measured  $K_d$  is 100, the scaled  $K_d$  for Equation (8 - 30 becomes

(8 - 50)

$$K_d = \left( \frac{0.003}{0.25} \right) 100 \frac{kg}{kg} = 1.2 \frac{kg}{kg}$$

For comparison with the TSPA-VA base case model, Table 8 - 34 shows the reaction parameters that are used to simulate the same system.

**Comparison Simulations** - The comparison simulations begin with a verification that the reactive colloid transport model simulates the same behavior as the TSPA-VA base case model when the same assumptions are made. The simulations are performed on the same 4 km, 1-D model described in Section 8.5.2.5.2. Reference cases (b) and (d) from Table 8 - 33 and Table 8 - 34 are simulated and compared in Figure 8 - 77. Case (b) has a  $K_c$  of 0.1 and is dominated by Pu(aq) transport and its associated sorption on the rock. Case (d) has a  $K_c$  of 10 and shows the effects of some unretarded, colloid-facilitated transport. By taking the reactive transport parameters used for Case (d) and adding in the effects of colloid filtration, the small travel times associated with colloid transport are significantly increased (Figure 8 - 78). Thus, whereas the

TSPA-VA base-case model currently neglects colloid filtration, it may play a significant retarding role when the colloid partitioning coefficient,  $K_c$ , is large.

Whereas colloid filtration mitigates fast colloid-facilitated transport, kinetic effects associated with the Pu-Colloid(aq) formation may have the opposite effect. For case (b), colloid-facilitated transport has very little effect on total Pu migration rates when the equations are represented as equilibrium formulations. However, when the reaction rates are reduced to capture potential kinetic effects, a small portion of the Pu may then stay on colloids and move faster than was previously predicted. Figure 8 - 79 shows three plots of Pu breakthrough curves for equilibrium and kinetic reaction formulations. The  $K_d$ s are the same in each case. When the Pu-Colloid reaction is formulated with rates three orders of magnitude lower than those used to ensure equilibrium, however, very early arrivals of low concentration Pu associated with colloid transport are predicted. As colloid filtration is factored into the formulation, the travel time of these Pu-Colloids is increased somewhat.

#### 8.5.2.5.4 TSPA-VA Streamtube Simulations

Simulations were also conducted using the entire TSPA 1-D SZ streamtube transport model and the reactive transport formulation for colloid-facilitated Pu transport. The streamtube consists of the pathway through three fractured volcanic tuff units and the alluvium-valley-fill unit, as described in Section 8.3.3.

The input aqueous phase Plutonium concentration,  $1 \times 10^{-11}$  M, is the same for this model as for the single material model described above. Likewise, the base-case aqueous phase colloid concentration is  $6.26 \times 10^{-9}$  M. Therefore, the primary differences between this model and the 4 km model are that the velocities change with distance in the model, depending on which unit is present in the streamtube at a particular location.

A few parameter combinations from the sensitivity tests described above are applied to the 25 km streamtube model. Table 8 - 35 shows which parameter sets are used and the corresponding figures. Initially, the parameters which represent the TSPA-VA case with  $K_c=10$  are compared with a kinetic formulation of the same problem and the addition of filtration. To achieve kinetic effects, significantly slower forward and reverse rates are required than were needed for the simpler test problem described above. Figure 8 - 80 shows the effect of the different processes and formulations on breakthrough curves at the end of the domain at 25 km. As with the 4 km test problem, a kinetic formulation leads to a small component of rapidly migrating Pu in comparison to the equilibrium formulation results (even with a  $K_c$  of 10). However, filtration may mitigate this behavior. The sorption  $K_d$  has the obvious effect of retarding transport. Unlike the sensitivity analysis, however the PuColloid(aq) appears to be controlled in an equilibrium fashion for the rates used. This may be due to the slow velocities in the alluvium, because unretarded travel times to the end of the tuff (18 km) are almost an order of magnitude less than to the end of the alluvium (25 km).

Rather than stepping through sensitivities to each parameter, the next simulation identifies a case within the feasible parameter domain in which Pu(aq) and PuColloid(aq) transport are not in equilibrium. By setting the filtration  $K_d$  to a low value, and forcing disequilibrium in the PuColloid formation process, the simulation illustrated in Figure 8 - 81 shows an interesting set

of breakthrough curves (Table 8 - 35). At an 18 km distance, the first arrival of PuColloid(aq) occurs sooner than Pu(aq) because the Pu(aq) sorption coefficient is larger than the colloid filtration coefficient. The two curves are not strongly linked due to disequilibrium in the PuColloid formation reaction. But, that also leads to PuColloid(aq) concentrations that are lower than would be computed under equilibrium conditions.

Figure 8 - 81 shows an interesting artifact of different flow velocities in the fractured rock and alluvium. The arrival time of Pu(aq) is earlier at 25 km than at 18 km, because once the PuColloid(aq) enters the alluvium, the velocity decreases substantially. This leads to residence times large enough that Pu(aq) and Colloid(aq) can form from PuColloid(aq). Thus, in the alluvium, PuColloid(aq) acts as a source of Pu(aq). Similarly, in the alluvium PuColloid(aq) can form from the abundance of Pu(aq) that arrives after  $10^4$  years.

### 8.5.2.5.5 Summary

A reactive colloid-transport model has been developed and tested against the TSPA-VA base-case equilibrium SZ transport model. When the same assumptions are made (e.g. equilibrium reactions and no colloid filtration), the two models produce similar results. Extending the comparison to include kinetic reaction formulations and colloid filtration shows that there are feasible parameter combinations that lead to both earlier arrivals and greater retardation than are predicted with the TSPA-VA equilibrium model. Because the effects of kinetics may be important, this study highlights the need to develop better data sets of reaction rates, rather than reaction  $K_d$ s.

The reactive transport model comparison does not cover the entire parameter space nor does it take into account many of the additional considerations incorporated in the TSPA-VA base-case analysis, such as the relative significance of effective porosity compared to larger  $K_c$  parameters. Therefore, this analysis serves primarily to highlight processes that should be evaluated in greater detail in the time frame between the VA and the LA analyses as well as to highlight the need for laboratory derived reaction rate parameters, specifically, the forward and reverse reaction rates for the sorption of Pu onto natural colloids.

### 8.5.3 Interpretation

The results of the sensitivity studies presented in this report have implications concerning the validity of assumptions used in the TSPA-VA base-case SZ analyses and with regard to future TSPA analyses. This section contains interpretations of the sensitivity studies results from the perspective of potential impacts on repository performance of these alternative analyses.

Analyses using the analytical solution for 3-D solute transport in the SZ indicate that the range for the dilution factor derived from the SZ Expert Elicitation (1 to 100) approximately corresponds to a range in vertical-transverse dispersivity of 0 to 14 m. The median value for the uncertainty distribution of the dilution factor (about 10) corresponds to a vertical-transverse dispersivity of about 0.16 m. The range of the uncertainty in vertical-transverse dispersivity (within two standard deviations of the mean) given by Lynn Gelhar in the SZ Expert Elicitation corresponds to a lower range in dilution factor than that used in the TSPA-VA base-case analyses (approximately 1 to 10, with a median of 2). This lower range for the uncertainty in the



dilution factor for SZ transport could be factored into the uncertainty distribution supplied by the three other experts or the lower range could be considered to be an alternative interpretation of dilution in the SZ. The dilution factor has a direct and primary influence on calculations of repository performance. High priority should be attached to reducing uncertainty or enhancing defensibility of assumptions regarding this parameter.

Results from the analytical solution for 3-D solute transport support the method used to combine the output from the six SZ streamtubes in the TSPA-VA base case. In this idealized representation of the flow and transport system, the sum of the concentrations in the six streamtubes overestimated the concentration by a factor of greater than two. However, the other options considered for combining the output (maximum concentration and averaged concentration) both underestimated the concentration. This result indicates that the sum of concentrations is the only defensible (though, admittedly conservative) option available for combining the transport results from the six streamtubes, within the context of the 1-D streamtube approach used in the TSPA-VA base case. The utilization of multiple streamtubes in SZ analyses in conjunction with implicit dispersion using the dilution factor requires a method for combining radionuclide results from the different streamtubes. The method has primary impact on calculations of repository performance and should be defensible and conservative, in the absence of an exact solution.

Geostatistical modeling of heterogeneity in bulk permeability within hydrostratigraphic units, in conjunction with groundwater flow and solute transport modeling using the TSPA 3-D flow model, demonstrated the potential influence of high-permeability pathways in the SZ on travel times, dilution, and transport paths. Geologically plausible representations of spatial variability in fracture network permeability and large-scale structural features resulted in significant variability in travel times and maximum simulated concentration for transport to a 20 km distance among 100 geostatistical realizations. Simulations that included the major faults as high-permeability features resulted in shorter travel times and higher maximum concentrations, on average. Simulations that included the major faults as high-permeability features also resulted in less variability in the location of the peak concentration at the 20 km fence.

Interestingly, the heterogeneities introduced into the TSPA 3-D flow model in this sensitivity study had little impact on the calibration of the flow model to observations of water levels in wells. The error in the calibration generally varied less than 10% among the 100 geostatistical realizations from the RMSE value obtained for homogeneous hydrostratigraphic units. The average error among the realizations with and without the high-permeability faults was slightly less than for the model with homogeneous units. This lack of sensitivity of the 3-D groundwater flow model to aquifer heterogeneity suggests that steady-state flow modeling of the SZ in this region is incapable of detecting the presence or absence of high-permeability pathways. Consequently, such features should be explicitly or implicitly considered in TSPA calculations of transport in the SZ.

An explicit dual-porosity representation of the 1-D SZ solute transport system was investigated as an alternative conceptual model, in terms of sensitivity to uncertain parameters and in comparison to the effective-porosity approach used in TSPA-VA base case analyses. As expected, the explicit dual-porosity model (two-dimensional single porosity model) showed great sensitivity to fracture spacing. Significant sensitivity of concentration breakthrough to the

sorption coefficient, matrix porosity, and Darcy velocity (specific discharge) was also observed in the simulation results. The dual-porosity modeling indicated minor sensitivity to molecular diffusion coefficient, radioactive decay (for  $^{99}\text{Tc}$ ), fracture porosity, and longitudinal dispersivity.

The solute transport solution using the one-dimensional dual-porosity model (FEHMN implementation) was found to be moderately accurate when compared to the two-dimensional single-porosity model, for the parameter set used in the base case. The one-dimensional dual-porosity model is significantly more efficient, in terms of computational effort, than the two-dimensional, single-porosity model. The accuracy of the one-dimensional, dual-permeability approach would have to be verified for a wider range of parameter values and model domains to use this approach for additional dual-porosity transport modeling.

Comparison of the two-dimensional single-porosity model to the one-dimensional single-porosity model (effective-porosity approach) that was used in the TSPA-VA SZ transport simulations indicates that the range of effective porosity used in the analyses approximately spans the range of response simulated with the explicit dual-porosity model. For a given value of equivalent effective-porosity and the corresponding explicit dual-porosity results, the effective-porosity model overestimates the concentration at later times, which is conservative behavior from the perspective of repository performance. The explicit dual-porosity transport simulations at intermediate values of fracture spacing (about 2 m to 20 m) exhibit substantially more apparent longitudinal dispersion in the concentration breakthrough curves than the effective-porosity model. Less apparent longitudinal dispersion, as simulated by the effective-porosity model, is also conservative from the perspective of repository performance because longitudinal dispersion contributes to dilution of peak radionuclide concentration from a transient mass source.

The explicit dual-porosity transport simulations at intermediate values of fracture spacing (about 2 m to 20 m) exhibit earlier arrival times for low concentrations relative to the effective porosity model, which is non-conservative from the perspective of repository performance.

The two-dimensional single-porosity model (explicit dual-porosity approach) results indicate solute transport behavior approximately equivalent to effective-porosity values in the fracture porosity range ( $< 1 \times 10^{-3}$ ) for fracture spacing of greater than about 100 m. Effective fracture spacing (in terms of significant groundwater flow) on the order of 100 m is not implausible, on the basis of flowmeter surveys in wells in the SZ. This suggests that the uncertainty range in effective porosity for transport in the SZ should include low values, on the order of fracture porosity.

The simplified analysis of average dose to a member of the critical group presented in the sensitivity studies indicates relatively low average-dose per person at the time of peak dose for the TSPA-VA base case, when the radiological dose is spread among a much larger critical group. Based on the average water use by the present residents of the Amargosa Valley, as many as 20 persons could receive the maximum calculated dose (about 300 mrem/y, occurring at 317,000 years in the future). Distributing the radionuclide contamination among a larger critical group would decrease the average dose proportionately.

A reactive colloid-transport model was evaluated as an alternative conceptual model for the colloid-facilitated transport of Pu in comparison to the equilibrium model employed in TSPA-VA SZ transport analyses. The reactive colloid-transport model has the advantage of utilizing a set of kinetic parameters that allow more flexibility in modeling observed colloid-facilitated transport behavior and is more closely based on physical processes.

Results of sensitivity studies indicate that travel times of total Pu are relatively sensitive to the Pu sorption coefficient, the relative values of the forward and reverse reaction rates for Pu sorption onto colloids, and the filtration of colloids. Equilibrium sorption coefficients have been measured in laboratory experiments for the sorption of Pu onto colloids, but critical information on the desorption reaction rates is not presently available. Relatively rapid transport of Pu on colloids, at concentrations well below the slower maximum aqueous phase Pu, can occur when Pu-Colloid desorption reaction rates are slow and colloid filtration is modest to low. This behavior maybe consistent with inferences from observations of Pu migration in the SZ at Pahute Mesa, where rapid transport of Pu at low concentrations associated with colloids has occurred (Thompson et al. 1998, vii). However, additional lab and field information regarding kinetic reaction rates are needed to bound the model parameters before any conclusions can be drawn.

The possibility of rapid migration of Pu associated with colloids has been included in the TSPA-VA base-case analyses through the concept of irreversible sorption of Pu onto colloids. A rather *ad hoc* method of defining the fraction of Pu that is available for transport as irreversibly sorbed onto colloids was used in the analyses (see Section 6.4.2). A reactive colloid-transport model would provide a more physically based representation of this process for use in TSPA analyses.

The comparisons between the TSPA-VA base-case model for colloid-facilitated Pu transport and the reactive transport model are not intended to indicate any serious deficiencies with the current TSPA model formulation. They are also not complete enough to elucidate the significance of any processes that lead to deviation from the PA model results. They are intended to provide an introduction to sensitivity work that can be performed between the VA and LA phase of the TSPA process. Our expectation is that the various reaction parameters in the reactive transport model can be formatted into distributions that can then be sampled just as any other uncertain parameter in the probabilistic method used for TSPA analyses.

## **8.6 SUMMARY AND RECOMMENDATIONS**

### **8.6.1 Summary of Methods and Results**

For the TSPA-VA, the saturated-zone flow and transport component of the analysis calculated the concentration of radionuclides in the groundwater as a function of time at a location 20 km from the repository. The radionuclide mass flux at the water table from downward percolating groundwater in the unsaturated zone was the source of radionuclides in the area beneath the repository used in the saturated zone transport calculations. A hypothetical pumping well, producing groundwater containing the radionuclides, was the mechanism assumed to transfer the contaminants to the biosphere.

Numerical modeling at several levels of abstraction was used in the TSPA-VA calculations of radionuclide transport in the SZ. A three-dimensional groundwater flow model of the saturated

zone was used to simulate the general direction of a contaminant plume from the repository and to identify the geologic units encountered along the flowpath. One-dimensional radionuclide-transport modeling in six streamtubes was performed to determine the radionuclide unit-concentration breakthrough curves at a distance of 20 km from the repository in response to a steady, unit-mass radionuclide flux from the unsaturated zone. Within the TSPA-VA calculations, the convolution integral method was used to combine the unit breakthrough curves with the time-varying radionuclide sources from the UZ. Finally, the radionuclide concentrations at 20 km were divided by a dilution factor to account for transverse dispersion during migration through the SZ.

The three-dimensional flow model used for this analysis incorporated an area of about 20 km by 36 km to a depth of 950 m below the water table. The hydrogeologic framework in the model was based on a refined version of the regional geologic-framework model used D'Agnese et al. (1997a). Sixteen different hydrogeologic units were represented in the model. Three linear, vertical features with low permeabilities to the west and north of Yucca Mountain were included to simulate the moderate-and large-hydraulic-gradient regions, respectively. Flow was modeled as steady state, through a single-continuum, porous medium. Focused recharge along Fortymile Wash, consistent with USGS measurements, was included as a specified flux. Specified-flux boundary conditions were applied to the lateral boundaries based on the interpolation of measured values of hydraulic head. The model was calibrated by an iterative procedure, and the simulated hydraulic heads were compared with measured head values in the model domain. The direction of groundwater movement in this flow model is consistent with the conceptual model of the system and is evident in the plot of simulated radionuclide pathlines at the water table shown in Figure 8 - 21. Particle tracking in the three-dimensional model's simulated flow field was used to estimate the flowpath lengths in the saturated zone through each of the hydrostratigraphic units downstream from the repository.

Simulations of radionuclide transport in the saturated zone for the TSPA-VA calculations were performed with six, one-dimensional flow tubes using the FEHMN computer code (Zyvoloski et al. 1995). Each of the six streamtubes is a continuation of a groundwater flow path from the repository in the unsaturated zone. The volumetric flow rate of groundwater through each streamtube was determined at the water table from flow simulations using the site-scale flow model developed by Bodvarsson et al. (1997) for the unsaturated zone. The specific discharge within the streamtubes in the saturated zone was 0.6 m/yr for current climatic conditions. The streamtubes are 20 km long (they reach to the Amargosa Valley), with a regular grid spacing in the tubes of 5 m. The four hydrostratigraphic units in the streamtubes are the middle volcanic aquifer, the upper volcanic aquifer, the middle volcanic confining unit, and the alluvium/valley fill. The lengths of these units within the streamtubes were defined by modeling transport with the three-dimensional flow model for the saturated zone. Output from the one-dimensional transport simulations for the SZ consists of a set of unit concentration breakthrough curves for different radionuclides at 20 km distance in response to a steady, unit radionuclide mass flux source from the unsaturated zone.

Uncertainty in radionuclide transport through the saturated zone was incorporated into the analysis by varying key transport parameters. The stochastic parameters used in the one-dimensional transport simulations were effective porosity in the volcanic units and the alluvium unit, distribution coefficients ( $K_d$ s) for sorbing radionuclides in the volcanic and alluvial units,

the ratio of the radionuclide mass in aqueous and colloidal forms ( $K_c$ ) for colloid-facilitated transport of plutonium, longitudinal dispersivity, the fraction of flowpath through the alluvium, and the dilution factor. This uncertainty was incorporated into the probabilistic TSPA-VA analyses by random sampling of the stochastic parameters and simulation of radionuclide transport in the resulting 100 realizations of the SZ system.

Colloid-facilitated transport of plutonium in the saturated zone was simulated using a conceptual model based on both equilibrium sorption of plutonium onto colloids and the potential for irreversible sorption of plutonium onto some colloidal particles. These two components of plutonium transport were included in the analysis. A large fraction of the plutonium mass was simulated to move through the saturated zone assuming chemical equilibrium among dissolved plutonium, plutonium sorbed onto colloids, and plutonium sorbed onto the aquifer material. A small fraction of the plutonium mass was simulated to be irreversibly attached onto colloids and to be transported relatively rapidly in the saturated zone, without significant retardation. The fraction of Pu subject to irreversible sorption onto colloids was assigned for each realization in the waste form degradation component of TSPA-VA. The rationale for this stochastic parameter is described in Chapter 6, Section 6.4.2.

The effects of climate change on radionuclide transport in the saturated zone are incorporated into the analysis by assuming instantaneous change from one steady-state flow condition to another steady-state condition in the saturated zone. Changes in climate state are assumed to affect the magnitude of groundwater flux through the saturated zone system but have a negligible impact on flowpaths. These effects are incorporated into the analysis by scaling the velocity of radionuclide breakthrough curves proportionally to the change in saturated zone specific discharge. Also, the concentrations of the radionuclide breakthrough curves are scaled proportionally to the change in volumetric groundwater flow rate from the unsaturated zone into the streamtubes. The regional-scale flow model for the saturated zone provided estimates of the relative change in specific discharge in the saturated zone for future climate states. The site-scale flow model for the unsaturated zone (Bodvarsson et al. 1997) provided estimates of changes in volumetric groundwater flow rate through the repository horizon.

The convolution integral method was used in the TSPA-VA calculations to determine the radionuclide concentration in the SZ, 20 km downgradient of the repository, as a function of the transient radionuclide mass flux at the water table beneath the repository. This computationally efficient method combines information about the unit response of the system (as simulated by the one-dimensional transport modeling) with the radionuclide source history to calculate transient system behavior. The most important assumptions of the convolution method are linear system behavior and steady-state flow conditions in the saturated zone.

The unit breakthrough curves of concentration from the one-dimensional transport model formed the basis for calculating radionuclide concentrations in the TSPA-VA using the convolution integral method. The breakthrough curves for unit concentration for the nine radionuclides at 20 km from the repository are shown in Figure 8 - 29. These curves were generated using the expected parameter values. Differences in the arrival times of different radionuclides are because of variations in sorption among the radionuclides. Differences in the maximum concentration among radionuclides are because of radioactive decay during transport through the saturated zone system.

The impact of uncertainty in the one-dimensional transport simulations for the saturated zone is illustrated in Figure 8 - 39. This figure shows the unit breakthrough curve  $^{99}\text{Tc}$  for all 100 realizations used in the base case analyses. Travel times for the non-sorbing  $^{99}\text{Tc}$  vary from a few hundred years to about 4000 years; maximum concentrations, primarily influenced by the dilution factor, vary over two orders of magnitude among these equally likely simulations. The uncertainty in longitudinal dispersion is shown by variations in the slopes of the breakthrough curves in Figure 8 - 39. The simulated unit breakthrough curves for the other radionuclides are shown in Figure 8 - 30 to Figure 8 - 40. Note that these unit breakthrough curves for the 100 stochastic realizations do not include the effects of radioactive decay, which was calculated in the convolution integral component of the analysis. Uncertainty in sorption parameters, in combination with uncertainty in effective porosity, results in significant variability in the simulated travel times for those radionuclides that experience sorption. The variability in travel times ranges over approximately 200,000 years for  $^{237}\text{Np}$  and  $^{234}\text{U}$ , as shown in Figure 8 - 32 and Figure 8 - 40, respectively. Extreme variability in simulated travel time (up to 1,000,000 years) occurs for those radionuclides with large uncertainties in values of  $K_d$  ( $^{231}\text{Pa}$  and  $^{79}\text{Se}$ ), as shown in Figure 8 - 33 and Figure 8 - 38. Uncertainties in the parameters of the equilibrium colloid sorption model of colloid-facilitated Pu transport result in extreme variability in travel times for  $^{239}\text{Pu}$  and  $^{242}\text{Pu}$  (see Figure 8 - 34 and Figure 8 - 36).

### 8.6.2 Implications for Repository Performance

For the TSPA-VA, the results of the flow and transport analysis for the saturated zone are the radionuclide concentration histories at the geosphere/biosphere interface, which is a well head located 20 km downgradient in the Amargosa Valley region. These concentrations are directly proportional to the dose calculated for possible future inhabitants.

Radionuclide migration through the saturated zone affects total system performance in two ways. First, the saturated zone may function as a mechanism for significant delay in releasing radionuclides to the biosphere. Second, there may be significant dilution of radionuclide concentrations that occurs during transport in the saturated zone. Both impacts are functions of the distance between the repository and the point of release to the biosphere.

Delays in radionuclide migration caused by processes in the saturated zone are potentially important to repository performance if the travel time for a radionuclide through the saturated zone system is long in comparison to its half life. For example, in the expected-value case shown in Figure 8 - 29, the maximum concentrations of Pu-239 (equilibrium colloid sorption) and  $^{79}\text{Se}$  are significantly attenuated relative to the other radionuclides because of radioactive decay. Delay in radionuclide migration in the saturated zone may also be significant if the travel time through the system is long relative to the time period of concern. For example, the travel time of unretarded radionuclides such as  $^{99}\text{Tc}$  (see Figure 8 - 39) may be relevant to repository performance in a 10,000-year time frame. However, the delay release from the saturated zone for a period of 100,000 years for unretarded radionuclides would be insignificant. Retardation in the saturated zone for most of the radionuclides that experience sorption is highly uncertain, particularly with regard to sorption characteristics of the alluvium-valley-fill material.

The dilution of radionuclide concentration in the saturated zone is handled in a straightforward manner in the TSPA-VA calculations through the dilution factor parameter. Although there is

significant uncertainty in this parameter and complexity in the underlying processes that lead to dilution, the relationship between the dilution factor and dose is a simple linear function for a steady radionuclide source from the UZ. Transient peaks in the radionuclide concentration at the source in the saturated zone are also attenuated by longitudinal dispersion during transport in the SZ.

### **8.6.3 Guidance for License Application**

The data and models used in the TSPA-VA saturated zone analyses could still be improved in several ways. The following list of suggested improvements is synthesized from comments offered by co-workers in the site-characterization effort, the Expert-Elicitation participants, the Performance Assessment Peer Review panel, external organizations (e.g., staff for the Nuclear Regulatory Commission, the Nuclear Waste Technology Review Board, and the Electrical Power Research Institute), and our experiences with producing the TSPA-VA.

Data are lacking in the saturated zone from a distance of approximately 10-km downgradient of the repository to the 20-km compliance boundary used in the TSPA-VA analyses. Important information needed in this area includes water level measurements, subsurface geology, hydrochemical data, and characterization of alluvium below the water table. Water level measurements would improve our understanding of the groundwater flow directions in this area and provide additional data for flow modeling calibration. There is significant uncertainty in the location at which flow in the shallow saturated zone enters the alluvium along the flow path from the repository or even if flow occurs in the alluvium within 20 km of the repository. This is particularly important with regard to the potentially higher sorption coefficients for some radionuclides (e.g., Np) in the alluvium. Hydrochemical data could provide valuable information to constrain flow paths in the saturated zone in this area. There are basically no site-specific data on the hydraulic, mineralogic, or geochemical characteristics of the alluvium in the saturated zone from this area. There is particularly great uncertainty in the sorption parameters for some radionuclides in the alluvial material. These data would greatly enhance confidence in SZ flow and transport models and could potentially influence TSPA results (in terms of travel times in the SZ) by allowing less conservative ranges in key parameter values (e.g., fraction of flowpath in alluvium and sorption coefficient for Np in the alluvium).

Additional geochemical and isotopic data from the saturated zone could provide important constraints on conceptual models of groundwater flow and on some key parameters for performance assessment. Enhanced vertical resolution of hydrochemical sampling could provide information on the degree of mixing in the flow system, with implications for the amount of transverse dispersion that would occur in the transport of contaminants from the repository. The data could also provide a better understanding of the flowpaths in the saturated zone downgradient from the repository and of the magnitude of recharge to the system from Fortymile Wash. Reliable age dating of groundwater along the flowpath from beneath the repository would constrain the travel times through the system and the appropriate range of effective porosity values in the fractured volcanic-tuff units. By inference, these data would provide information on the process of matrix diffusion in the fractured units. Data on groundwater travel times through the SZ could result in much less conservative TSPA simulations of transport in the SZ, with regard to the delay in release of radionuclides afforded by the SZ.

An improved 3-D saturated-zone flow model could provide the basis for defensible radionuclide transport simulations that explicitly model relevant processes. An improved site-scale flow model should be consistent with all of the available data from the site. In addition, development of the flow model should be focused on simulation capabilities that are needed for accurate and defensible transport modeling for use in TSPA calculations. These capabilities include the ability to incorporate variability and uncertainty in aquifer properties and numerical methods for simulating solute transport with minimal numerical dispersion. A more realistic 3-D SZ flow model would increase confidence in the abstracted transport modeling employed in TSPA analyses and is probably a prerequisite for acceptance of a license application.

The dilution factor in the saturated zone has been shown to be a sensitive parameter for TSPA-VA. The appropriate range of uncertainty for dilution (and/or vertical transverse dispersivity) is also a controversial topic. Reduction in the uncertainty in this parameter will probably have to rely on inferences from analog sites or potentially from analysis of natural solute tracers in the saturated zone at the site. Additional effort should be devoted to an evaluation of potential analog systems of saturated flow in fractured media or in highly heterogeneous porous media. Although significant uncertainties will undoubtedly remain with regard to dispersive dilution processes in SZ transport, the dilution factor plays a direct role in calculations of dose and must be more defensibly assessed. Accurate, direct simulation of dispersive processes that result in dilution would be preferable to the use of the dilution factor as a parameter in TSPA analyses.

Climate change has an effect on the saturated zone that was grossly simplified in TSPA-VA. The water-table rise was not considered in the saturated-zone modeling. Changes in flow paths were not considered. Changes in groundwater flux were based on regional-scale modeling, but without an estimate of uncertainty. The effect of additional discharge locations and the presence of surface water was not considered. The effect of additional recharge at Yucca Mountain, Fortymile Wash, and regions upgradient was not considered. The saturated zone modeling should attempt to better reflect the wetter climates that might be the norm for the Yucca Mountain region.

More realistic models of colloid-facilitated transport should be implemented in the saturated zone models. These models should be tied to site-scale observations of colloidal transport and to observations of apparent colloid-facilitated transport of actinides from underground nuclear tests on the Nevada Test Site. The reactive colloid transport modeling presented in the sensitivity studies section of this chapter was developed in collaboration with environmental restoration research of underground nuclear testing on the Nevada Test Site. The equilibrium colloid sorption model employed in the TSPA-VA transport calculations is inadequate for modeling colloid-facilitated transport processes that may be dominated by kinetic sorption-desorption reactions onto colloids. Colloid-facilitated transport model development for the SZ in the Yucca Mountain project is planned to occur in conjunction with modeling of radionuclide migration from underground nuclear testing. Laboratory measurements to estimate the Pu desorption reaction rates from colloids should be obtained to constrain kinetic models of colloid-facilitated Pu transport and are currently planned. Colloid-facilitated transport of other radionuclides should be considered if Pu transport associated with colloids in the enhanced modeling proves to be an important contributor to dose in future TSPA calculations.



In TSPA-VA, the geosphere/biosphere interface was defined as a well at the point of highest concentration of contaminants in the groundwater. Natural discharge points were not considered. Dilution from mixing contaminated water with uncontaminated water during well pumping was not considered. An improved definition and modeling of this interface would lend further credibility to the TSPA calculations. Explicit regulatory guidance concerning the groundwater release scenarios that should be considered in performance assessment calculations would greatly aid in the planning for TSPA-LA and for Yucca Mountain site-characterization activities.

## 8.7 REFERENCES

- Altman, S.J.; Arnold, B.W.; Barnard, R.W.; Barr, G.E.; Ho, C.K.; McKenna, S.A.; and Eaton, R.R. 1996. *Flow Calculations for Yucca Mountain Groundwater Travel Time (GWTT-95)*. SAND96-0819. Albuquerque, New Mexico: Sandia National Laboratories. MOL.19961209.0152.
- Anderson, L.A. 1994. *Water Permeability and Related Rock Properties Measured on Core Samples from the Yucca Mountain USW GU-3/G-3 and USW G-4 Boreholes, Nevada Test Site, Nevada*. Open-File Report 92-201, 36 pp. Denver, Colorado: U.S. Geological Survey. NNA.19940218.0001.
- Andrews, R.W.; Dale T.F.; and McNeish, J.A. 1994. *Total System Performance Assessment - 1993: An Evaluation of the Potential Yucca Mountain Repository*. B000000000-01717-2200-00099, Rev. 01. Las Vegas, Nevada: INTERA, Inc. NNA.19940406.0158.
- Apps, J.A.; Carnahan, C.L.; Lichtner, P.C.; Michel, M.C.; Perry, D.; Silva, R.J.; Weres, O.; and White, A.F. 1983. *Status of Geochemical Problems Relating to the Burial of High-Level Radioactive Waste, 1982*. NUREG/CR-3062; LBL-15103. Washington, D.C.: U.S. Nuclear Regulatory Commission, Office of Nuclear Material Safety and Safeguards; Berkeley, California: Lawrence Berkeley Laboratory. HQS.19880517.1941.
- Arnold, B.W.; Gauthier, J.H.; Tucci, P.; and Robinson, B.A. 1997. *Saturated Zone Flow and Transport Abstraction/Testing Workshop Results*. B000000000-01717-2200-00190. Las Vegas, Nevada: TRW Environmental Safety Systems, Inc. MOL.19980528.0038.
- Arnold, B.W. and McKenna, S.A. 1998. "Influences of Aquifer Heterogeneity and Channelization on Saturated-Zone Flow and Transport at Yucca Mountain: Sub-Site-Scale Modeling Results." *High Level Radioactive Waste Management, Proceedings of the Eighth International Conference, Las Vegas, Nevada, May 11-14, 1998*, 213-215. La Grange Park, Illinois: American Nuclear Society
- Atkins, J.E.; Lee, J.H.; Lingineni, S.; Mishra, S.; McNeish, J.A.; Sassani, D.C.; Sevougian, S.D.; Andrews, R.W.; and Younker, J.L. 1995. *Total System Performance Assessment - 1995: An Evaluation of the Potential Yucca Mountain Repository*. B000000000-01717-2200-00136, Rev. 01. Las Vegas, Nevada: TRW Environmental Safety Systems, Inc. MOL.19960724.0188.
- Barnard, R.W. and Dockery, H.A., Editors. 1991. *Technical Summary of the Performance-Assessment Computational Exercises for 1990 (PACE-90), Vol. 1: 'Nominal Configuration' Hydrogeologic Parameters and Computational Results*. SAND90-2726. Albuquerque, New Mexico: Sandia National Laboratories. NNA.19910523.0001.
- Barnard, R.W.; Wilson, M.L.; Dockery, H.A.; Gauthier, J.H.; Kaplan, P.G.; Eaton, R.R.; Bingham, F.W.; and Robey, T.H. 1992. *TSPA 1991: An Initial Total-System Performance Assessment for Yucca Mountain*. SAND91-2795. Albuquerque, New Mexico: Sandia National Laboratories. NNA.19920630.0033.

Barton, C.C. and Larsen, E. 1985. "Fractal Geometry of Two-Dimensional Fracture Networks at Yucca Mountain, Southwestern Nevada." *Fundamentals of Rock Joints, Proceedings of the International Symposium, Bjorkliden, Lapland, Sweden, September 15-20, 1985*, 77-84. Editor: Stephansson, O. Lulea, Sweden: Centek Publishers. TIC Catalog Number: 217581.

Barton, C.C. 1995. "Fractal Analysis of Scaling and Spatial Clustering of Fractures." *Fractals in the Earth Sciences*, 141-178. Editors: Barton, C.C. and La Pointe, P.R. New York, New York: Plenum Press. TIC Catalog Number: 238243.

Bedinger, M.S.; Langer, W.H.; and Reed, J.E. 1989a. "Ground-Water Hydrology." *Studies of Geology and Hydrology in the Basin and Range Province, Southwestern United States, for Isolation of High-Level Radioactive Waste - Characterization of the Death Valley Region, Nevada and California*. Professional Paper 1370-F, 28-35. Editors: Bedinger, M.S.; Sargent, K.A.; and Langer, W.H. Denver, Colorado: U.S. Geological Survey. NNA.19920131.0251.

Bedinger, M.S.; Langer, W.H.; and Reed, J.E. 1989b. "Hydraulic Properties of Rocks in the Basin and Range Province." *Studies of Geology and Hydrology in the Basin and Range Province, Southwestern United States, for Isolation of High-Level Radioactive Waste - Basis of Characterization and Evaluation*. Professional Paper 1370-A, 16-18. Editors: Bedinger, M.S.; Sargent, K.A.; Langer, W.H.; Sherman, F.B.; Reed, J.E.; and Brady, B.T. Denver, Colorado: U.S. Geological Survey. NNA.19910524.0125.

Bedinger, M.S.; Sargent, K.A.; and Langer, W.H., Editors. 1989c. *Studies of Geology and Hydrology in the Basin and Range Province, Southwestern United States, for Isolation of High-Level Radioactive Waste - Characterization of the Death Valley Region, Nevada and California*. Professional Paper 1370-F, 49 pp. Denver, Colorado: U.S. Geological Survey. NNA.19920131.0251.

Bedinger, M.S.; Sargent, K.A.; Sherman, F.B.; Langer, W.H.; and Brady, B.T. 1989d. "Regional Characterization and Guidelines for Evaluation." *Studies of Geology and Hydrology in the Basin and Range Province, Southwestern United States, for Isolation of High-Level Radioactive Waste - Basis of Characterization and Evaluation*. Professional Paper 1370-A, 6-15. Editors: Bedinger, M.S.; Sargent, K.A.; Langer, W.H.; Sherman, F.B.; Reed, J.E.; and Brady, B.T. Denver, Colorado: U.S. Geological Survey. NNA.19910524.0125.

Benson, L.V.; Robison, J.H.; Blankennagel, R.K.; and Ogard, A.E. 1983. *Chemical Composition of Ground Water and the Locations of Permeable Zones in the Yucca Mountain Area, Nevada*. Open-File Report 83-854, 19 pp. Denver, Colorado: U.S. Geological Survey. NNA.19890511.0102.

Benson, L.V. and McKinley, P.W. 1985. *Chemical Composition of Ground Water in the Yucca Mountain Area, Nevada, 1971-84*. Open-File Report 85-484, 10 pp. Denver, Colorado: U.S. Geological Survey. NNA.19900207.0281.

Blankennagel, R.K. and Weir, J.E., Jr. 1973. *Geohydrology of the Eastern Part of Pahute Mesa, Nevada Test Site, Nye County, Nevada*. Professional Paper 712-B, 35 pp. Denver, Colorado: U.S. Geological Survey. NNA.19870406.0202.

Bodvarsson, G.S.; Bandurraga, T.M.; and Wu, Y.S., Editors. 1997. *The Site-Scale Unsaturated Zone Model of Yucca Mountain, Nevada, for the Viability Assessment*. LBNL - 40376. Berkeley, California: Lawrence Berkeley National Laboratory. MOL.19971014.0232.

Bredehoeft, J.D. 1992. "Response of the Ground-Water System at Yucca Mountain to an Earthquake." *Ground Water at Yucca Mountain: How High Can It Rise?*, 212-222. Washington, D.C.: National Academy Press. MOL.19960708.0340.

Bredehoeft, J.D. 1997. "Fault Permeability Near Yucca Mountain." *Water Resources Research*, 33, 11, 2459-2463. Washington, D.C.: American Geophysical Union. MOL.19980506.0039.

Caine, J.S.; Evans, J.P.; and Forster, C.B. 1996. "Fault Zone Architecture and Permeability Structure." *Geology*, 24, 11, 1025-1028. Boulder, Colorado: Geological Society of America. TIC Catalog Number: 238244.

Carr, W.J. 1984. *Regional Structural Setting of Yucca Mountain, Southwestern Nevada, and Late Cenozoic Rates of Tectonic Activity in Part of the Southwestern Great Basin, Nevada and California*. Open-File Report 84-854, 109 pp. Denver, Colorado: U.S. Geological Survey. NNA.19870325.0475.

Carrigan, C.R.; King, G.C.P.; Barr, G.E.; and Bixler, N.E. 1991. "Potential for Water-Table Excursions Induced by Seismic Events at Yucca Mountain, Nevada." *Geology*, 19, 12, 1157-1160. Boulder, Colorado: Geological Society of America. NNA.19920427.0050.

Champ, D.R.; Merritt, W.F.; and Young, J.L. 1982. "Potential for Rapid Transport of Plutonium in Groundwater as Demonstrated by Core Column Studies." *Scientific Basis for Nuclear Waste Management V, Proceedings of the Materials Research Society Fifth International Symposium, Berlin, Germany, June 7-10, 1982*, 11, 745-754. Editor: Lutze, W. New York, New York: North-Holland. TIC Catalog Number: 224867.

Claassen, H.C. 1985. *Sources and Mechanisms of Recharge for Ground Water in the West-Central Amargosa Desert, Nevada —A Geochemical Interpretation*. U.S. Geological Survey Professional Paper 712-F, 31 pp. Washington, D.C.: United States Government Printing Office. NNA.19900117.0150.

Clayton, R.W.; Zelinski, W.P.; and Rautman, C.A. 1997. *ISM2.0: A 3-D Geologic Framework and Integrated Site Model of Yucca Mountain*. B00000000-01717-5700-00004, Rev. 00. Las Vegas, Nevada: Civilian Radioactive Waste Management System, Management and Operating Contractor for U.S. Department of Energy, Yucca Mountain Site Characterization Office. MOL.19970724.0215.

Cohen, A.J.B.; Oldenburg, C.M.; Simmons, A.M.; Mishra, A.K.; and Hinds, J. 1997. *S<sup>4</sup>Z: Sub-Site-Scale Saturated-Zone Model for Yucca Mountain*. Level 4 Milestone SP25UM4. Berkeley, California: Lawrence Berkeley National Laboratory. MOL.19971204.0732.

Cooley, R.L. and Naff, R.L. 1990. *Regression Modeling of Ground-Water Flow*. Techniques of Water-Resources Investigations, Book 3, Chapter B4, 232 pp. Washington, D.C.: U.S. Government Printing Office; Denver, Colorado: For Sale by the U.S. Geological Survey, Books and Open-File Reports Section. TIC Catalog Number: 234709.

Craig, R.W. and Johnson, K.A. 1984. *Geohydrologic Data for Test Well UE-25p#1, Yucca Mountain Area, Nye County, Nevada*. Open-File Report 84-450, 63 pp. Denver, Colorado: U.S. Geological Survey. NNA.19870406.0256.

Craig, R.W. and Robison, J.H. 1984. *Geohydrology of Rocks Penetrated by Test Well UE-25p No. 1, Yucca Mountain Area, Nye County, Nevada*. Water-Resources Investigations Report 84-4248, 62 pp. Denver, Colorado: U.S. Geological Survey. NNA.19890905.0209.

CRWMS M&O. 1997. *Report of Results of Hydraulic and Tracer Tests at the C-Holes Complex*. Yucca Mountain Project Deliverable SP23APM3. Las Vegas, Nevada: TRW Environmental Safety Systems. MOL.19971024.0074.

CRWMS M&O. 1998. *Saturated Zone Flow and Transport Expert Elicitation Project*. Yucca Mountain Project Deliverable SL5X4AM3. Las Vegas, Nevada: TRW Environmental Safety Systems. MOL.19980224.0347.

Czarnecki, J.B. and Waddell, R.K. 1984. *Finite-Element Simulation of Ground-Water Flow in the Vicinity of Yucca Mountain, Nevada-California*. Water-Resources Investigations Report 84-4349, 38 pp. Denver, Colorado: U.S. Geological Survey. NNA.19870407.0173.

Czarnecki, J.B. 1985. *Simulated Effects of Increased Recharge on the Ground-Water Flow System of Yucca Mountain and Vicinity, Nevada-California*. Water-Resources Investigations Report 84-4344. Denver, Colorado: U.S. Geological Survey. NNA.19870407.0008.

Czarnecki, J.B. 1990. *Geohydrology and Evapotranspiration at Franklin Lake Playa, Inyo County, California*. Open-File Report 90-356, 96 pp. Denver, Colorado: U.S. Geological Survey. NNA.19920131.0238.

Czarnecki, J.B.; Faunt, C.C.; Gable, C.W.; and Zyvoloski, G.A. 1998. *Hydrogeology and Preliminary Three-Dimensional Finite-Element Ground-Water Flow Model of the Site Saturated Zone, Yucca Mountain, Nevada*. MOY-971211-03-04. Denver, Colorado: U.S. Geological Survey. MOL.19980204.0519.

D'Agnese, F.A. 1994. *Using Geoscientific Information Systems for Three-Dimensional Modeling of Regional Ground-Water Flow Systems, Death Valley Region, Nevada and California*. Ph.D. Dissertation, 331 pp. Golden, Colorado: Colorado School of Mines. MOL.19971009.0127.

D'Agnese, F.A.; Faunt, C.C.; Turner, A.K.; and Hill, M.C. 1997a. *Hydrogeologic Evaluation and Numerical Simulation of the Death Valley Regional Ground-Water Flow System, Nevada and California*. Water-Resources Investigations Report 96-4300. Denver, Colorado: U.S. Geological Survey. MOL.19971009.0062.

D'Agnese, F.A.; O'Brien, G.M.; Faunt, C.C.; and San Juan, C.A. 1997b. *Simulated Effects of Climate Change on the Death Valley Regional Ground-Water Flow System, Nevada and California*. DTN GS970708312144.003. TDIF: 306208. Denver, Colorado: U.S. Geological Survey. MOL.19980204.1023.

Deguelldre, C.A. 1994. *Colloid Properties in Groundwaters from Crystalline Formations*. PSI Bericht Nr. 94-21, NTB-92-05. Wurenlingen und Villigen, Switzerland: Paul Scherrer Institut; Baden, Switzerland: Nationale Genossenschaft für die Lagerung Radioaktiver Abfälle (NAGRA). MOL.19950330.0395.

Deguelldre, C.; Triay, I.; Kim, J.; Vilks, P.; Laaksoharju, M.; and Miekeley, N. 1997. "Groundwater Colloid Properties: A Global Approach." submitted to *NatureTIC* Catalog Number: 234027.

Deutsch, C.V. and Journel, A.G. 1992. *GSLIB Geostatistical Software Library and User's Guide*. New York, New York: Oxford University Press. NNA.19930507.0081.

EPA (U.S. Environmental Protection Agency). 1985. "40 CFR 191: Environmental Standards for the Management and Disposal of Spent Nuclear Fuel, High-Level and Transuranic Radioactive Wastes; Final Rule." *Federal Register*, 50, 182, 38066-38089.

Washington, D.C.: Superintendent of Documents, U.S. Government Printing Office. MOL.19980116.0231.

Ervin, E.M.; Luckey, R.R.; and Burkhardt, D.J. 1994. *Revised Potentiometric-Surface Map, Yucca Mountain and Vicinity, Nevada*. Water-Resources Investigations Report 93-4000, 17 pp. Denver, Colorado: U.S. Geological Survey. NNA.19930212.0018.

Faunt, C.C. 1994. *Characterization of the Three-Dimensional Hydrogeologic Framework of the Death Valley Region, Nevada and California*. Ph.D. Dissertation, 235 pp. Golden, Colorado: Colorado School of Mines. MOL.19980623.0372.

Faunt, C.C. 1997. *Effect of Faulting on Ground-Water Movement in the Death Valley Region, Nevada and California*. Water-Resources Investigations Report 95-4132. Denver, Colorado: U.S. Geological Survey. MOL.19980429.0119.

Fetter, C.W. 1993. *Contaminant Hydrogeology*. New York, New York: Macmillan Publishing Co. TIC Catalog Number: 226280.

Flint, L.E. and Flint, A.L. 1990. *Preliminary Permeability and Water-Retention Data for Nonwelded and Bedded Tuff Samples, Yucca Mountain Area, Nye County, Nevada*. Open-File Report 90-569, 57 pp. Denver, Colorado: U.S. Geological Survey. NNA.19901015.0200.

Flint, L.E. 1998. *Characterization of Hydrogeologic Units Using Matrix Properties, Yucca Mountain, Nevada*. Water-Resources Investigations Report 97-4243. Denver, Colorado: U.S. Geological Survey. TIC Catalog Number: 236515.

- Freeze, R.A. and Cherry, J.A. 1979. *Ground Water*. Englewood Cliffs, New Jersey: Prentice-Hall, Inc. NNA.19870406.0444.
- Fridrich, C.J.; Dudley, W.W., Jr.; and Stuckless, J.S. 1994. "Hydrogeologic Analysis of the Saturated-Zone Ground-Water System, Under Yucca Mountain, Nevada." *Journal of Hydrology*, 154, 1-4, 133-168. Amsterdam; New York, New York: Elsevier Science. MOL.19940811.0102.
- Geldon, A.L. 1993. *Preliminary Hydrogeologic Assessment of Boreholes UE-25c#1, UE-25c#2, and UE-25c#3, Yucca Mountain, Nye County, Nevada*. Water-Resources Investigations Report 92-4016, 176 pp. Denver, Colorado: U.S. Geological Survey. MOL.19960808.0136.
- Geldon, A.L. 1996. *Results and Interpretation of Preliminary Aquifer Tests in Boreholes UE-25c #1, UE-25c #2, and UE-25c #3, Yucca Mountain, Nye County, Nevada*. Water-Resources Investigations Report 94-4177, 119 pp., 3 sheets. Denver, Colorado: U.S. Geological Survey. MOL.19960229.0127.
- Geldon, A.L.; Umari, A.M.A.; Fahy, M.F.; Earle, J.D.; Gemmell, J.M.; and Darnell, J. 1997. *Results of Hydraulic and Conservative Tracer Tests in Miocene Tuffaceous Rocks at the C-Hole Complex, 1995 to 1997, Yucca Mountain, Nye County, Nevada*. 1997 Milestone Report SP23PM3. Denver, Colorado: U.S. Geological Survey - Yucca Mountain Project Branch. MOL.19980122.0412.
- Gelhar, L.W. 1986. "Stochastic Subsurface Hydrology From Theory to Applications." *Water Resources Research*, 22, 9, 135S-145S. Washington, D.C.: American Geophysical Union. NNA.19890523.0133.
- Graves, R.P.; Tucci, P.; and O'Brien, G.M. 1997. *Analysis of Water Level Data in the Yucca Mountain Area, Nevada, 1985-95*. U.S. Geological Survey Water Resources Investigations Report 96-4256, 140 p. Denver, Colorado: U.S. Geological Survey.
- Grisak, G.E. and Pickens, J.F. 1980. "Solute Transport Through Fractured Media 1. The Effect of Matrix Diffusion." *Water Resources Research*, 16, 4, 719-730. Washington, D.C.: American Geophysical Union. NNA.19890315.0006.
- Herzig, J.P.; Leclerc, D.M.; and Le Goff, P. 1970. "Flow of Suspensions Through Porous Media: Application to Deep Filtration." *Industrial and Engineering Chemistry I&EC*, 62, 5, 8-35. Washington, D.C.: American Chemical Society. TIC Catalog Number: 223585.
- Hill, M.C. 1992. *A Computer Program (MODFLOWP) for Estimating Parameters of a Transient, Three-Dimensional, Ground-Water Flow Model Using Nonlinear Regression*. Open-File Report 91-484, 358 pp. Denver, Colorado: U.S. Geological Survey. MOL.19961118.0122.
- Hillel, D. 1980. *Fundamentals of Soil Physics*. New York, New York: Academic Press, Inc. TIC Catalog Number: 215655.

Ho, C.K.; Francis, N.D.; Arnold, B.W.; Xiang, Y.; McKenna, S.A.; Mishra, S.; Barr, G.E.; Altman, S.J.; Yang, X.H.; and Eaton, R.R. 1996. *Thermo-Hydrologic Modeling of the Potential Repository at Yucca Mountain, Including the Effects of Heterogeneities and Alternative Conceptual Models of Fractured, Porous Media*. Level 3 Milestone T6536. Albuquerque, New Mexico: Sandia National Laboratories. MOL.19961219.0269.

Hodge, V.F.; Johannesson, K.H.; and Stetzenbach, K.J. 1996. "Rhenium, Molybdenum, and Uranium in Groundwater From the Southern Great Basin, USA: Evidence for Conservative Behavior." *Geochimica et Cosmochimica Acta*, 60, 17, 3197-3214. Amsterdam; New York, New York: Elsevier Science. TIC Catalog Number: 236469.

Istok, J.D.; Rautman, C.A.; Flint, L.E.; and Flint, A.L. 1994. "Spatial Variability in Hydrologic Properties of a Volcanic Tuff." *Ground Water*, 32, 751-760. Dublin, Ohio: Ground Water Publishing Company. TIC Catalog Number: 224518.

Johannesson, K.H.; Stetzenbach, K.J.; Hodge, V.F.; Kreamer, D.K.; and Zhou, X. 1997. "Delineation of Ground-Water Flow Systems in the Southern Great Basin Using Aqueous Rare Earth Element Distributions." *Ground Water*, 35, 5, 807-819. Worthington, Ohio: Water Well Journal Pub. Co. MOL.19980505.0200.

Jones, B.F. 1966. "Geochemical Evolution of Closed Basin Water in the Western Great Basin." *Second Symposium on Salt*, 1, 181-200. Editor: Rau, J.L. Cleveland, Ohio: Northern Ohio Geological Society. TIC Catalog Number: 224269.

Kerrisk, J.F. 1987. *Groundwater Chemistry at Yucca Mountain, Nevada, and Vicinity*. LA-10929-MS, 124 pp. Los Alamos, New Mexico: Los Alamos National Laboratory. NNA.19870507.0017.

Kreamer, D.K.; Hodge, V.F.; Rabinowitz, I.; Johannesson, K.H.; and Stetzenbach, K.J. 1996. "Trace Element Geochemistry in Water from Selected Springs in Death Valley National Park, California." *Ground Water*, 34, 1, 95-103. Worthington, Ohio: Water Well Journal Pub. Co. TIC Catalog Number: 236534.

La Camera, R.J. and Westenburg, C.L. 1994. *Selected Ground-Water Data for Yucca Mountain Region, Southern Nevada and Eastern California, Through December 1992*. Open-File Report 94-54, 161 pp. Carson City, Nevada: U.S. Geological Survey. TIC Catalog Number: 211474.

Lahoud, R.G.; Lobmeyer, D.H.; and Whitfield, M.S., Jr. 1984. *Geohydrology of Volcanic Tuff Penetrated by Test Well UE-25b No. 1, Yucca Mountain, Nye County, Nevada*. Water-Resources Investigations Report 84-4253, 49 pp. Denver, Colorado: U.S. Geological Survey. NNA.19890511.0117.

LeCain, G.D. 1997. *Air-Injection Testing in Vertical Boreholes in Welded and Nonwelded Tuff, Yucca Mountain, Nevada*. Water-Resources Investigations Report 96-4262, 33 pp. Denver, Colorado: U.S. Geological Survey. TIC Catalog Number: 233455.



- Leij, F.J.; Skaggs, T.H.; and van Genuchten, M.Th. 1991. "Analytical Solutions for Solute Transport in Three-Dimensional Semi-infinite Porous Media." *Water Resources Research*, 27, 10, 2719-2733. Washington, D.C.: American Geophysical Union.
- Lessoff, S.C. and Konikow, L.F. 1997. "Ambiguity in Measuring Matrix Diffusion with Single-Well Injection/Recovery Tracer Tests." *Ground Water*, 35, 1, 166-176. Worthington, Ohio: Water Well Journal Pub. Co. TIC Catalog Number: 238363.
- Levy, S.S. 1991. "Mineralogic Alteration History and Paleohydrology at Yucca Mountain, Nevada." *High Level Radioactive Waste Management, Proceedings of the Second Annual International Conference, Las Vegas, Nevada, April 28-May 3, 1991*, 1, 477-485. La Grange Park, Illinois: American Nuclear Society, Inc.; New York, New York: American Society of Civil Engineers. TIC Catalog Number: 210390.
- Lobmeyer, D.H. 1986. *Geohydrology of Rocks Penetrated by Test Well USW G-4, Yucca Mountain, Nye County, Nevada*. Water-Resources Investigations Report 86-4015, 42 pp. Denver, Colorado: U.S. Geological Survey. NNA.19890918.0510.
- Luckey, R.R.; Tucci, P.; Faunt, C.C.; Ervin, E.M.; Steinkampf, W.C.; D'Agnese, F.A.; and Patterson, G.L. 1996. *Status of Understanding of the Saturated-Zone Ground-Water Flow System at Yucca Mountain, Nevada, as of 1995*. Water-Resources Investigations Report 96-4077, 71 pp. Denver, Colorado: U.S. Geological Survey. MOL.19970116.0039.
- Ludwig, K.R.; Peterman, Z.E.; Simmons, K.R.; and Gutentag, E.D. 1993. " $^{234}\text{U}/^{238}\text{U}$  as a Ground-Water Tracer, SW Nevada-SE California." *High Level Radioactive Waste Management, Proceedings of the Fourth International Conference, Las Vegas, Nevada, April 26-30, 1993*, 4, 1567-1572. La Grange Park, Illinois: American Nuclear Society, Inc.; New York, New York: American Society of Civil Engineers. TIC Catalog Number: 224405.
- Marshall, B.D.; Peterman, Z.E.; and Stuckless, J.S. 1993. "Strontium Isotopic Evidence for a Higher Water Table at Yucca Mountain." *High Level Radioactive Waste Management, Proceedings of the Fourth Annual International Conference, Las Vegas, Nevada, April 26-30, 1993*, 2, 1948-1952. La Grange Park, Illinois: American Nuclear Society, Inc.; New York, New York: American Society of Civil Engineers. TIC Catalog Number: 225324.
- Matsuka, N.A. and Hess, J.W. 1989. *The Relationship of the Yucca Mountain Repository Block to the Regional Groundwater System—A Geochemical Model*. NWPO-TR-011-89. 149 pp. Reno, Nevada: University of Nevada. Washington, DC: Water Resources Center, U.S. Department of Energy. TIC Catalog Number: 206801.
- McCord, J.T.; Gotway C.A.; and Conrad, S.H. 1997. "Impact of Geologic Heterogeneity on Recharge Estimation Using Environmental Tracers: Numerical Modeling Investigation." *Water Resources Research*, 33, 6, 1229-1240. Washington, DC: American Geophysical Union. TIC Catalog Number: 238284.

McDonald, M.G. and Harbaugh, A.W. 1988. *A Modular Three-Dimensional Finite-Difference Ground-Water Flow Model*. Techniques of Water Resources Investigations, Book 6, Chapter A1, 576 pp. Denver, Colorado: U.S. Geological Survey. NNA.19921202.0002.

McKinley, P.W.; Long, M.P.; and Benson, L.V. 1991. *Chemical Analyses of Water from Selected Wells and Springs in the Yucca Mountain Area, Nevada and Southeastern California*. Open-File Report 90-355, 47 pp. Denver, Colorado: U.S. Geological Survey. NNA.19901031.0004.

Moench, A.F. 1989. "Convergent Radial Dispersion: A Laplace Transform Solution for Aquifer Tracer Testing." *Water Resources Research*, 25, 3, 439-447. Washington, DC.: American Geophysical Union. TIC Catalog Number: 238281.

Montazer, P.; Weeks, E.P.; Thamir, F.; Yard, S.N.; and Hofrichter, P.B. 1985. "Monitoring the Vadose Zone in Fractured Tuff, Yucca Mountain, Nevada." *Proceedings of the NWWA Conference on Characterization and Monitoring of the Vadose (Unsaturated) Zone, Denver, Colorado, November 19-21, 1985*, 439-469. Worthington, Ohio: National Water Well Association. NNA.19900924.0023.

National Research Council. 1995. *Technical Bases for Yucca Mountain Standards*. Committee on Technical Bases for Yucca Mountain Standards, Board on Radioactive Waste Management. National Academy of Science. Washington, DC: National Academy Press. 205 p. TIC Catalog Number: 104273.

Neretnieks, I. 1980. "Diffusion in the Rock Matrix: An Important Factor in Radionuclide Migration?" *Journal of Geophysical Research*, 85, B8, 4379-4397. Washington, DC.: American Geophysical Union. NNA.19870406.0365.

Ogard, A. 1987. "Appendix B Importance of Radionuclide Transport by Particulates Entrained in Flowing Groundwaters." *Groundwater Geochemistry at Yucca Mountain, Nevada, and Vicinity*. LA-10929-MS, 114-118. Kerrisk, J.F. Los Alamos, New Mexico: Los Alamos National Laboratory. Appendix B of NNA.19930607.0078.

Ogard, A.E. and Kerrisk, J.F. 1984. *Groundwater Chemistry Along Flow Paths Between a Proposed Repository Site and the Accessible Environment*. LA-10188-MS, 49 pp. Los Alamos, New Mexico: Los Alamos National Laboratory. TIC Catalog Number: 202356.

Perfect, D.L.; Faunt, C.C.; Steinkampf, W.C.; and Turner, A.K. 1995. *Hydrochemical Data Base for the Death Valley Region, California and Nevada*. Open-File Report 94-305, 10 pp. Denver, Colorado: U.S. Geological Survey. MOL.19940718.0001.

Peterman, Z.E. and Stuckless, J.S. 1993. "Isotopic Evidence of Complex Ground-Water Flow at Yucca Mountain, Nevada, USA." *High Level Radioactive Waste Management, Proceedings of the Fourth Annual International Conference, Las Vegas, Nevada, April 26-30, 1993*, 2, 1559-1566. La Grange Park, Illinois: American Nuclear Society, Inc.; New York, New York: American Society of Civil Engineers. NNA.19940120.0074.

Peters, R.R. and Klavetter, E.A. 1988. "A Continuum Model for Water Movement in an Unsaturated Fractured Rock Mass." *Water Resources Research*, 24, 3, 416-430. Washington, D.C.: American Geophysical Union. NNA.19890523.0139.

Plume, R.W. and Carlton, S.M. 1988. *Hydrogeology of the Great Basin Region of Nevada, Utah, and Adjacent States*. Hydrologic Investigations Atlas 694-A. Denver, Colorado: U.S. Geological Survey. NNA.19910215.0252.

Pruess, K.; Wang, J.S.Y.; and Tsang, Y.W. 1990a. "On Thermohydrologic Conditions Near High-Level Nuclear Wastes Emplaced in Partially Saturated Fractured Tuff. 1. Simulation Studies With Explicit Consideration of Fracture Effects." *Water Resources Research*, 26, 6, 1235-1248. Washington, D.C.: American Geophysical Union. NNA.19910328.0073.

Pruess, K.; Wang, J.S.Y.; and Tsang, Y.W. 1990b. "On Thermohydrologic Conditions Near High-Level Nuclear Wastes Emplaced in Partially Saturated Fractured Tuff. 2. Effective Continuum Approximation." *Water Resources Research*, 26, 6, 1249-1261. Washington, D.C.: American Geophysical Union. NNA.19890522.0315.

Reeves, M.; Ward, D.S.; Johns, N.D.; and Cranwell, R.M. 1986a. *Theory and Implementation for SWIFT II, The Sandia Waste-Isolation Flow and Transport Model for Fractured Media, Release 4.84*. NUREG/CR-3328, SAND83-1159, 189 pp. Albuquerque, New Mexico: Sandia National Laboratories. TIC Catalog Number: 216521.

Reeves, M.; Ward, D.S.; Johns, N.D.; and Cranwell, R.M. 1986b. *Data Input Guide for SWIFT II, The Sandia Waste-Isolation Flow and Transport Model for Fractured Media, Release 4.84*. NUREG/CR-3162, SAND83-0242, 144 pp. Albuquerque, New Mexico: Sandia National Laboratories. TIC Catalog Number: 227804.

Reeves, M.; Freeze, G.A.; Kelly, V.A.; Pickens, J.F.; Upton, D.T., and Davies, P.B. 1987. *Regional Double-Porosity Solute Transport in the Culebra Dolomite Under Brine-Reservoir-Breach Release Conditions: An Analysis of Parameter Sensitivity and Importance*. SAND89-7069. Albuquerque, New Mexico: Sandia National Laboratories. TIC Catalog Number: 203705.

Reeves, M.; Baker, N.A.; and Duguid, J.O. 1994. *Review and Selection of Unsaturated Flow Models*. B00000000-01425-2200-00001, Rev. 00. Las Vegas, Nevada: INTERA, Inc. MOL.19970203.0025.

Reimus, P.W. and Turin, H.J. 1997. *Results, Analyses, and Interpretation of Reactive Tracer Tests in the Lower Bullfrog Tuff at the C-Wells, Yucca Mountain, Nevada*. Yucca Mountain Project Milestone Report SP2370M4, 33 pp. Los Alamos, New Mexico: Los Alamos National Laboratory. TIC Catalog Number: 234030.

Robinson, B.A. 1994. "A Strategy for Validating a Conceptual Model for Radionuclide Migration in the Saturated Zone Beneath Yucca Mountain." *Radioactive Waste Management and Environmental Restoration*, 19, 1-3, 73-96. Yverdon, Switzerland: Harwood Publishers; Newark, New Jersey: Distributed by International Publishers Distributor. TIC Catalog Number: 222513.

Robinson, B.A.; Wolfsberg, A.V.; Viswanathan, H.S.; Bussod, G.Y.; Gable, C.W.; and Meijer, A. 1997. *The Site-Scale Unsaturated Zone Transport Model of Yucca Mountain*. YMP Milestone Report SP25BM3. Los Alamos, New Mexico: Los Alamos National Laboratory. MOL.19980203.0570.

Rush, F.E.; Thordarson, W.; and Pyles, D.G. 1984. *Geohydrology of Test Well USW H-1, Yucca Mountain, Nye County, Nevada*. Water-Resources Investigations Report 84-4032, 56 pp. Denver, Colorado: U.S. Geological Survey. NNA.19870518.0067.

Sass, J.H.; Lachenbruch, A.H.; Dudley, W.W., Jr.; Priest, S.S.; and Munroe, R.J. 1988. *Temperature, Thermal Conductivity, and Heat Flow Near Yucca Mountain, Nevada: Some Tectonic and Hydrologic Implications*. Open-File Report 87-649, 122 pp. Denver, Colorado: U.S. Geological Survey. NNA.19890123.0010.

Schenker, A.R.; Guerin, D.C.; Robey, T.H.; Rautman, C.A.; and Barnard, R.W. 1995. *Stochastic Hydrogeologic Units and Hydrogeologic Properties Development for Total-System Performance Assessments*. SAND94-0244, 150 pp. Albuquerque, New Mexico: Sandia National Laboratories. MOL.19960318.0528.

Schwartz, F.W. and Smith, L. 1988. "A Continuum Approach for Modeling Mass Transport in Fractured Media." *Water Resources Research*, 24, 8, 1360-1372. Washington, D.C.: American Geophysical Union. TIC Catalog Number: 225296.

Scott, R.B.; Spengler, R.W.; Diehl, S.; Lappin, A.R.; and Chornack, M.P. 1983. "Geologic Character of Tuffs in the Unsaturated Zone at Yucca Mountain, Southern Nevada." *Role of the Unsaturated Zone in Radioactive and Hazardous Waste Disposal, Philadelphia, Pennsylvania, May 31-June 4, 1982*, 289-335. Editors: Mercer, J.W.; Rao, P.S.C.; and Marine, I.W. Ann Arbor, Michigan: Ann Arbor Science Publishers. NNA.19870406.0034.

Sinnock, S.; Lin, Y.T.; and Brannen, J.P. 1984. *Preliminary Bounds on the Expected Postclosure Performance of the Yucca Mountain Repository Site, Southern Nevada*. SAND84-1492, 179 pp. Albuquerque, New Mexico: Sandia National Laboratories. NNA.19920131.0332.

Sinnock, S.; Lin, Y.T.; and Tierney, M.S. 1985. *Preliminary Estimates of Groundwater Travel Time and Radionuclide Transport at the Yucca Mountain Repository Site*. SAND85-2701, 156 pp. Albuquerque, New Mexico: Sandia National Laboratories. NNA.19891129.0550.

Spengler, R.W.; Braun, C.A.; Linden, R.M.; Martin, L.G.; Ross-Brown, D.M.; and Blackburn, R.L. 1993. "Structural Character of the Ghost Dance Fault, Yucca Mountain, Nevada." *High Level Radioactive Waste Management, Proceedings of the 4th Annual International Conference, Las Vegas, Nevada, April 26-30, 1993*, 1, 653-659. La Grange Park, Illinois: American Nuclear Society, Inc.; New York, New York: American Society of Civil Engineers. TIC Catalog Number: 224016.

StatSoft, Inc. 1997. *STATISTICA (Release 5, '97 Edition)*. Tulsa, Oklahoma: STATISTICA.

Stuckless, J.S.; Whelan, J.F.; and Steinkampf, W.C. 1991. "Isotopic Discontinuities in Ground Water Beneath Yucca Mountain, Nevada." *High Level Radioactive Waste Management, Proceedings of the Second Annual International Conference, Las Vegas, Nevada, April 28-May 3, 1991*, 2, 1410-1415. La Grange Park, Illinois: American Nuclear Society, Inc.; New York, New York: American Society of Civil Engineers. NNA.19920117.0093.

Sweetkind, D.S. and Williams-Stroud, S.C. 1996. *Characteristics of Fractures at Yucca Mountain, Nevada: Synthesis Report*. 93 pp. Denver, Colorado: U.S. Geological Survey. MOL.19961213.0181.

Szymanski, J.S. 1989. *Conceptual Considerations of the Yucca Mountain Groundwater System with Special Emphasis on the Adequacy of This System to Accommodate a High-Level Nuclear Waste Repository*, 390 pp. Las Vegas, Nevada: U.S. Department of Energy, Nevada Operations Office, Yucca Mountain Project Office. NNA.19890831.0152.

Tang, D.H.; Frind, E.O.; and Sudicky, E.A. 1981. "Contaminant Transport in Fractured Porous Media: Analytical Solution for a Single Fracture." *Water Resources Research*, 17, 3, 555-564. Washington, D.C.: American Geophysical Union. NNA.19900711.0084.

Thibault, D.H.; Sheppard, M.I.; and Smith, P.A. 1990. *A Critical Compilation and Review of Default Soil Solid/Liquid Partition Coefficients,  $K_d$ , for Use in Environmental Assessments*. AECL-10125, 115 pp. Pinawa, Manitoba, Canada: Whiteshell Nuclear Research Establishment, Atomic Energy of Canada Limited. MOL.19980623.0375.

Thomas, J.M.; Lyles, B.F.; and Carpenter, L.A. 1991. *Chemical and Isotopic Data for Water From Wells, Springs, and Streams in Carbonate-Rock Terrain of Southern and Eastern Nevada and Southeastern California, 1985-88*. Open-File Report 89-422, 24 pp. Denver, Colorado: U.S. Geological Survey. NNA.19940510.0008.

Thompson, J.L.; Dozier, B.L.; Duncan, D.W.; Efurd, D.W.; Finnegan, D.L.; Kersting, A.B.; Martinez, B.A.; Ortega, P.K.; Rokop, D.J.; Smith, D.K.; and Thompson, B.K. 1998. *Laboratory and Field Studies Related to Radionuclide Migration at the Nevada Test Site, October 1, 1996 — September 30, 1997*. LA-13419-PR, 38 pp. Los Alamos, New Mexico: Los Alamos National Laboratory. MOL.19980625.0450.

Thordarson, W. 1983. *Geohydrologic Data and Test Results from Well J-13, Nevada Test Site, Nye County, Nevada*. Water-Resources Investigations Report 83-4171, 63 pp. Denver, Colorado: U.S. Geological Survey. NNA.19870518.0071.

Triay, I.R.; Meijer, A.; Conca, J.L.; Kung, K.S.; Rundberg, R.S.; Strietelmeier, B.A.; Tait, C.D.; Clark, D.L.; Neu, M.P.; and Hobart, D.E. 1997. *Summary and Synthesis Report on Radionuclide Retardation for the Yucca Mountain Site Characterization Project*. Yucca Mountain Site Characterization Program Milestone 3784M. LA-13262-MS. Editor: Eckhardt, R.C. Los Alamos, New Mexico: Los Alamos National Laboratories. MOL.19971210.0177.

Tsang, C.F. and Mangold, D.C., Editors. 1984. *Panel Report on Coupled Thermo-Mechanical-Hydro-Chemical Processes Associated with a Nuclear Waste Repository*. LBL-18250, 89 pp. Berkeley, California: Lawrence Berkeley Laboratory. NNA.19871014.0047.

Tsang, C.-F. 1997. *Drift-Scale Heterogeneous Permeability Field Conditioned to Field Data*. Yucca Mountain Project Level 4 Milestone SP331BM4. Berkeley, California: Lawrence Berkeley National Laboratory. MOL.19971125.0911.

Tucci, P. 1997. e-mail message to Bill Arnold, December 11, 1997.

Tucci, P. and Burkhardt, D.J. 1995. *Potentiometric-Surface Map, 1993, Yucca Mountain and Vicinity, Nevada*. Water-Resources Investigations Report 95-4149, 15 pp. Denver, Colorado: U.S. Geological Survey. MOL.19960924.0517.

Tucci, P. 1998. Particle-tracking Analysis of Saturated-Zone Flow from Yucca Mountain, Nevada: U.S. Geological Survey Administrative Report, 8 p.

van Genuchten, M.Th. 1981. *Non-Equilibrium Transport Parameters From Miscible Displacement Experiments*. Research Report 119, 88 pp. Riverside, California: U.S. Department of Agriculture, Science and Education Administration, U.S. Salinity Laboratory.

Waddell, R.K. 1982. *Two-Dimensional, Steady-State Model of Ground-Water Flow, Nevada Test Site and Vicinity, Nevada-California*. Water-Resources Investigations Report 82-4085, 72 pp. Denver, Colorado: U.S. Geological Survey. NNA.19870518.0055.

Waddell, R.K.; Robison, J.H.; and Blankennagel, R.K. 1984. *Hydrology of Yucca Mountain and Vicinity, Nevada—California: Investigative Results Through Mid-1983*. Water-Resources Investigations Report 84-4267, 72 pp. Denver, Colorado: U.S. Geological Survey. NNA.19870406.0343.

Watermark Computing. 1994. *PEST Model-Independent Parameter Estimation: User's Manual*. Oxley, Australia: Watermark Computing. MOL.19961202.0179.

White, A.F. 1979. *Geochemistry of Ground Water Associated with Tuffaceous Rocks, Oasis Valley, Nevada*. Hydrology of Nuclear Test Sites. Geological Survey Professional Paper 712-E, E1-E25. Reston, Virginia: U.S. Geological Survey; Washington, D.C.: For Sale by the Superintendent of Documents, U.S. Government Printing Office. NNA.19870519.0034.

White, A.F.; Claassen, H.C.; and Benson, L.V. 1980. *The Effect of Dissolution of Volcanic Glass on the Water Chemistry in a Tuffaceous Aquifer, Rainier Mesa, Nevada*. Water-Supply Paper 1535-Q, 34 pp. Reston, Virginia: U.S. Geological Survey; Washington, D.C.: For Sale by the Superintendent of Documents, U.S. Government Printing Office. NNA.19870519.0065.

Whitfield, M.S., Jr.; Eshom, E.P.; Thordarson, W.; and Schaefer, D.H. 1985. *Geohydrology of Rocks Penetrated by Test Well USW H-4, Yucca Mountain, Nye County, Nevada*. Water-Resources Investigations Report 85-4030, 37 pp. Reston, Virginia: U.S. Geological Survey. NNA.19870407.0328.

Wilson, M.L.; Gauthier, J.H.; Barnard, R.W.; Barr, G.E.; Dockery, H.A.; Dunn, E.; Eaton, R.R.; Guerin, D.C.; Lu, N.; Martinez, M.J.; Nilson, R.; Rautman, C.A.; Robey, T.H.; Ross, B.; Ryder, E.E.; Schenker, A.R.; Shannon, S.A.; Skinner, L.H.; Halsey, W.G.; Gansemer, J.D.; Lewis, L.C.; Lamont, A.D.; Triay, I.R.; Meijer, A.; and Morris, D.E. 1994. *Total-System Performance Assessment for Yucca Mountain—SNL Second Iteration (TSPA-1993)*. SAND93-2675, 882 pp. Albuquerque, New Mexico: Sandia National Laboratories. NNA.19940112.0123.

Winograd, I.J. and Thordarson, W. 1975. *Hydrogeologic and Hydrochemical Framework, South-Central Great Basin, Nevada-California, With Special Reference to the Nevada Test Site*. Professional Paper 712-C, 126 pp. Washington, D.C.: U.S. Geological Survey. NNA.19870406.0201.

Wood, W.W.; Kraemer, T.F.; and Hearn, P.P., Jr. 1990. "Intragranular Diffusion: An Important Mechanism Influencing Solute Transport in Clastic Aquifers?" *Science*, 247, 4950, 1569-1572. Washington, D.C.: American Association for the Advancement of Science. TIC Catalog Number: 238109.

Yao, K.M.; Habibian, M.T.; and Omelia, C.R. 1971. "Water and Waste Water Filtration: Concepts and Applications." *Environmental Science and Technology*, 5, 11, 1195-1112. Washington, D.C.: American Chemical Society. MOL.19950110.0086.

Zhang, H.; Schwartz, F.W.; Wood, W.W.; Garabedian, S.P.; and LeBlanc, D.R. 1998. "Simulation of Variable-Density Flow and Transport of Reactive and Nonreactive Solutes During a Tracer Test at Cape Cod, Massachusetts." *Water Resources Research*, 34, 1, 67-82. Washington, D.C.: American Geophysical Union. TIC Catalog Number: 238299.

Zyvoloski, G. 1983. "Finite Element Methods for Geothermal Reservoir Simulation." *International Journal for Numerical and Analytical Methods in Geomechanics*, 7, 1, 75-86. London; New York, New York: John Wiley & Sons. NNA.19910806.0017.

Zyvoloski, G.A. 1986. "Incomplete Factorization for Finite Element Methods." *International Journal for Numerical Methods in Engineering*, 23, 6, 1101-1109. London; New York, New York: John Wiley & Sons. NNA.19890523.0138.

Zyvoloski, G.A. and Dash, Z.V. 1990. *Software Verification Report FEHMN: Version 1.0*. TWS-EES-5/5-90-3. Los Alamos, New Mexico: Los Alamos National Laboratory. NNA.19910806.0018.

Zyvoloski, G.A.; Robinson, B.A.; Dash, Z.V.; and Trease, L.L. 1995. *Models and Methods Summary for the FEHMN Application, Revision 1*. LA-UR-94-3787, 70 pp. Los Alamos, New Mexico: Los Alamos National Laboratory. TIC Catalog Number: 222337.

Zyvoloski, G.A.; Robinson, B.A.; Birdsell, K.H.; Gable, C.W.; Czarnecki, J.; Bower, K.M.; and Faunt, C. 1997. *Saturated Zone Radionuclide Transport Model September 29, 1997*. Milestone SP25CM3A. Los Alamos, New Mexico: Los Alamos National Laboratory. MOL.19980127.0089.

INTENTIONALLY LEFT BLANK